Participation of Ste20-like kinase-deficient neurons in the abnormal circuitry of focal epileptogenic lesions

Doctoral thesis

to obtain a doctorate (PhD)

from the Faculty of Medicine

of the University of Bonn

Pedro Xavier Royero Rodriguez

Guarenas, Venezuela

2022

Written with authorization of

the Faculty of Medicine of the University of Bonn

First reviewer: Prof. Dr. Heinz Beck

Second reviewer: Prof. Dr. Dirk Isbrandt

Day of oral examination: 21.12.2021

For the Institute of Experimental Epileptology and Cognition Research

Director: Prof. Dr. Heinz Beck

Table of Contents

List of abbreviations

4-AP	4-aminopyridine
ACSF	Artificial cerebrospinal fluid
AMPA	α-amino-3-hydroxy-5-methyl-4-isoxazolepropionic acid
ANOVA	Analysis Of Variance
aRGCs	Apical radial glial cells
ATP	Adenosine 5′-triphosphate
BSA	Bovine serum albumin
CNQX	6-Cyano-7-nitroquinoxaline-2,3-dione disodium salt
D-AP5	D-(-)-2-Amino-5-phosphonopentanoic acid
DAPI	4′,6-diamidino-2-phenylindole
DE	Differentially expressed
E/I	Excitatory/inhibitory
EGTA	Ethylenglycole-bis(2-aminoethylether)-N,N,N′,N′-tetraacetic acid
EPSC	Excitatory postsynaptic current
EPSP	Excitatory postsynaptic potential
FCD	Focal cortical dysplasias
FF	Feedforward
FingR	Fibronectin intrabodies generated with mRNA display
FS	Fast spiking
GABA	Gamma-aminobutyric acid
GCK	Germinal center kinase
GFAP	Glial fibrillary acidic protein
GG	Ganglioglioma
GOPC	Golgi-associated PDZ and coiled-coil motif-containing protein
HEPES	4-(2-hydroxyethyl)-1-piperazineethanesulfonic acid
ILAE	International League Against Epilepsy
ILAE	Neoplastic glioneuronal tumors
I.p.	Intraperitoneal
IPC	Intermediate progenitor cell
IPSC	Inhibitory postsynaptic current

IPSP	Inhibitory postsynaptic potential
IUE	In utero electroporation
IZ/SP	Intermediate zone or subplate
KD	knockdown
KO	Knockout
Ldb	LIM domain-binding transcriptional cofactor protein
MAP 2	Microtubule-associated protein 2
MAPK	Mitogen-activated protein kinase
MCD	Malformations of cortical development
mEPSC	Miniature excitatory postsynaptic current
mIPSC	Miniature inhibitory postsynaptic current
mTOR	Mechanistic target of rapamycin
NEC	Neuroepithelial cells
nFS	non-fast spiking
NMDA	N-Methyl-d-aspartic acid
PAK	p21-activated kinase
Patch-seq	Patch-clamp RNA sequencing
PBS	Phosphate-buffered saline
PC	Pyramidal cell
PC	Pyramidal cells
PCA	Principal Components Analysis
PFA	Paraformaldehyde
pS6	Phosphorylated ribosomal S6 protein
PSD-95	Postsynaptic density protein 95
PTZ	Pentylenetetrazol
QX314	N-(2,6-Dimethylphenylcarbamoylmethyl) triethylammonium
S.c.	Subcutaneous
scRNA-seq	Single-cell RNA sequencing
SEM	Standard error of the mean
shRNA	Short hairpin RNA
shSLK	shRNA for SLK
SLK	Ste20-like kinase

Ste20	Sterile 20
SVZ	Subventricular zone
Thal	Thalamus
t-SNE	t-Distributed Stochastic Neighbor Embedding
TTX	Tetrodotoxin
Vip	Vasointestinal peptide
VZ	Ventricular zone
XFP	X fluorescence proteins (control plasmid)

1. Introduction

1.1 Epilepsy

Epilepsy comprises more than 40 clinical syndromes affecting around 50 million people worldwide, representing one of the most common neuropathologies in the human population (Najm et al., 2018; World Health Organization, 2019). According to the International League Against Epilepsy (ILAE), epilepsy is a disorder of the brain function characterized by a susceptibility to generate recurrent and spontaneous seizures, resulting in neurological, cognitive, psychological, and social consequences (Fisher et al., 2014). Diagnosing epilepsy is a complex process that requires a multi-level classification framework, focusing on the seizure type, epilepsy type, and epilepsy syndrome (Scheffer et al., 2017). In addition, features such as etiology, age of onset, response to drugs, and electrophysiological and structural findings also assist in the classification of the epilepsy type (Berg and Scheffer, 2011; Scheffer et al., 2017).

Epileptic seizures are transient clinical manifestations of excessive or synchronous neuronal activity in the brain (Fisher et al., 2005). They can differ in their initiation mechanism, propagation, and frequency, and are classified into seizures of focal, generalized, and unknown onset (Fisher et al., 2017b, 2017a). Generalized seizures quickly spread bilaterally to extended brain areas causing impaired consciousness. Generalized seizures can be divided into motor (e.g. tonic or tonic-clonic seizures) and non-motor (absence) seizures (Fisher et al., 2017a). Focal seizures begin in a limited region and spread locally within the same hemisphere or bilaterally. Furthermore, focal seizures can also impair the level of awareness and show motor and non-motor symptoms (Fisher et al., 2017a, 2017b). In some cases, however, seizure triggering may involve different areas and more than one seizure type, but each individual seizure has a consistent area of onset (Berg et al., 2010; Berg and Scheffer, 2011).

Epilepsy is considered a spectrum disorder with a wide variety of causes. They can have a genetic, infectious, structural, metabolic, immune, as well as an unidentified origin. The etiologies of epilepsies are not mutually exclusive nor hierarchical; therefore, some epilepsy types may have a multifactorial origin (Scheffer et al., 2017). In this study, we aimed to better understand the mechanisms of excitability in developmental brain lesions,

distinct structural abnormalities generated during the development of the cortex that are frequently associated with drug-resistant seizures.

1.2 Developmental brain lesions and epilepsy

Developmental brain lesions represent the most common cause of untreatable epilepsy in children and young adults. Such focal epileptogenic lesions encompass a wide range of locally restricted brain architectural abnormalities and cell growth alterations that arise as a consequence of disturbances during brain development (Aronica and Crino, 2014; Kuzniecky, 2015; Pallud and McKhann, 2019). Neoplastic glioneuronal tumors (GNTs) and the non-neoplastic malformations of cortical development (MCD) are two major classes of developmental brain lesions associated with high epileptogenicity in human patients. Gangliogliomas (GGs) and focal cortical dysplasias (FCDs) are the most common disorder belonging to each class, respectively. Even though their molecular mechanisms and pathological alterations are diverse, the presence of either, GNT or MCD, usually requires long-term treatments and/or removal of the abnormal brain tissue when refractory seizures are observed (Moosa and Wyllie, 2013).

GNTs are epilepsy-associated tumors characterized by their low-grade appearance, slow growth, and preferential cortical location observed in young patients with drug-resistant complex partial seizures (Moosa and Wyllie, 2013; Aronica and Crino, 2014). These cortical neoplasms generally display a mixed glial and neuronal phenotype (Gatto et al., 2020). GGs, the most common GNT causing chronic focal epilepsy, consists of a mixture of neurons with altered morphology (known as dysplastic or dysmorphic neurons) and proliferative glial tumor cells (**Fig. 1E-H**) (Pasquier et al., 2002; Giulioni, 2014). The benign character of GGs usually leads to a favorable prognosis after surgical resection. However, removal of the tumor itself might not be sufficient to avoid the generation of seizures, due to epileptogenic peritumoral changes (Aronica et al., 2007; van Breemen et al., 2007; Englot et al., 2012).

On the other hand, MCDs are non-neoplastic disorders that result from the alteration of one or more developmental steps, generating focal cortical malformations and in some cases abnormal changes in brain size (Represa, 2019; Severino et al., 2020). Approximately 40-50% of patients with drug-resistant epilepsy that undergo surgery suffer

from an MCD (Pasquier et al., 2002). In addition, MCDs have been related to mental retardation and congenital neurological deficits (Lee, 2017; Severino et al., 2020). MCDs include a wide spectrum of cortical anomalies exhibiting diverse anatomical alterations, genetic profiles, and clinical manifestations (Benova and Jacques, 2019; Severino et al., 2020). They are classified according to the disrupted developmental stage that triggered the structural anomalies, including proliferation or apoptosis (microcephaly, megalencephaly, tuberous sclerosis, and FCD), cellular migration (heterotopias, lissencephaly, and Cobblestone malformations), and post-migrational development (polymicrogyria and FCD group III.C) (Barkovich et al., 2012; Severino et al., 2020). Among MCDs, FCD type IIB (FCD-IIB) is considered one of the major causes of untreatable epilepsy in the pediatric population (Sisodiya et al., 2009; Jayalakshmi et al., 2019). FCD-IIB is characterized by marked disrupted cortical lamination (**Fig. 1A**) and the appearance of both dysplastic neurons with abnormal shape, size, and orientation, and immature cells exhibiting neuronal and glial features known as balloon cells (**Fig. 1B-D**) (Lamparello et al., 2007; Crino, 2015a).

The exact mechanism of seizure generation in developmental brain lesions is still unsolved. In GGs, Ictal activity may originate intrinsically at the tumor itself, with experimental evidence showing that dysplastic neurons are hyperexcitable and that an excitatory-inhibitory (E/I) imbalance exists within the affected cortical areas (Wolf et al., 1995; Aronica et al., 2001; Andres et al., 2005; Barba et al., 2011; Koh et al., 2018; Goz et al., 2020). In addition, the infiltrated peritumoral cortex may also be key for the generation of seizures, due to neurotransmitter and ionic changes, acidosis, inflammation, and the possible coexistence of a second pathology such as an FCD in the tumor vicinity (Prayson et al., 2010; Giulioni, 2014; Huberfeld and Vecht, 2016; Slegers and Blumcke, 2020).

As for GGs, dysplastic neurons in FCD-IIB appear to play an important role in the generation of ictal activity due to their hyperexcitable intrinsic properties (Cepeda et al., 2003, 2005b; André et al., 2004; Abdijadid et al., 2015). In contrast, balloon cells do not show excitable properties and seem to be synaptically disconnected from the local network (Mathern et al., 2000; Cepeda et al., 2003, 2005b). In addition, an imbalance of excitation and inhibition has been described in FCD-IIB, due to remarkable changes in the

expression of neurotransmitter receptors and voltage-gated channels across principal cells and interneurons (Roesler et al., 2001; Calcagnotto et al., 2005; Cepeda et al., 2005a; Möddel et al., 2005; Yu et al., 2012). In this sense, dysplastic brain areas in FCD-IIB have been shown to retain features of the immature cortex, including the preservation of immature gamma-aminobutyric acid (GABA) signaling acting as a depolarizing neurotransmitter (Cepeda et al., 2006, 2007; Hanai et al., 2010; Talos et al., 2012). Spontaneous pacemaker synaptic activity exclusively driven by GABA receptors has also been observed, which may explain the benzodiazepine resistance in patients with FCD-IIB (Hammers et al., 2001; Cepeda et al., 2014).

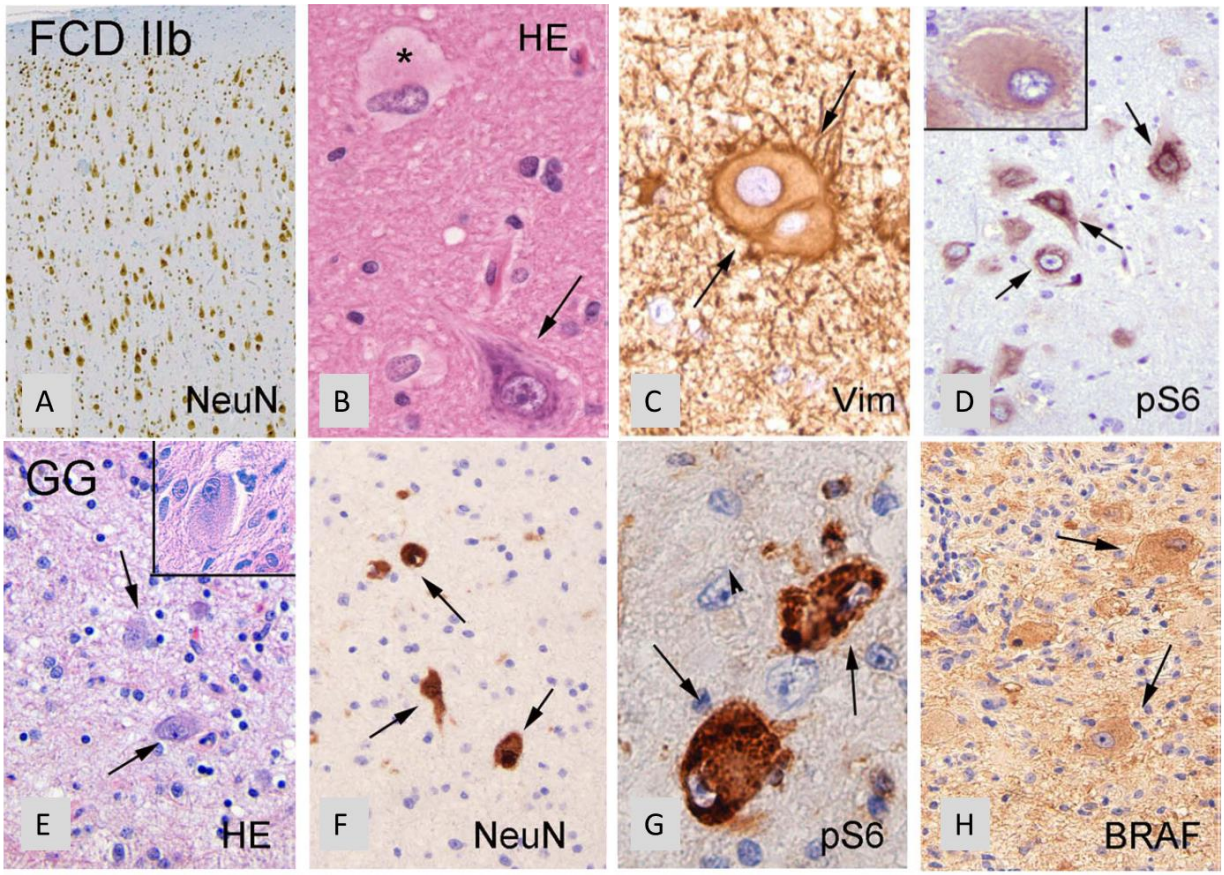

Figure 1. Dysplastic neurons in FCD-IIB and GGs. A, FCD-IIB NeuN staining showing cortical dyslamination. B, Hematoxylin/eosin (HE) staining revealing a dysplastic neuron with enlarged nucleus (arrow) and a balloon cell (asterisk). C, Staining of the cytoskeletal protein vimentin in balloon cells. D, Phosphorylated ribosomal S6 protein (pS6) expression in dysplastic neurons (arrows) and a balloon cell (inset), suggesting hyperactivation of the mechanistic target of rapamycin (mTOR) pathway. E, Hematoxylin/eosin staining of a GG specimen showing dysplastic neurons (arrows and inset) and glial cells. F, NeuN staining shows the neuronal component of GGs. G, pS6 expression of dysplastic neurons in a GG

specimen. H, BRAFV600E immunostaining showing large expression in dysplastic cells (arrows). Modified from Arorica and Crino, 2014.

The presence of these developmentally disrupted cellular elements, altered cortical architecture, and immature circuits, suggest a complex interaction between pathological and normal cortical networks within and outside developmental brain lesions, which may be responsible for their highly epileptogenicity and resistance to drug treatments (Aronica and Crino, 2014; Abdijadid et al., 2015; Iffland and Crino, 2017). This means that studies addressing the role of individual pathological alterations are necessary to understand precisely what drives the emergence of hyperexcitability and to find efficient therapeutic targets to treat refractory seizures. This thesis focuses on studying the microcircuit features of morphological-altered neurons within cortical networks.

1.3 Dysplastic neurons and developmental brain lesions

Although the physiopathology and associated comorbidities between GGs and FCD-IIB may differ, these developmental brain lesions are among the most common types of surgical specimens removed from patients with refractory seizures (Aronica and Crino, 2014). Moreover, these focal epileptogenic lesions share the presence of dysplastic neurons as a striking unifying feature that may represent a common mechanism leading to the emergence of severe hyperexcitability (Blümcke and Wiestler, 2002; Cepeda et al., 2003).

As stated above, dysplastic neurons are a heterogeneous population of pathological cellular elements displaying disrupted morphological features such as aberrant dendritic arbors, reduced number of spines, altered orientation, ectopic location, abnormal distribution of neurofilaments, and changes in soma size (Duong et al., 1994; Cepeda et al., 2003; Mühlebner et al., 2014). Dendrites of dysplastic neurons with enlarged somata may be tortuous and slightly shorter with branching reported to be decreased (Cepeda et al., 2003) or increased (Rossini et al., 2021), with abnormal apical and basal organization. Dendritic arbors of dysplastic neurons with normal soma size exhibit a dramatic simplification of dendritic branching complexity (Rossini et al., 2021). It has been shown that dysplastic neurons express cytoskeletal, layer-specific, and neurochemical markers found in normal pyramidal neurons, suggesting that they originated from neuronal progenitors during cortical development (Lamparello et al., 2007; Blümcke et al., 2011).

In addition, they may also express cytoskeletal regulatory proteins that are markers of cellular immaturity, indicating a mixed developmental phenotype and pointing to a failure in proper morphological maturation (Crino et al., 1997; Taylor et al., 2001; Boer et al., 2009; Hanai et al., 2010).

Dysplastic neurons are thought to be major contributors to epileptiform dischargers in FCD-IIB and GGs (Abdijadid et al., 2015; Iffland and Crino, 2017; Slegers and Blumcke, 2020). A recent publication found that phase-amplitude coupling, spikes, ripples, and seizure onset are related to the density of dysplastic neurons in human FCD-IIB (Rampp et al., 2021). Similarly, in-vitro electrophysiological recordings from dysplastic neurons within human FCDs revealed an increase in macroscopic Ca^{2+} currents and Ca^{2+} influx accompanied by a reduced sensitivity to Mg^{2+}, which may lead to hyperexcitability (Cepeda et al., 2003; André et al., 2004). In addition, dysplastic neurons exhibit an increased expression of N-Methyl-d-aspartic acid (NMDA; NR2A/B, NR2B, and NR1) and α-amino-3-hydroxy-5-methyl-4-isoxazolepropionic acid (AMPA; GluA2/3) glutamatergic receptor subunits, as well as Nav1.3 voltage-gated Na^{+} channel subunit (Babb et al., 1998; Ying et al., 1999, 2004; Najm et al., 2000; Roesler et al., 2001; Yamanouchi, 2005; Yu et al., 2012). The fact that dysplastic neurons display an abnormal expression of neurotransmitter and Cl^{-} transporters that are characteristics of immature neurons, indicates that these neurons possess electrophysiological properties of underdeveloped neurons (including depolarizing responses to GABAergic inputs) that contribute to their increased excitability phenotype (Möddel et al., 2005; Talos et al., 2012).

Increasing evidence has suggested that the abnormal activation of the mechanistic target of rapamycin (mTOR) pathway may be a common cause for the cytoarchitectural alterations observed in developmental brain lesions, including not only FCDs and GGs but also tuberous sclerosis and hemimegalencephaly (Crino, 2015b; Majolo et al., 2018; Mühlebner et al., 2019). mTOR pathway modulates cellular migration, mobility, proliferation, growth, and death, playing a crucial role during normal cortical development (Crino, 2015b; Mühlebner et al., 2019). Morphologically altered elements (including dysplastic neurons) show an enhanced mTOR activation in FCD-IIB and GGs (Baybis et al., 2004; Miyata et al., 2004; Ljungberg et al., 2006; Samadani et al., 2007; Boer et al., 2010). Consistently, somatic and germline mutations that result in the hyperactivation of

the mTOR pathway have been described in patients with FCD-IIB and GG (Schick et al., 2006; Dougherty et al., 2010; Prabowo et al., 2014; Lim et al., 2015, 2017; Nakashima et al., 2015; Møller et al., 2016; Ehrstedt et al., 2020). These findings have led to the classification of these disorders as ‘mTORpathies’, and to the association of the mTOR aberrant activation with developmental malformations and refractory seizures (Curatolo et al., 2018; Iffland et al., 2019).

More recently, somatic gene modifications generated in mice using in utero electroporation (IUE) have been used to prove the casual relationship between the mTOR pathway, dysplastic neurons, and epileptic seizures. Genetic alterations that lead to the hyperactivation of mTOR are sufficient to generate neurons with aberrant morphology and cortical dyslamination, hallmark features of FCD-IIB (Lim et al., 2015, 2017; Park et al., 2018). These dysplastic neurons showed a decrease in threshold and an increase in the firing rates of action potentials (Williams et al., 2015; Ribierre et al., 2018). More importantly, the presence of IUE-targeted neurons displaying morphological alterations leads to spontaneous behavioral seizures that occur independently from cortical dyslamination and that can be prevented using mTOR inhibitors (Lim et al., 2015, 2017; Hsieh et al., 2016; Park et al., 2018; Ribierre et al., 2018). Similarly, the induction of the somatic BRAFV600E mutation in cortical neurons (which enhances mTOR signaling and has been detected in GGs), triggers the emergence of dysmorphic and hyperexcitable phenotypes in cortical neurons that are accompanied by generalized tonic-clonic seizures (Faustino et al., 2012; Koh et al., 2018; Goz et al., 2020; Slegers and Blumcke, 2020).

Brain somatic mutations of mTOR and/or other pathways occurring in subpopulations of cells during brain development are thought to cause the cellular mosaicism and the focal nature of developmental brain lesions (Lee, 2016; Marsan and Baulac, 2018). Nonetheless, is it still unknown how specific changes in similar molecular pathways are able to generate the heterogeneous features of each specific focal epileptogenic lesion and the diversity of morphological altered cellular elements. In addition, even though dysplastic neurons are a common feature in some of these disorders, the exact molecular mechanisms underlying their emergence and hyperexcitability remain largely unknown.

1.4 Cortical development

1.4.1 Cell proliferation and migration

The development of the nervous system is an intricate but organized process that originates from the folding of the ectoderm to form the neuronal tube, followed by a series of orchestrated stages encompassing massive neurogenesis, migration, and complex architectural organization (Jiang and Nardelli, 2016). Specifically, the cerebral cortex arises from the most rostral area of the neuronal tube, which consists of a single cell layer of highly polarized neuroepithelial cells (NEC) (Fernández et al., 2016; Quezada et al., 2018). These cells extend their processes throughout the cortical wall, stretching from the ventricular zone (VZ) surface to the outer pial lamina. NCEs exclusively undergo symmetric divisions, where each progenitor generates two daughter cells and therefore exponentially increase their population size (**Fig. 2**) (Fernández et al., 2016). Since all neuronal progenitors eventually originate from NCEs, their pool size is fundamental to determine the final magnitude of the mature cortex (Rakic, 2009).

Prior to neurogenesis, NCECs become apical radial glial cells (aRGCs) and begin to express the transcription factor Pax6 and glial markers (Asami et al., 2011). aRGCs display apical-basal polarity and undergo symmetric division as observed in NCEs (Fernández et al., 2016). However, aRGCs progressively start dividing asymmetrically, generating another aRGC and either one neuron or one intermediate progenitor cell (IPC) which then gives rise to two neurons (indirect neurogenesis) in a self-consuming division (Noctor et al., 2004). IPCs reside and divide in the subventricular zone (SVZ), a secondary proliferative layer superficial to the VZ. During the last stages of neurogenesis, aRGCs go through terminal symmetric division, ultimately generating two neurons (**Fig. 2**). Asymmetric and indirect neurogenesis increases markedly as new cells are formed, and is viewed as a key process that amplifies the production of cortical neurons during the formation of the brain cortex (Jiang and Nardelli, 2016). Decreased or increased proliferation at this stage may result in microcephaly or megalencephaly, while abnormal proliferation or dysgenesis can trigger the emergence of neurons with altered morphology (Severino et al., 2020).

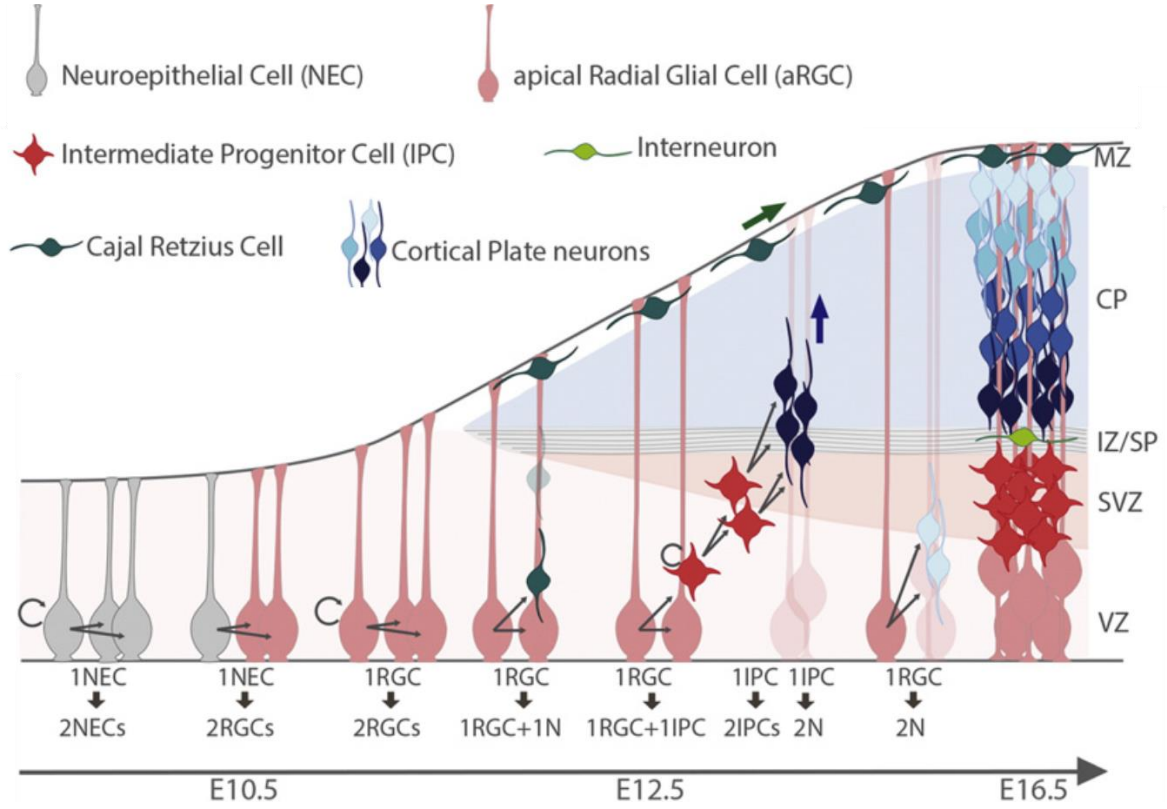

Figure 2. Development of the mouse cortex. At early developmental stages, neuroepithelial cells (NECs, grey) increase their size population by undergoing symmetric division, which later generate apical radial glial cells (aRGCs, pink) that face either symmetrical mitosis to self-renew, or asymmetrical mitosis to give rise to neurons (direct neurogenesis). aRGCs may also generate intermediate progenitor cells (IPC, red) which occupy the subventricular zone (SVZ) and generate cortical layer neurons (indirect neurogenesis). Cortical neurons (blue) migrate alongside the processes of aRGCs through the intermediate zone or subplate (IZ/SP) in the direction of their layer of destination. Modified from Jiang and Nardelli, 2016.

As neurogenesis continues in the VZ and SVZ, newborn neurons migrate radially towards the cortical surface, forming the cortical layers in an inside-out pattern (Rakic, 1972). Radial glial fibers, which extent perpendicularly between the VZ and the cortical pial surface, work as primary scaffolds and provide the necessary substrate for migrating neurons, defining their trajectory and final location along the developing cortical plate (**Fig. 2**) (Casanova and Trippe, 2006; Fernández et al., 2016). During this process, migrating neurons display a series of cytoskeletal rearrangements that shape them into a multipolar morphology when leaving the SVZ, and subsequently to a bipolar phenotype featuring leading and trailing processes, both alterations regulated by a complex interaction between intrinsic and extrinsic cues (Marín et al., 2006).

Radial inside-out migration patterns lead to the formation of columnar, radial units within the laminated cortex. This type of migration is mostly carried out by excitatory projection neurons that ultimately create the six layers of the cortex. In contrast, GABAergic interneurons generated within the ganglionic eminences migrate tangentially (parallel to the pial surface and perpendicular to the radial glial fibers) over longer distances to finally integrate into their cortical layer of destination (Barber and Pierani, 2016). Glial cells, cortical constituents crucial to maintain the homeostasis of mature brain circuits, originate from the same progenitors that give rise to neurons in the VZ. However, gliogenesis starts at a late embryonic stage, being rodent cortical astrocytes firstly detected around E16 and oligodendrocytes around birth, in contrast to neuron proliferation that starts at about E12 (Rowitch, 2004; Rowitch and Kriegstein, 2010). Incomplete neuronal migration may result in the accumulation of neurons near the VZ or ectopically located across cortical layers, generating heterotopias, lissencephaly, and dysgyria, In contrast, cortical over-migration result in polymicrogyria and cobblestone malformations (Severino et al., 2020).

1.4.2 Neurite extension and synaptogenesis

During or shortly after neuronal migration, cortical cells begin a process of terminal differentiation that includes soma size increase, axonal/dendritic outgrowth and branching, development of spines and boutons, and formation/maturation of synapses. This process is also fundamental to define the final dimension of the cerebral cortex since it influences cell size and neuropile volume. Neuronal morphological changes continue after birth, as synapses and neuronal connections show activity-dependent alterations induced by interactions with the environment (Fernández et al., 2016).

Axonal and dendritic branching starts with the initial formation of short processes called neurites. One of the neurites rapidly elongates and becomes the future axon, which is guided by attractive and repulsive environmental chemical cues (Tessier-Lavigne and Goodman, 1996). Cell-surface adhesion molecules and extracellular matrix components participate in the process of retracting or elongating the growth cone (the growing axon's tip) into the proper direction towards its synaptic target (Dickson, 2002; Kolodkin and Tessier-Lavigne, 2011). This cue-mediated guidance triggers architectural changes of the cytoskeleton, in which actin filaments and microtubules dynamically assemble and disassemble causing neurite elongation and movement (Witte and Bradke, 2008).

Neurites that start growing later acquire dendritic branch characteristics, showing mix-orientated microtubules associated with the microtubule-associated protein 2 (MAP 2), in contrast to axons that show uniformly oriented microtubules complemented with tau proteins (Baas et al., 1988). The patterns of axonal and dendritic arborization in different neurons are tightly regulated by cytoskeleton remodeling, cell surface receptors, and the expression levels of key proteins, which lead to the distinctive morphologies observed among different neuronal subclasses (Grueber et al., 2003; Parrish et al., 2006).

Once a growing tip reaches its final target, it becomes a presynaptic axon terminal. Presynaptic compartments develop active zones in which structural proteins such as synapsins, rim, and SNARE complex, help to dock, fuse and release neurotransmitter-filled synaptic vesicles (Ziv and Garner, 2004; Sigrist and Schmitz, 2011). Cell-surface molecules mediate the alignment of presynaptic axon terminals with postsynaptic membrane regions where excitatory or inhibitory neurotransmitter receptors are enriched (Li and Sheng, 2003). Excitatory postsynapses reside on actin-rich dendritic spines and contain large numbers of glutamate receptors stabilized by scaffold proteins such as the postsynaptic density protein 95 (PSD-95), homer, and shank (Jiang and Nardelli, 2016). In contrast, inhibitory postsynapses are established onto dendritic shafts, the axon or soma, and cluster $GABA_A$ receptors through the scaffold protein gephyrin (Tyagarajan and Fritschy, 2014). These presynaptic and postsynaptic structures undergo structural and functional maturation, showing changes in the type and subunit composition of neurotransmitter receptors and voltage-gated channels over time (Ziv and Garner, 2004; Ethell and Pasquale, 2005).

The formation and stabilization of new synapses are influenced by spontaneous activity patterns in the embryo and continues in the postnatal period when interactions with the environment and learning lead to activity-dependent changes (Momose-Sato and Sato, 2013; Makino et al., 2016). Unused or weak synapses are eliminated to enable the strengthening of more efficient connections, a process called pruning. In humans, synaptic pruning continues for about 15 years after birth, during which nearly 50% of all formed synapses are removed. Stablished synapses require continuous maintenance to remain functional. This process guarantees fine-tuned neuronal circuitries that are required to

support general brain function, cognition, and behavior (Hashimoto and Kano, 2013; Jiang and Nardelli, 2016).

1.5 Cortical circuits

The cortex participates in most ethologically relevant brain functions such as sensory perception, execution of motor commands, learning, and memory (Feldmeyer et al., 2013; Li et al., 2015). Each cortical area is formed by a densely interconnected array of neuronal networks, whose cell diversity and sophisticated connectivity patterns define its capacity to process and integrate information (Harris and Mrsic-flogel, 2013). The neuronal computations required to support sensory coding and goal-directed behavior are not restricted to a specific cortical circuit, but instead involve the interconnection of different cortical regions and subcortical structures across the brain (Feldmeyer et al., 2018).

Due to the large diversity of sensory signals and association processes that take place in the cortex, specialized cortical areas display unique network features to assist in the processing of particular patterns of information (Harris and Mrsic-flogel, 2013; Adesnik and Naka, 2018). Nonetheless, the circuits of different cortical regions and mammalian species display prominent similarities in the cell types they expressed, their intrinsic properties, and in the synaptic connections between them (Douglas and Martin, 2004; Harris and Mrsic-flogel, 2013). For this reason, in the following sections we will focus on the general principles of circuitry architecture and information processing commonly observed across cortical areas.

Horizontal lamination and vertical interconnected columns are the structural hallmarks of the cortex. Six layers are generally distinguished, with excitatory and inhibitory neurons occupying specific layers and with distinctive input-output connections (Harris and Shepherd, 2015). Cortical columns are considered the basic modules of cortical processing, each one spanning 200–600 μm in diameter and containing several thousand neurons depending on area and species (Lübke and Feldmeyer, 2007; Feldmeyer et al., 2013, 2018). Local connections within a column are formed between cells of the same layer or stretching across the cortex vertically in characteristic pathways. Furthermore, columns receive and send inputs from and to other columns, different cortical areas, and subcortical structures (Feldmeyer et al., 2018). This modular concept presumes that a

cortical column executes basic signal processing, which is then integrated with the activity of other neuronal networks (Lübke and Feldmeyer, 2007).

1.5.1 Cortical excitatory neurons

Cortical neurons are divided into two major classes, excitatory and inhibitory neurons. Principal excitatory neurons, which release L-glutamate as neurotransmitter, comprise approximately 80% or more of all neurons in the cortex. Cortical excitatory neurons mostly consist of pyramidal cells and their variants, characterized by a pyramidal soma, complex dendritic arborization, and a single axon that emanates from the base of the soma and branches locally and distally (Spruston, 2008; Wang et al., 2018b). Pyramidal neurons display relatively short basal dendrites and a long apical dendrite that bifurcates and gives rise to tuft dendrites. These distinctive dendritic domains play an important role in the computational properties of pyramidal neurons. Proximal dendrites receive inputs mostly from local excitatory sources, while distal apical dendrites are targeted by excitatory inputs from more distal areas, where an interplay of coincident inputs along dendrites might control the overall responsiveness of neurons and cooperate to generate supra-threshold responses (Larkum et al., 2004; Spruston, 2008). On the other hand, although most inhibitory inputs reach pyramidal neurons at the soma and axon, distinct populations of inhibitory cells target specific cellular compartments of pyramidal neurons. This targeted inhibition causes that some GABAergic interneurons act by reducing the probability of firing an action potential close the initiation site while others regulate non-linear events and control the integration of glutamatergic inputs at distal dendrites (Tremblay et al., 2016; Cardin, 2018).

Cortical excitatory neurons can be subdivided based on their axonal projection patterns. Intratelencephalic principal neurons are located in layers 2-6 and project only within the telencephalon (including the cortex), being responsible for most of the vertical communication within columns. Pyramidal tract neurons are thick tufted depolarized neurons residing in layer 5B that project to subcerebral destinations, in addition to the ipsilateral cortex, striatum, and thalamus. Finally, corticothalamic neurons of layer 6 send connections mainly to the ipsilateral thalamus and show sparse coding capabilities (Harris and Shepherd, 2015).

The morphophysiological features of cortical excitatory neurons can vastly vary within their axonal projection subclass. For example, layer 4 intratelencephalic neurons can be regular or fast-spiking and show rapid sensory responses in vivo (Arkhipov et al., 2018; Scala et al., 2019). In contrast, intratelencephalic neurons from layers L2/3 are known for encoding information sparsely and for their low spontaneous and evoked firing rates in awake animals (Adesnik and Scanziani, 2010; Mateo et al., 2011). These diverse intrinsic and synaptic characteristics are key to properly manage information flowing through multiple entries and exit points, and provide cortical networks with their sophisticated computational properties.

1.5.2 Inhibitory cortical neurons

The second major class of cortical constituents are inhibitory neurons, which utilize the derivate of glutamate GABA as main neurotransmitter. GABAergic cells (also called interneurons due to the restraint location of their axons within local networks), are responsible for regulating information flow and shaping the dynamics of cortical circuits (Tremblay et al., 2016; Feldmeyer et al., 2018). The activity of interneurons is crucial to modulate the temporal precision of pyramidal cell firing, sensory feature selectivity in sensory areas, plasticity network changes, neuronal synchronization, and generation of cortical rhythms (Muñoz and Rudy, 2014; Tremblay et al., 2016; Cardin, 2018). In addition, interneurons assure the maintenance of the excitatory and inhibitory balance necessary for proper information processing while avoiding network hyperexcitation (Paz and Huguenard, 2015).

To maximize flexibility and shape network dynamics in a large variety of input signals and connectivity features, the cortex relies on the existence of a large diversity of GABAergic interneurons. These inhibitory cells exhibit extraordinary variations in their morphology, intrinsic membrane properties, and connectivity, which can have tremendous consequences on their cellular and network functional capabilities (Markram et al., 2004; Ascoli et al., 2008). Although there is still no clear agreement on a precise taxonomical framework for their classification, it is widely accepted the existence of three broad non-overlapping interneuron subpopulations characterized by the expression of specific molecular markers (Zeisel et al., 2015; Tasic et al., 2016). These subpopulations express either the calcium-binding protein parvalbumin (PV), the neuropeptide somatostatin

(SST), or the ionotropic serotonin receptor 5HT3a (5HT3aR), which account for nearly 100% of all GAD-67 mRNA-expressing neurons in the somatosensory cortex (Lee et al., 2010). Each of these groups shows strong functional and genetic similarities that are exclusive or not as prominent in other groups (Zeisel et al., 2015; Tasic et al., 2016), suggesting that the expression of these markers is a good starting point for hierarchical classification of interneurons. Due to the relevance to this project, in this section we will mostly focus on the molecular and functional features of PV and SST interneurons.

The most abundant type of inhibitory cells in the cortex are PV-expressing interneurons (around 40%), which include perisomatic-targeting basket cells and axo-axonic chandelier cells (Hu et al., 2014). These inhibitory neurons are distributed across cortical layers 2-6, being basket cells preferentially located in layer 4 and chandelier cells in layers 2 and 6 (Karube et al., 2004; Taniguchi et al., 2013). PV interneurons are strongly innervated by thalamic afferents from which they receive depressing excitatory postsynaptic potentials (EPSPs) (Beierlein et al., 2003; Cruikshank et al., 2007; Sermet et al., 2019). After activation, PV cells display fast-spiking properties that allow them to trigger reliable, robust, and temporally precise hyperpolarization and/or shunting inhibition close to where action potentials are generated in local neurons (Gibson et al., 1999; Thomson and Lamy, 2007; Goldberg et al., 2011; Rossignol et al., 2013; Tremblay et al., 2016). The inhibitory postsynaptic potentials (IPSPs) from PV neurons are initially very strong and then depress rapidly, which precisely narrows the window for temporal summation of EPSPs and thus impeding action potential generation (Galarreta and Hestrin, 1999; Beierlein et al., 2000; Pouille and Scanziani, 2001; Hu et al., 2014). This remarkable fast and timely precise inhibition is assured through a series of molecular and cellular specializations observed in PV cells. Among them, it can be mentioned the expression of fast Ca^{2+} permeable AMPA receptors (Hull et al., 2009), low input resistance and very fast time constant (Goldberg et al., 2011), expression of K^+ channels specialized for rapid repolarization (Erisir et al., 1999), expression of voltage-gated Na^+ channels with slower inactivation and faster recovery (Martina and Jonas, 1997), and expression of fast presynaptic Ca^{2+} channels that produce reliable GABA release (Zaitsev et al., 2007).

The millisecond time-scaled, precise inhibition carried out by PV interneurons is able to tightly constrain the initial component of sensory information arriving to the cortex,

(Panzeri et al., 2001; Pouille and Scanziani, 2001; Cardin, 2018; Resulaj et al., 2018). In addition, their robust reciprocal synaptic interconnectivity (via chemical and electrical synapses) and with nearby excitatory neurons allow them to synchronize and orchestrate network oscillations that have been linked to higher brain functions (Gibson et al., 1999; Tamás et al., 2000). In vivo recordings coupled to optogenetic stimulation in the somatosensory cortex have shown that PV-expressing interneurons have a critical role in the generation and maintenance of gamma oscillations (30–80 Hz), a range of frequencies thought to enhance information processing and cognition (Cardin et al., 2009; Sohal et al., 2009; Stark et al., 2013). Moreover, PV interneurons' firing frequency increases during running and exploratory behavior (Polack et al., 2013; Kim et al., 2016a), and its activity regulates the gain of sensory responses (Cardin et al., 2009; Atallah et al., 2012; Lee et al., 2012; Wilson et al., 2012; Agetsuma et al., 2018) and certain forms of learning (Yazaki-Sugiyama et al., 2009; Letzkus et al., 2011; Donato et al., 2013). These experiments in awake animals have revealed that the fast-spiking properties and synchronized activity of PV interneurons are required to enhance signal processing in the cortex, and to modulate network oscillations coupled to behavioral states (Cardin, 2018; Ferguson and Gao, 2018a).

SST expressing cells constitute a second major class of interneurons, representing around 30% of all GABAergic cells in the cortex (Yavorska and Wehr, 2016). In terms of morphology, SST interneurons can be divided into two broad classes: Martinotti and non-Martinotti cells. Martinotti cells (layers 2/3 and 5/6) represent the larger fraction of SST interneurons, which commonly show spindle or ovoid-shaped somata with dense axonal ramifications (Wang et al., 2004; Ma et al., 2006; Riedemann et al., 2018). On the other hand, non-Martinotti interneurons comprise a more heterogeneous population, including basket cells (layer 4), double-bouquet cells (layers 2-5), and long-range GABAergic projection cells (layer 6) (Riedemann, 2019).

Despite their high degree of morphological variability, SST interneurons can be characterized by their more depolarized membrane potential, higher input resistance, shorter membrane time constant, and slower spike kinetics (regular, low threshold, or burst spiking) compared to fast-spiking cells (Kawaguchi and Kubota, 1996; Bacci et al., 2003; Riedemann et al., 2018). In addition, excitatory inputs onto SST interneurons are

strongly facilitating (Beierlein et al., 2003; Kapfer et al., 2007). These excitatory inputs seem to come mostly from neighboring excitatory cells, in which the stimulation of a single layer 2/3 pyramidal neuron can activate up to 30% of SST interneurons within its microcircuit (Kwan and Dan, 2012; Naka et al., 2019). Given their relatively high input resistance, depolarized membrane potential, and EPSP summation from their facilitating synapses, SST cells show supralinear responses that make them much more excitable compared to fast-spiking interneurons (Beierlein et al., 2003; Fanselow et al., 2008). Therefore, a single high-frequency input can recruit SST neurons and produce strong feedback inhibition, in contrast to PV cells that require the synchronous firing of pre-synaptic neurons due to their strongly depressing excitatory synapses (Kapfer et al., 2007; Silberberg and Markram, 2007; Tremblay et al., 2016).

SST cells preferentially target the dendrites of layer 2/3 and 5/6 pyramidal neurons. Their axons target the basal dendrites of local excitatory neurons or project vertically up to layer 1 where they spread horizontally and target tuft dendrites (Ma et al., 2006; Riedemann, 2019). SST interneuron-mediated IPSPs onto distal dendrites have weak facilitating properties that progressively attenuate due to the cable properties of the postsynaptic cells. Therefore, inhibition triggered by SST interneurons is more effective locally at the targeted dendrite, where it regulates non-linear events such as Ca^{2+} spikes and controls the efficacy and integration of glutamatergic inputs (Tremblay et al., 2016; Yavorska and Wehr, 2016). This dendritic-targeted inhibition tends to be weak when the cortex shows low neuronal activity, but becomes robust at higher frequencies and therefore regulates neuronal responses to prolonged excitation (Gibson et al., 1999; Kapfer et al., 2007; Murayama et al., 2009).

Cell-type-specific optogenetic experiments in behaving animals have identified dendritic-targeting SST interneurons as regulators of visual-induced beta/low-gamma (20–30 Hz) oscillations in the neocortex (Chen et al., 2017; Veit et al., 2017). SST cells-mediated lateral inhibition produces surround suppression of layer L2/3 visual pyramidal neurons that is critical for the efficient tune and representation of visual stimuli (Adesnik et al., 2012). Moreover, SST interneurons show sensory habituation and learning-dependent potentiation of their synaptic transmission in the auditory and prefrontal cortex (Kato et al., 2015; Natan et al., 2015; Cummings and Clem, 2020). In contrast, the activity of SST

interneurons is reduced during locomotion via dishinbition, being motor learning impaired after their optogenetic activation (Ayaz et al., 2013; Chen et al., 2015; Fu et al., 2015; Adler et al., 2019). Therefore, the activity of SST interneurons has a direct, context-dependent impact on the responsiveness of neuronal networks in behaving animals. This modulation may have a special effect on inputs coming from associative brain areas and higher-order thalamic nuclei, given that SST cells preferentially target the apical dendrites of pyramidal neurons where most of these signals are integrated (Riedemann, 2019).

5HT3aR cells are the third major subpopulation of interneurons in the cortex. These are the most heterogeneous interneuron group and represent around 30% of all GABAergic cells in the cortex (Lee et al., 2010). 5HT3aR cells express functional 5HT3a (the only ionotropic serotonin receptor) which after activation with molecular agonists, produce fast and robust depolarization in all 5HT3aR cells regardless of location and electrophysiological properties (Lee et al., 2010; Rudy et al., 2011). In addition to glutamate and serotonin, cholinergic agonists acting on nicotinic receptors also excite 5HT3aR interneurons (Férézou et al., 2002; Lee et al., 2010). These cells are preferentially located in the upper cortical layers, being the majority of neurons in layer I 5HT3aR positive (Lee et al., 2010). This restricted location in superficial layers where corticocortical and long-distance connections are integrated, in addition to their recruitment by modulatory systems, make 5HT3aR interneurons ideal to mediate converging cortical activity depending on the brain state and behavior context (Fu et al., 2014; Zhang et al., 2014; Ayzenshtat et al., 2016; Nelson and Mooney, 2016; Wood et al., 2017).

Vasointestinal peptide-expressing (Vip) interneurons comprise the best-characterized 5HT3aR cell subtype, which features vertically-oriented bipolar or multipolar cells located mainly in layers 2-3 (Tremblay et al., 2016). Vip interneurons are known to trigger potent dishinbition in cortical networks, preferentially forming synapses onto dendritic-targeting SST inhibitory cells (Lee et al., 2013; Pfeffer et al., 2013; Pi et al., 2013). Feedback connection from high-order cortical areas such as motor cortex and cingulate cortex, efficiently recruit Vip neurons that then inhibit local SST cells, allowing the dendrites of pyramidal cells to be dishinbited and more likely to integrate excitatory inputs from these areas (Lee et al., 2013; Zhang et al., 2014). This dishinbition network can be observed in

behaving animals, where the activity of Vip cells increases during whisking while the activation of SST cells is reduced, showing opposite effects during quiescence (Gentet et al., 2012; Lee et al., 2013).

1.5.3 Circuit motifs of the cortex

While the intrinsic characteristics of cortical neurons influence how synaptic inputs are processed by neuronal units, the connectivity features of neuronal microcircuits dictate how incoming information is initially filtered and processed before being integrated into larger neuronal networks. The main connectivity motifs in which cortical excitatory and inhibitory cells are embedded are the so-called feedforward and feedback circuits. Feedforward excitation and inhibition occur when excitatory inputs from external brain regions recruit local networks. In contrast, in a feedback motif, local principal cells provide recurrent excitatory inputs onto excitatory and inhibitory neurons of the same network. It is important to note that these microcircuit motifs coexist in probably all cortical neurons; however, certain cellular subtypes exhibit a more potent role in one motif over another (Paz and Huguenard, 2015; Tremblay et al., 2016; Feldmeyer et al., 2018).

1.5.3.1 Feedforward circuits

Incoming sensory and motor information traveling from the thalamus represents the major source of feedforward inputs to the cortex. These signals are processed in a canonical top-bottom vertical pathway, through the sequential flow of information across a cortical column (**Fig. 3A**). Glutamatergic axons from motor and sensory thalamic nuclei target virtually all cortical layers but show their highest density in layer 4, which is considered to be the mayor and dominant input layer of the cortex (Petreanu et al., 2009; Wimmer et al., 2010; Oberlaender et al., 2012; Hunnicutt et al., 2014). The thalamus also innervates considerably layer 1, mostly sending contextual information from high order nuclei (Hunnicutt et al., 2014). These feedforward thalamic inputs strongly depolarize layer 4 excitatory pyramidal and spiny stellate cells, whose electrophysiological features and coding strategies do not seem to differ from each other (Brecht and Sakmann, 2002). Layer 4 cells spread thalamic excitation to other cortical layers, with preferential synaptic output onto the basal dendrites of layer 2/3 neurons and neighboring cells in their home layer (Lefort et al., 2009; Feldmeyer, 2012; Harris and Shepherd, 2015). Next, Layer 2/3

neurons project vertically to deeper layers in their home column, mainly to layers 5A and 5B, and horizontally across the same layer (Hardingham et al., 2010; Feldmeyer, 2012). Once thalamic information reaches layer 5, activity flows toward the local 2/3 layer or distally to higher-order cortices and thalamic nuclei. This way, layer 5 excitatory neurons accumulate and distribute arriving feedforward information of an entire column, which is later integrated with signals from different columns and other sensory and motor areas (Feldmeyer, 2012; Feldmeyer et al., 2013; Harris and Shepherd, 2015).

In contrast to feedforward excitation in which external excitatory inputs directly target local principal cells, in feedforward inhibitory circuits afferent excitatory axons synapse onto local interneurons, which subsequently provide disynaptic inhibition to principal cells. Thalamocortical axons preferentially recruit fast-spiking PV cells over other subtypes of cortical interneurons (**Fig. 3B**) (Pala and Petersen, 2018), with faster and stronger connections than those made onto pyramidal neurons (Inoue and Imoto, 2006; Cruikshank et al., 2007). Given its disynaptic nature, cortical feedforward inhibition reaches pyramidal neurons after monosynaptic feedforward excitation. Nonetheless, due to the specialized synaptic (**Fig. 3C**) and intrinsic properties of PV interneurons (see above), this delay is only about 1-2 ms, producing a limited time window for feedforward excitatory inputs to summate and evoke an output on the postsynaptic cell (Pinto et al., 2000; Alonso and Swadlow, 2005). As a result, feedforward inhibition participates in feature selectivity by suppressing slow and asynchronous thalamic activity and by constraining strong sensory information that arrives in the cortex (Tremblay et al., 2016). This tight inhibitory regulation guarantees the maintenance of cortical network stability since failures in proper feedforward inhibition have been linked to the development of hyperexcitability and seizures (Sun et al., 2005; Sasaki et al., 2006; Maheshwari et al., 2013).

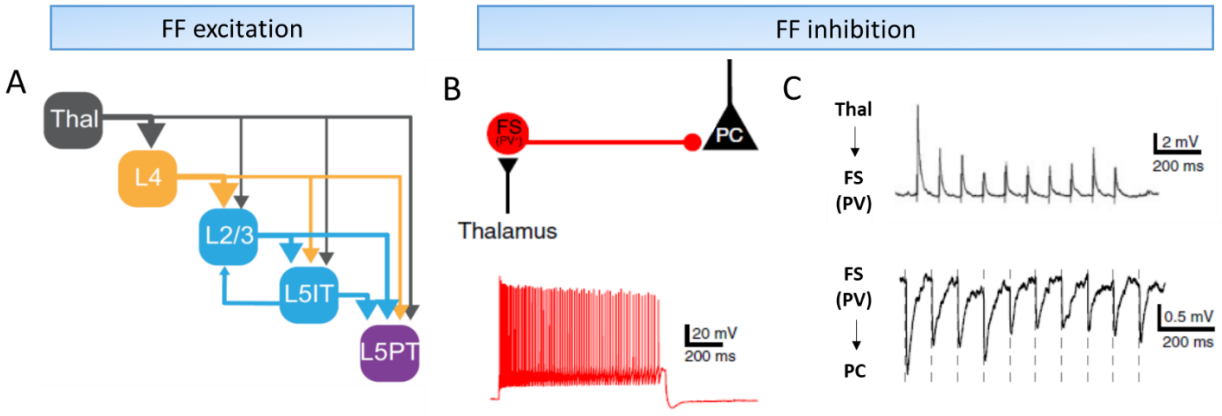

Figure 3. Feedforward circuits in the cortex. A, Excitatory feedforward connectivity in the cortex occurs through the sequential flow across cortical layers of information arriving from the thalamus. B, Cortical feedforward inhibition occurs when thalamic inputs activate local interneurons (preferentially fast-spiking PV interneurons) which then inhibit pyramidal cells. C, PV interneurons receive initially strong inputs from the thalamus that quickly depress over time. Similarly, they produce robust depressing inhibitory potentials in neighboring pyramidal cells that narrow their window for temporal summation of EPSPs. Feedforward (FF), thalamus (thal), fast-spiking (FS), pyramidal cells (PC). Modified from Adesnik and Naka, 2018 (A) and Feldmeyer et al., 2018 (B, C).

1.5.3.2 Feedback circuits

In contrast to feedforward circuitry, feedback excitation and inhibition occur when local principal cells activate neighboring neuronal elements (**Fig. 4A**). Most synapses in the cortex are formed between local excitatory neurons, which frequently feedback to its source creating recurrent interconnected networks (Douglas et al., 1995; Miller, 2016). Local recurrent connections between excitatory cells are overrepresented in the cortex, occurring more frequently than expected by chance, and being more common between principal cells that receive common inputs (Yoshimura et al., 2005; Otsuka and Kawaguchi, 2011). Hence, interconnected subnetworks in sensory cortices are heavily composed of groups of neurons that are tuned for similar sensory features (Harris and Mrsic-flogel, 2013). This is greatly beneficial for sensory processing since local recurrent excitation is able to increase the number of neurons recruited by an incoming thalamic input, which in turn amplifies cortical responses to peripheral sensory signals (Li et al., 2013a, 2013b; Lien and Scanziani, 2013; Peron et al., 2020). In addition, feedback loops between local excitatory cells prolong cortical responses to sensory information, allowing short stimuli to be maintained in time to interact with succeeding inputs or contextual

information arriving from other cortical areas (Douglas and Martin, 2004; Harris and Mrsic-flogel, 2013).

In addition to local recurrent connections between excitatory neurons, feedback interactions can also be observed between different cortical areas. Sensory inputs leaving primary sensory cortices are forwarded to secondary sensory, motor, and associative areas that in turn can project back carrying information about the state of the whole sensory circuitry (Harris and Mrsic-flogel, 2013; Pennartz et al., 2019). These cortico-cortical connections arrive mainly to superficial layers, where they activate the apical tuft dendrites of principal cells and interneurons. Feedback inputs are not able to reliably recruit principal cells, but rather increase their overall gain to excitatory inputs by the generation of dendritic calcium spikes (Larkum et al., 1999, 2004). Therefore, feedback inputs between cortical areas amplify sensory and motor responses and modulate their activity by integrating contextual information coming from other cortical areas (Shuler and Bear, 2006; Reynolds and Heeger, 2009).

Feedback inhibition is recruited when a principal neuron synapses onto an interneuron, which then synapses back onto the same excitatory cell (recurrent inhibition) or another cell of a similar type (lateral inhibition) (Feldmeyer et al., 2018). This circuit mechanism acts by tracking the local activation of excitatory neurons, in contrast to feedforward inhibition whose action does not depend on local activity level. Therefore, feedback inhibition limits further discharges from excitatory cells and controls the excitatory-inhibitory balance of local neuronal populations (Tremblay et al., 2016). Due to the dense local connectivity of interneurons, feedback inhibition can potently restrain local excitation and create networks with sparse activity (Kapfer et al., 2007; Fino and Yuste, 2011; Barth and Poulet, 2012). Moreover, interneurons can extend their axons and inhibit neighboring populations that might have not provided them with excitation (Tremblay et al., 2016; Feldmeyer et al., 2018). These inhibitory motifs have been associated with the generation of complex neuronal patterns and assemblies such as grid field formation, surround suppression, and oscillatory coupling (Adesnik et al., 2012; Couey et al., 2013; Shao et al., 2013).

Intracortical axons are able to recruit both, PV and SST interneurons. However, due to the differences in their synaptic and intrinsic properties, SST cells appear to be preferentially

activated in cortical feedback inhibitory circuits (**Fig. 4B**) (Silberberg and Markram, 2007; Kwan and Dan, 2012; Paz and Huguenard, 2015; Callaway, 2016). The initially weak but facilitating inputs that SST interneurons receive from principal cells, make these interneurons to be more dependent on the increase in local excitatory firing rates (**Fig. 4C**). EPSPs summation causes that the high-frequency activation of even a single pyramidal cell is capable to recruit SST interneuron-mediated inhibition (Kapfer et al., 2007; Silberberg and Markram, 2007; Kwan and Dan, 2012). In contrast, the depressing synapses of PV interneurons make them more sensitive to synchronized inputs distributed among different excitatory cells (Beierlein et al., 2003; Cruikshank et al., 2007; Sermet et al., 2019). Moreover, feedback connections from other cortical areas and local pyramidal neurons mostly target superficial cortical layers, which has contributed to the hypothesis that SST interneurons might favorably regulate feedback inhibition at the apical tufts of principal neurons (Callaway, 2016). Thus, feedback activation of SST interneurons might work as a burst and rate detector over longer timescales, preventing over excitation by generating inhibitory outputs proportional to the magnitude of the excitatory state of the network (Kwan and Dan, 2012; Tremblay et al., 2016).

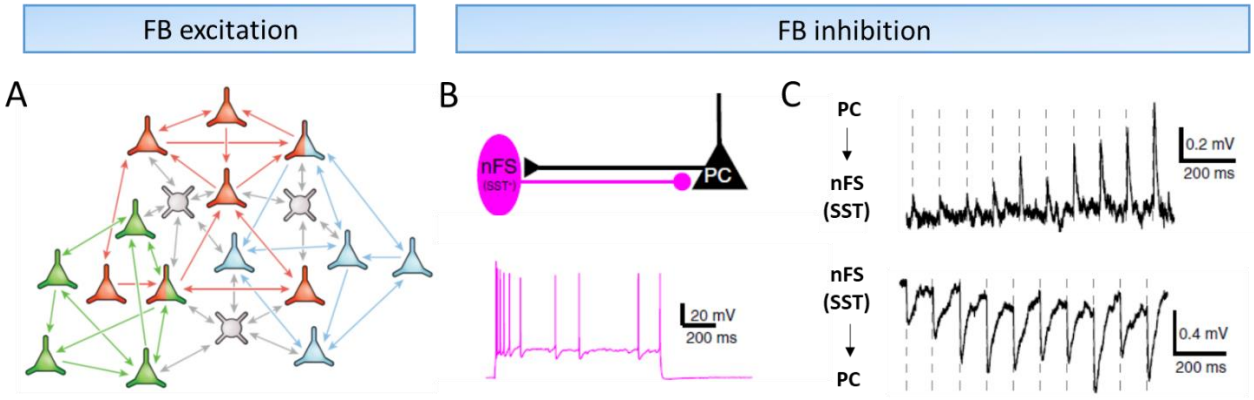

Figure 4. Feedback circuits in the cortex. A, Cortical networks display subpopulations of highly interconnected pyramidal cells (each color represents a subpopulation) where recurrent excitation occurs. Not all neurons of a subpopulation are connected, and any neuron can be part of more than one subnetwork (striped triangles). B, Cortical feedback inhibition occurs when pyramidal cells activate local interneurons (preferentially non-fast spiking SST interneurons) which then synapse back to the pyramidal cell population. C, SST interneurons receive initially weak and gradually facilitating excitatory inputs, which then elicit facilitating (or weakly depressing) inhibitory inputs onto pyramidal cells. Feedback (FB), non-fast spiking (nFS), pyramidal cells (PC). Modified from Adesnik and Naka, 2018 (A) and Harris and Mrsic-Flogel (B, C).

1.6 Ste20-like kinase (SLK)

The Sterile 20 (Ste20) protein family encompasses more than 60 serine/threonine kinases involved in migration, cellular proliferation, and apoptosis (Al-Zahrani et al., 2013). These proteins are characterized by their conserved kinase domain and a structural-variable non-catalytic region that allows them to interact with a diverse group of signaling proteins and regulatory molecules of the cytoskeleton (Dan et al., 2001). Based on their protein structure, Ste20 kinases can be divided into 2 major groups: the p21-activated kinases (PAKs), which regulates the actin cytoskeleton to promote cell motility and survival, and the germinal center kinases (GCKs), which transduce stress signals to trigger cell cycle arrest and apoptosis (Miller et al., 2019).

The Ste20-like kinase (SLK) is a member of the Ste20 family firstly isolated from guinea pig liver with identified homologs in mice and humans (Itoh et al., 1997; Sabourin and Rudnicki, 1999; Yamada et al., 2000). SLK is ubiquitously expressed in mammals and is particularly enriched during embryogenesis in myocytes and neurons, where it may play an important role in muscle and brain development (Zhang et al., 2002). The SLK protein is formed by 1204-1235 amino acids, containing an N-terminal Ste20 catalytic kinase domain and protein interaction (coiled-coil) regions. SLK also contains phosphorylation sites at T183 and S189 and a dimerization domain at the C-terminal region, which have been shown to mediate the activation of its kinase activity (Delarosa et al., 2011; Luhovy et al., 2012; Cybulsky et al., 2017).

The regulation of the catalytic activity of SLK is complex and may involve several molecular mechanisms. mRNA stabilization, dimerization, phosphorylation, and protein-protein interactions are critical to enabling the kinase function of SLK (Cybulsky et al., 2007, 2017; Storbeck et al., 2009; Delarosa et al., 2011; Luhovy et al., 2012). Autophosphorylation, which leads to key posttranslational modifications required for kinase activation (Luhovy et al., 2012; Cybulsky et al., 2017), has been shown to be enabled by protein homodimerization (Pike et al., 2008). Dimerization and autophosphorylation may ease the establishment of a bond between E79 and the ATP binding site, which keeps SLK into an active conformation suitable for substrate binding (Luhovy et al., 2012). Further regulation of SLK activity or cellular localization may be driven by interactions with other proteins, including the LIM domain-binding transcriptional

cofactor proteins (Ldb1 and Ldb2), Tpr, and actinin-4 (Storbeck et al., 2009; Jaberi et al., 2015). LDB1/2 were identified as SLK-binding factors, which reduce SLK kinase activity by stabilizing its auto-inhibitory region in the C-terminal domain (Yan et al., 2007). These observations suggest that the catalytic activity of SLK is under tight regulation and that additional studies are necessary to comprehend its regulatory mechanisms.

SLK has been implicated in a diverse set of physiological processes in different tissues, but its precise roles and functions remain poorly understood. Global deletion of SLK or gene-trap mediated SLK truncation that results in loss of kinase function, lead to severe developmental defects and lethality at around E12-E15, suggesting an important involvement of SLK in embryogenesis (Al-Zahrani et al., 2014; Pryce et al., 2017). In muscle, where it mediates actin polymerization (Wang et al., 2020), deletion of SLK causes alterations in myofiber maintenance and integrity, resulting in a progressive myopathy and delayed muscle regenerative capacity (Pryce et al., 2017). SLK expression and activity in kidney peak at late developmental stages and during the recovery phase from ischemia-reperfusion injury (Cybulsky et al., 2004). Moreover, deletion of SLK in kidney's podocytes results in marked podocyte injury and albuminuria (Cybulsky et al., 2018; Woychyshyn et al., 2020).

It has been shown that SLK mediates apoptosis by taking part in mitogen-activated protein kinase (MAPK)-dependent signaling pathways in fibroblast and myoblast (Sabourin and Rudnicki, 1999). SLK triggers apoptosis by the release of cytochrome c and activation of caspase-8 and -9 via the apoptosis signal-regulating kinase-1 and p38 MAPK (Hao et al., 2006). Furthermore, SLK is needed for proper cell migration and motility, a process in which SLK activation causes disassembly of actin stress fibers, loss of cell adhesion, and relocation of actin to the cell periphery (Wagner et al., 2008; Wagner and Sabourin, 2009). Through the phosphorylation of Rac1 and RhoA, two major regulators of the cytoskeleton dynamics, SLK mediates cytoskeletal reorganization and fiber breakdown (Wagner et al., 2002; Guilluy et al., 2008). In addition, SLK co-localizes with adhesion components and microtubules at the leading edge of migrating cells and is necessary for adhesion turnover after Src kinases activation. Related to this, SLK seems to have an important role in the invasion and progression of certain types of cancer (Roovers et al., 2009; Wang et al., 2018a).

In summary, SLK displays critical roles for cell migration and growth in non-neuronal cells, modifying the cytoskeleton dynamics through a series of complex regulatory mechanisms that depend on the biological context. These characteristics may suggest similar molecular involvement in neurons; however, further studies of this kinase in the nervous system are required to understand its overall biological relevance in mammals.

1.6.1 Role of SLK in dendritic and inhibitory synaptic formation

Schoch and collaborators (2021) found that SLK expression is strongly reduced in dysmorphic neurons of FCD-IIB and GG biopsies from patients with refractory epilepsy. In order to verify a possible role of the loss of SLK in the generation of neurons with altered dendritic morphology, these researchers performed a knockdown of SLK in vivo via delivery of a validated short hairpin RNA (shRNA) for SLK (shSLK) by performing IUEs at E14. SLK knockdown (SLK-KD) caused a subset of neurons to be located ectopically in deeper cortical layers (**Fig. 5A**), suggesting a possible impairment in their migration process. In addition, neurons lacking SLK showed alterations in the complexity of the distal dendritic tree, with a selective reduction in the number of secondary and higher-order dendrites (**Fig. 5B-C**). These effects were not observed when shSLK was delivered by intracortical viral injections in adult animals, indicating that SLK is required for the generation of normal dendritic trees during the development but not for the maintenance of established dendrites (Schoch et al., 2021).

SLK protein expression was detected at high levels in the cell body and dendrites of cultured primary cortical neurons, where it colocalized with the dendritic marker protein MAP-2. Remarkably, SLK showed a high degree of overlap with the scaffold protein of inhibitory synapses gephyrin in dendritic shafts, but was virtually absent in dendritic spines and did not co-localized with PSD-95. These results suggested that the kinase activity of SLK might have a role in regulating the structure of inhibitory synapses. Thus, to examine the effect of SLK loss on the formation of excitatory and inhibitory synapses, quantifications of PSD-95 and gephyrin were performed in SLK-KD neurons. There was no difference in the initial formation of inhibitory postsynapses (P5 and P15) in SLK-KD neurons compared to control cells. However, at P30 and P60 inhibitory postsynapse density displayed a significant decrease (**Fig. 5D-E**). In contrast, no significant alterations in the density of excitatory postsynapses were detected at any time point. This indicates

that SLK is specifically required for the stabilization/maintenance of inhibitory synapses during development in vivo (Schoch et al., 2021).

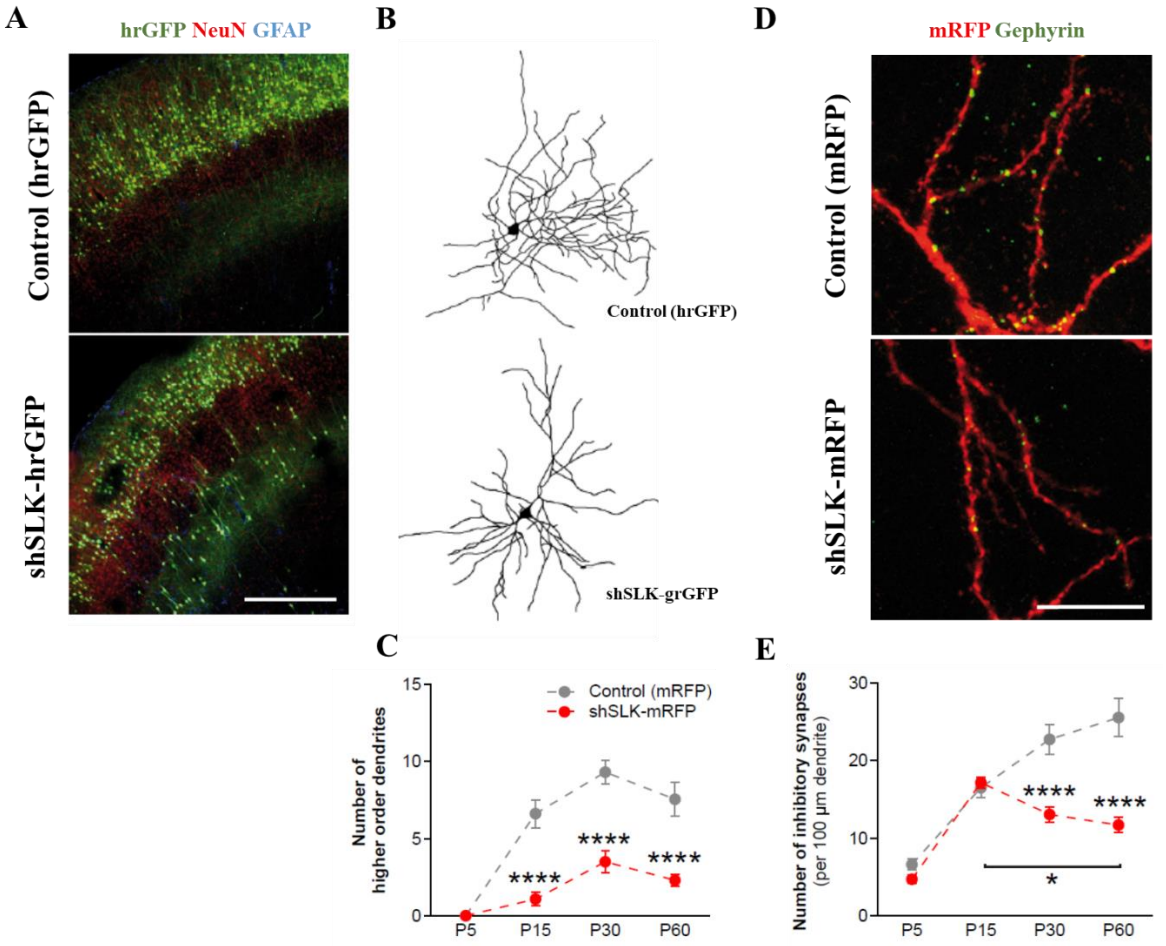

Figure 5. SLK-KD neurons display impaired dendritic arbors and a reduction of inhibitory postsynapses in vivo. A, Immunohistochemical staining against NeuN and glial fibrillary acidic protein (GFAP) in hrGFP (control) or shSLK-hrGFP (SLK-KD) electroporated brain slices, showing ectopic cells located in deeper layers when an SLK-KD was performed; Scale bar 400 µm. B, High magnification images of reconstructed cortical neurons electroporated with either hrGFP or shSLK-hrGFP plasmids. C, Quantification of higher-order dendrites of hrGFP or shSLK-hrGFP electroporated cells, showing that the lack of SLK reduced the number of higher-order dendrites in animals from P15 to P60. D, Representative images of cortical neurons electroporated with gephyrin-GFP-fibronectin intrabodies generated with mRNA display (FingRs) together with mRFP or shSLK-mRFP; Scale bar 100 µm. E, Inhibitory synapse density quantifications at P5, P15, P30, and P60 revealed no differences at P5 and P15 but a significant reduction at P30 and P60 in shSLK-mRFP electroporated neurons when compared to mRFP electroporated cells. Modified from Schoch et al., 2021.

Electrophysiological recordings in acute slices showed a marked reduction in miniature inhibitory postsynaptic current (mIPSC) frequency but no corresponding change in miniature excitatory postsynaptic current (mEPSC) frequency, indicating a profoundly disrupted balance between inhibition and excitation. In addition, the cell capacitance of SLK-KD neurons was significantly reduced, consistent with a smaller dendritic arbor. Finally, mice in utero electroporated with shSLK exhibited an increased severity of acute seizures induced by pentylenetetrazol (PTZ). These observations suggest that SLK has an important role in the development of a normal dendritic tree and inhibitory synapse stabilization/maintenance. Consequently, a decrease in neuronal SLK levels during the development might contribute to the emergence of morphological alterations and an excitatory-inhibitory imbalance in neurons within epileptogenic brain lesions (Schoch et al., 2021).

1.7 Key Questions

Developmental focal lesions featuring dysmorphic neurons are frequently associated with devastating and therapy-refractory epilepsies. However, it is still unknown how these malformative neurons contribute to increasing the propensity to generate seizures. SLK protein was found to be downregulated in dysmorphic neurons in certain types of developmental focal lesions and its experimental knockdown strongly impairs dendritic and inhibitory synapse formation. Therefore, this thesis addresses the functional connectivity consequences at the microcircuit level of the morphological and physiological changes induced by SLK-deficiency. To this end, we addressed the following aims:

- Examine how SLK-KD neurons differentially recruit excitatory and inhibitory inputs
- Determine whether the functional impairments of SLK-KD neurons are circuit-specific
- Examine the cellular basis of the inhibitory deficit of SLK-KD neurons
- Address the relevance of SLK-KD neurons for network hyperexcitability
- Determine molecular mechanisms underlying the inhibitory alterations of SLK-KD neurons

2. Materials and methods

2.1 Animals

All experimental procedures were conducted in accordance with the federal law of the state of North Rhine-Westphalia, Germany (Project number: AZ84–02.04.2017.A363). Timed- pregnant mice were used for in utero electroporations (IUE) at embryonic day 14 (E14). Male C57Bl/6 and female CD1 mice were allowed to mate overnight, and the day of mating was defined as E0. For viral transduction into specific GABAergic interneurons subtypes, wild type CD1 females were bred with homozygous Parvalbumin (PV)-cre ($Pvalb^{tm1(cre)Arbr}$, JAX stock #017320) or heterozygous somatostatin (SST)-IRES-Cre ($SST^{tm2.1(cre)Zjh}$, JAX stock #018973) males. The offspring of SST-IRES-Cre breedings were genotyped using the primers TCAGGTACATGGATCCACTAGTTCT (mutant forward), GAGGTCTGCCAACTCGAAC (wild type forward), and AGTCAAACG CTTGCTCTTCA (common), being classified as heterozygous if amplified fragments at 198 and 257bp were observed. IUE animals were assigned to experimental groups based on the electroporated plasmids irrespective of sex. Animals were housed under controlled conditions (12 h light-dark cycle, temperature 22 ± 2 °C, and humidity 55 ± 10 %) with food and water *ad libitum*.

2.2 Generation of constructs

Constructs were generated as described before (Schoch et al., 2021). shRNA constructs against SLK were designed based on sequences in the RNAi Codex database (http://cancan.cshl.edu/cgibin/ Codex/Codex.cgi), ordered as oligonucleotides from Invitrogen life technologies and annealed in 100 mM Tris pH7.5, 1 M NaCl and 10 mM EDTA solution for 10 min at 95°C. Afterward, samples were slowly cooled down to room temperature and inserted into the vectors pAAV-U6-shRNA-CBA-hrGFP / pAAV-U6-shRNA-CBA-mRFP via BamHI and HindIII restriction sites, respectively.

2.3 Intraventricular in utero electroporation

In utero electroporation was performed as described before (Grote et al., 2016; Schoch et al., 2021). In short, time pregnant (E14) CD1 wild-type mice were deeply anesthetized with isoflurane inhalation and injected with Ketoprofen (5 mg/kg - Mibe) and

Buprenorphine (0.05 mg/kg - Bayer) as analgesia. Uterine horns were exposed from the abdominal cavity and each embryo was injected once into the lateral ventricle with 1-2 µl DNA with a concentration of 1.5 µg/µl and fast green (1 mg/ml, Sigma, USA) with a pulled and beveled glass capillary (Drummond Scientific, USA) using a microinjector (Picospritzer III, Parker Hannifin Corporation, USA). Five electric pulses with 50 ms duration were delivered at 950 ms intervals with a triple-electrode using a CUY21SC Square Wave Electroporator charged to 30 V (Nepa Gene, Japan). Electrode forceps were placed to target cortical progenitor cells in the somatosensory and motor cortex (Szczurkowska et al., 2016). Animals were in utero electroporated either with control plasmids to only express a fluorescent protein (XFP; hrGFP or mRFP) or with SLK-shRNA-hrGFP/mRFP (shSLK) plasmids to downregulate SLK in targeted cells.

2.4 Stereotaxic viral gene transfer

Electroporated animals (3 weeks old) were anesthetized with an injection of fentanyl/midazolam/medetomidine mixture (0.05 / 5.0 / 0.5 mg/kg body weight, i.p.) and received ketoprofen subcutaneously (s.c.) as analgesia (5 mg/kg body weight). Next, animals were head-fixated in a stereotactic frame while keeping a constant temperature of 37 °C using a regulated heating plate (TCAT-2LV, Physitemp). After removal of the head hair and superficial disinfection, the surface was locally anesthetized with a drop of 10 % lidocaine and the skull was exposed. The IUE brain area was identified by using a dual fluorescent protein flashlight (DFP-1, Nightsea). Then, a hole was carefully open with a dental drill at the target site and the tip of a precision syringe (cannula size 34 G) was stereotactically inserted through the burrhole in order to slowly deliver the virus particles into the brain area of interest. For activation of feedforward inputs, AAV-syn-ChR2-EYFP (250 nl at 50 nl/min) was injected to reach the ventral posterior medial nucleus (VPM) and the posteriormedial complex (POm) of the thalamus of the electroporated hemisphere (AP: -1.7, ML: +/-1.2, DV: -3.6, relative to bregma) (Paxinos and Franklin, 2001). For the activation of feedback inputs, a mixed injection (1:1, 250nl at 50nl/min) of pENN.AAV.CamKII0.4.Cre.SV40 (Addgene, plasmid #105558) and AAV-EF1a-double-floxed-hChR2(H134R)-EYFP-WPRE-HGHpA (Addgene, plasmid #20298) was performed in 3 locations of the identified cortical electroporated area (500 µm apart across the anterior-posterior axis; 300µm deep from the pia surface). The same approach was used

for the specific activation of PV- and SST-expressing interneurons, but only AAV-EF1a-double-floxed-hChR2(H134R)-EYFP-WPRE-HGHpA (Addgene, plasmid #20298) was injected in PV-cre and SST-IRES-Cre animals. At the end of the surgery, the scalp was stitched and the anesthesia was terminated by injection of the antagonist naloxone/flumazenil/atipamezole mixture (1.2 / 0.5 / 2.5 mg/kg body weight, i.p.). Postoperative analgesia was carried out over 3 days with one daily administration of ketoprofen (5 mg/kg body weight, s.c.). In vitro patch-clamp recordings were performed 2 to 3 weeks after virus injection.

2.5 Slice preparation

Electroporated animals ranging from age 4 to 6 weeks were decapitated under deep isoflurane anesthesia. The brain was quickly removed and immersed in ice-cold sucrose-containing artificial cerebrospinal fluid (ACSF; in mM: NaCl 60, sucrose 100, KCl 2.5, $CaCl_2$ 1, $MgCl_2$ 5, NaH_2PO_4 1.25, D-glucose 20, $NaHCO_3$ 26; pH 7.4, 310 mOsmol, equilibrated with 5 % CO_2 : 95 % O_2). 300 µm-thick coronal brain slices were prepared with a vibratome (Microm HM650 V, Thermo Scientific). Slices containing transfected cells in motor and somatosensory cortices were identified and incubated at 35 °C in the same solution for 20 min. Then, slices were maintained for at least 1 hour and up to 6 hours in ACSF (in mM: NaCl 125, KCl 3.5, $CaCl_2$ 2, $MgCl_2$ 2, NaH_2PO_4 1.25, D-glucose 15, $NaHCO_3$ 26; pH 7.4, 310 mOsmol, equilibrated with 5 % CO_2 : 95% O_2) at room temperature.

2.6 Electrophysiological recordings

Slices were transferred into a submerged chamber and superfused with carbogen-saturated ACSF (3 ml/min, 35 ºC). Layer II/III pyramidal cells were visualized using infrared oblique illumination contrast microscopy in a 60x water immersion objective (Nikon, N60X-NIR Apo, NA1.0W) on an upright microscope (Nikon Eclipse FN1, Tokyo, Japan). Electroporated cells expressing shSLK or control plasmids were identified visually by hrGFP or mRFP fluorescence using a long-life mercury light source and a FITC (EX465-495, DM505, BA515-555; Nikon, Tokyo, Japan) or TRITC filter cube set (EX515-565, DM565, BA550-660; Nikon, Tokyo, Japan), respectively. For postsynaptic currents (PSCs) measurements, whole-cell voltage-clamp configuration was established with a cesium-methane-sulfonate based intracellular solution (in mM: cesium methanesulfonate

120, $MgCl_2$ 0.5, 4-(2-hydroxyethyl)-1-piperazineethanesulfonic acid (HEPES) 5, ethylenglycole-bis(2-aminoethylether)-N,N,N′,N′-tetraacetic acid (EGTA) 5, Adenosine 5′-triphosphate disodium salt (Na_2-ATP) 5, N-(2,6-Dimethylphenylcarbamoylmethyl) triethylammonium chloride ($QX314Cl^-$) 5; pH adjusted to 7.25 with CsOH, 295 mOsmol). The resistance of the patch pipettes ranged from 4 to 6 MΩ. Recordings were performed with a Multiclamp 700B (Molecular Devices) and signals were sampled at 20 kHz with a Digidata 1322A (Molecular Devices) controlled by Clampex 10.2 (Molecular Devices). Holding potentials were corrected offline for a liquid junction potential of 10 mV. For pharmacology experiments, it was used 50 µM 6-Cyano-7-nitroquinoxaline-2,3-dione disodium salt (CNQX, Tocris), 200 µM D-(-)-2-Amino-5-phosphonopentanoic acid (D-AP5, Tocris), 10 µM gabazine (SR 95531 hydrobromide, Tocris), 1 µM tetrodotoxin (TTX, Tocris) and 200 µM 4-aminopyridine (4-AP, Sigma Aldrich). All compounds were applied to the ACSF recording solution and continuously perfused for at least 10 minutes before continuing with the measurements. Amplitudes of PSCs from pharmacological experiments were normalized to the ACSF condition.

2.7 Electric and optogenetic stimulation

Electrically- and light-evoked PSCs were recorded from layer II/III electroporated neurons (either shSLK or control XFP). Subsequently, an adjacent pyramidal cell (PC) not targeted by the electroporation in the same slice (<50 µm apart, paired-control) was patched and PSCs were evoked without repositioning the stimulation electrode/light fiber. The excitatory and inhibitory components of evoked PSCs were separated by clamping the patched cell at the chloride reversal potential (-80 mV, calculated with Nernst equation) and the cation reversal potential (0 mV), respectively. To achieve synaptic activation of patched cells, a concentric bipolar electrode (FHC, USA) was placed in the subcortical white matter and stimuli with increasing intensities were applied until PSCs were evoked in the recorded cell (240.92 ± 38.62 µA average stimulation intensity, **Fig.6C**). The same stimulation intensity was used to evoke PSCs in the adjacent paired-control PC. Stimulation frequencies ranged from 1 to 10 Hz (10 pulses). For light-based activation of ChR2-expressing cells and axons, it was used a diode 473 nm laser (LuxX, Omicron) attached to an optical fiber. The end of the light fiber was immediately above the brain slice to illuminate the electroporated cortical area. Light stimuli with different pulse times

(0.5–15 ms) and intensities (0.72-20.96 mW) were applied at frequencies ranging from 1 to 10 Hz (10 pulses). In addition, a long light pulse of 500 ms was applied at a holding potential of -80 mV in order to assess whether the current patched cell displayed photocurrents generated by the expression of ChR2 in its own membrane (**Fig. 10E**). Few electroporated cells displayed intrinsic photocurrents, which were not considered for further quantifications.

2.8 Patch-clamp recording analysis

Amplitudes and kinetics of evoked PSCs were analyzed in Clampfit (Molecular Devices) and using a custom routine programmed in Python. For feedforward inputs experiments, PSCs evoked at 100 % laser output (20.96 mW) with 10 ms pulse time were plotted and analyzed. In the case of feedback inputs, PCSs resulted from the stimulation at 30% laser output (6.45 mW) and 10 ms pulse time were selected for further analyses due to the appearance of a slow component in EPSC decay at higher laser powers. For the light activation of PV- and SST-expressing interneurons, PCSs evoked at 30% laser output (6.45 mW) and 10 ms pulse time were plotted and analyzed. PSCs ratios were computed by dividing the PSC amplitude of XFP or shSLK neurons by the amplitude of their paired-control PC. Excitatory/inhibitory (E/I) ratios were calculated by dividing the EPSC by the IPSC of each individual recorded cell. Short-term plasticity features of recorded neurons were assessed by normalizing synaptic responses to the first response evoked by stimulation trains at 10. Pair-pulse ratios were obtained by dividing the second to the first response of pair stimulations at different frequencies (5, 10, 20, 30, 50 Hz). For patch-clamp RNAseq experiments, passive membrane properties were calculated with a custom routine programmed in R. The input resistance was obtained from the steady-state current responses to 5 and 10 mV voltage steps (200 ms) from a holding potential of -80 mV. Capacitance was defined as the area under the capacitive peak divided by the amplitude of the applied voltage step. Frequencies and amplitudes of mEPSC and mIPSC were calculated offline with a custom routine programmed in IGOR Pro. mEPSC were detected by calculating the first derivative of current traces and selecting events for which the first derivative was > 5x than the standard deviation of the baseline 0-3 ms before the event. mIPSCs were detected if the difference between the mean current amplitudes in two

adjacent moving windows (0.5 ms) was > 5 pA. All detected events were assessed by visual inspection and sorted manually.

2.9 Immunohistochemistry

Electroporated animals (4 to 6 weeks old) were heart perfused with ice-cold 4 % paraformaldehyde (PFA). Brains were dissected and transferred into 4 % PFA for 48 hours at 4 ºC for post-fixation. 80 µm slices were cut on a vibratome (Microm HM 650 V, Thermo Scientific) and blocked with 0.25 % Triton X-100 and 3% bovine serum albumin (BSA) in phosphate-buffered saline (PBS) overnight at 4 ºC. Next, slices were incubated with the primary antibodies rabbit anti-c-fos (1:500, PC05, Millipore), rabbit anti-parvalbumin (1:500, AB15736, Millipore), or rabbit anti-somatostatin (1:500, T-4102, Peninsula Laboratories International) overnight at 4ºC. After three washing steps, slices were incubated with the secondary antibody Alexa Fluor® 647 (Life Technologies, USA) for 2 hours and mounted on glass slides. Controls consisted of the omission of primary antibodies. Counterstaining of brain sections was achieved using 4′,6-diamidino-2-phenylindole (DAPI). Images were acquired with a Leica SP8 Confocal Microscope using a 10X (PV and SST staining) or 40X (c-fos staining) objective and quantified manually using ImageJ software.

For the quantification of c-fos positive cells, hrGFP signal was used to delimitate the area of electroporated cells and to create a mask that was superposed on the c-fos labeling images. The average pixel intensity of c-fos labeling was quantified in hrGFP contours and normalized by the average intensity of negative controls. Contours displaying an average intensity 3x higher than the average intensity of negative controls were classified as c-fos positive cells. PV and SST quantifications were performed manually across all cortical layers and within IUE-targeted brain areas.

2.10 Patch-clamp recordings and RNA collection

Patch-clamp RNA sequencing (patch-seq) experiments were performed following an adapted protocol from previous publications consisting of several steps, including whole-cell patch-clamp recordings, aspiration of cell contents, cDNA synthesis, sequencing, and data analysis (Cadwell et al., 2015, 2017a, 2017b; Fuzik et al., 2016). Several modifications of the aforementioned patch-clamp protocol were applied in order to avoid RNA degradation during sample collection. Preparations and sample handling were

executed under a safety hood with strict RNAse-free conditions, using certified RNase-free disposable products and tools and glassware previously treated with RNaseZap (Invitrogen, AM9780). Cells electroporated with XFP or shSLK (and 3 non-electroporated striatal cells for downstream comparisons) were recorded using baked (200 °C, 2 hours) borosilicate patch pipettes (2–4 MΩ) filled (maximum 1 µl) with an intracellular solution containing (in mM): 123 potassium gluconate, 12 KCl, 10 HEPES, 0.2 EGTA, 4 MgATP, 0.3 NaGTP, 10 sodium phosphocreatine, pH: 7.25. On the day of the experiment, 1 U/µl recombinant RNase inhibitor (Takara, 2313A) and 20 µg/ml glycogen (Sigma-Aldrich, G1767) were added to the intracellular solution in order to preserve and help to collect the RNA from the recorded cell (Cadwell et al., 2017b). Slices were kept in a submerged chamber and superfused with carbogen-saturated ACSF with TTX (1 µM). Once the whole-cell configuration was achieved, miniature EPSCs and IPSCs were recorded by clamping the cell at -80 mV for 2 min and 0 mV for 30 s, respectively. In addition, voltage steps (200 ms) of 5 and 10 mV from a holding potential of -80 mV were applied in order to determine the passive properties of the cell. After recording the electrophysiological parameters of interest, negative pressure was applied (20-100 mbar for 1-2 min) to aspirate the cell contents into the patch pipette until the cell body dramatically decreased in size. Next, the recording pipette was quickly removed and the sample ejected into an RNase-free PCR tube containing 1 µl lysis buffer (40 mM Guanidine hydrochloride, 0.1 µM Smart dT30VN primer, 5 mM dNTPs), which was immediately frozen in liquid nitrogen and stored at -80 °C.

2.11 Library preparation, sequencing, and gene alignment

Individual lysed cells were treated according to the Smart-Seq2 library preparation protocol (Picelli et al., 2014). Preamplified cDNA was quantified and the average size distribution was determined via D5000 assay on a tapestation4200 system (Agilent). Tagmentation and subsequent next-generation sequencing (NGS) library generation were performed using 200 pg of cDNA per sample following the Smart-Seq2 protocol. NGS libraries were quantified by HS dsDNA assay on a Qubit (Invitrogen) and the average size distribution was determined via D5000 assay on a TapeStation 4200 system (Agilent). Libraries were equimolarly pooled, clustered at 1.4 pM, and sequenced SR 75 cycles using High Output v2 chemistry on a NextSeq500 system (Illumina). Raw sequencing data

were demultiplexed and converted into fastq format using bcl2fastq2 v2.20 and aligned to mouse genome M16 via STAR aligner considering both, exonic and intronic reads.

2.12 Patch-seq analysis

Exonic and intronic aligned reads were added and used to maximize gene counts as reported for other patch-seq datasets (Cadwell et al., 2017b; Scala et al., 2020). Read counts were used to compute basic quality control metrics for each cell, such as library size, the total number of expressed genes, and the proportion of mitochondrial reads (Lun et al., 2016b; Amezquita et al., 2020). Cells deviating at least three median absolute deviations (MADs) from the median value of any of the metrics were classified as poor-quality samples and therefore removed from the analysis (final number of cells 69; 28 hrGFP, 38 shSLK, 3 striatum). A $\log_{10}$-transformation was used to improve resolution at small values. Low abundance genes (which are likely to be dominated by zero counts) were filtered by choosing genes expressed in at least 28 cells (the size of the smallest experimental group; final number of genes: 3287). Next, expression levels were normalized using a library size deconvolution approach (Lun et al., 2016a). Briefly, read counts of multiple cells were pooled and then deconvolved to determine size factors for individual cells. Read counts were divided by their specific cell-based size factor and then $\log_2$-transformed. This helps to account for systematic differences in sequencing coverage (technical differences that arise during library preparation) while considering composition biases introduced by differentially expressed genes in subsets of cells. These normalized $\log_2$-transformed values were the basis of further analysis unless state otherwise.

In order to compress multiple features of the gene expression data into single dimensions, we applied Principal Components Analysis (PCA) and t-Distributed Stochastic Neighbor Embedding (t-SNE) to achieved 2D representations of the expression profiles of patched cells (using the scater package in R). The principal components that retained 60% of the variability in the data were used as input to initiate t-SNE analyses, using a set value of 15 for the perplexity of the Gaussian distributions.

To identify changes in gene expression driven by the absence of SLK, we performed differential expression analysis between the transcriptomic profile of XFP and shSLK neurons. Even though our patch-seq approach provided us with the cellular resolution needed to achieve our goals, this kind of data displays some characteristics that need to

be considered. First, due to the low concentration and low capture efficiency of RNAs in patched cells, read counts can be inflated with zero values or “drop-out” events, which introduce noise to the data and makes it difficult to find biological differences among groups (Saliba et al., 2014). Second, since the recording and collecting these samples is extremely challenging, we could not collect the high number of cells usually obtained for scRNA-seq from dissociated tissues, which also makes more noisy our data due to the heterogeneity of individual neurons. To overcome these problems, we used an analysis pipeline specially design for single-cell data that was shown to work well for data sets with a large number of zero counts and a small number of samples, compared to more traditional pipelines made for bulk-RNAseq (Wang et al., 2019). This approach, called DESingle, uses a zero-inflated negative binomial model to estimate the fraction of real biological zero counts and drop-out events. With this, DEsingle classifies DE genes into three categories; genes that have differences only in the proportion of real zeros between groups, genes that are differentially expressed between the groups without significant difference in the proportion of real zeros, and genes that have significant differences in both the proportions of real zeros and the expression abundances between the two groups (Miao et al., 2018). We implemented this approach in R using the raw count data since DEsingle applies a normalization step in its pipeline. Genes with an adjusted p-value ≤ 0.05 were considered as differentially expressed.

We next investigated whether the DE genes found in SLK-deficient neurons were associated with human diseases. For this purpose, we use Disgenet2r, a platform with a large collection of curated repositories, genome-wide association studies, and scientific publications of genes and variants involved in human pathologies. We explore the number of diseases associated with each DE gene based on DisGeNET scores, which mirrors the recurrence of a specific gene-disease association across multiple data sources (Piñero et al., 2017).

Finally, to explore possible group-specific gene expression signatures related to excitability, we performed Spearman’s rank correlations between the DE genes and the electrophysiological properties of XFP and shSLK neurons. The package Hmisc in R was used to generate a correlation matrix of the 24 DE genes found with DEsingle and the electrophysiological parameters that displayed differences between groups (capacitance

and mIPSC frequency). Along with the correlation coefficients, *p*-values from t-tests were obtained to determine significant paired correlations using a significant level of 0.05.

2.13 Statistical analysis

Average values in the text and figures are expressed as mean ± standard error of the mean (SEM). The significance level was set to $p<0.05$. The statistical tests and the resulted statistical values are described in the text for each individual test performed.

3. Results

3.1 Altered synaptic excitation/inhibition balance in SLK-deficient neurons

SLK protein was found to be downregulated in dysplastic neurons from human FCD-IIB and GGs, and its experimental knockdown strongly impairs dendritic and inhibitory synapse formation (Schoch et al., 2021). In order to address the functional consequences at the microcircuit level of the focal loss of SLK in cortical networks, we in utero electroporated mice at E14 either with control plasmids to only express a fluorescent protein (XFP; hrGFP or mRFP) or with SLK-shRNA-hrGFP/mRFP (shSLK) plasmids to downregulate SLK in targeted cells. Slices obtained from shSLK electroporated animals showed a higher dispersion of targeted cells across cortical layers compared to XFP electroporated animals (**Fig. 6A**). In both experimental conditions, patch-clamp recordings were performed in neurons located in layer II/III within the cortical electroporated area.

To examine if decreased SLK expression also affects inhibition in cortical circuits, we examined stimulation-evoked inhibitory and excitatory transmission. We recorded from XFP and shSLK neurons, as well as from at least one immediately adjacent pyramidal cell (PC) not targeted by the electroporation in the same slice (paired-control PCs, **Fig. 6B**). We then evoked excitatory and inhibitory postsynaptic currents (EPSCs and IPSCs) by stimulation of the subcortical white matter with a bipolar electrode, using an average intensity of 240.92 ± 38.62 µA (**Fig. 6B, C**). We assessed the IPSCs amplitude by holding neurons at 0 mV, resulting in $GABA_A$ receptor-mediated outward currents that were blocked by gabazine (**Fig. 6D**, 10 µM). The remaining inward currents were completely abolished by the subsequent application of CNQX and D-AP5 (**Fig. 6D**, 50 µM, and 200 µM). EPSCs were recorded by holding neurons at -80 mV, close to the Cl^- reversal potential, resulting in PSCs entirely blocked by the combined application of CNQX and D-AP5 (**Fig. 6E**).

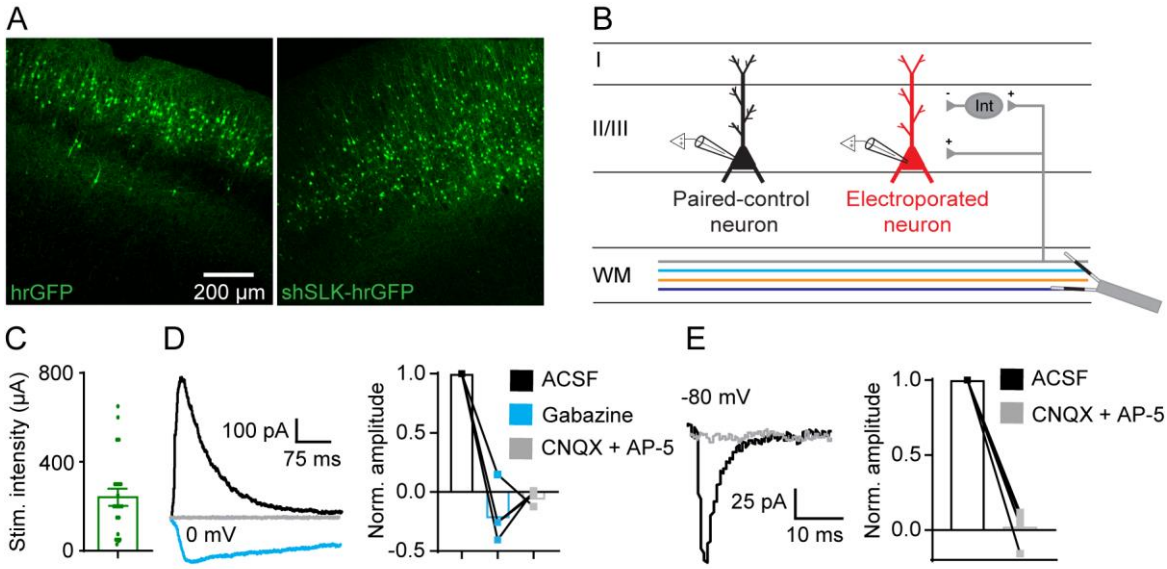

Figure 6: White matter stimulation evokes IPSCs and EPSCs in electroporated cortical neurons. A, Representative micrograph of neurons expressing hrGFP in mice in utero electroporated at E14 either with only the fluorescent protein or with SLK-shRNA-hrGFP plasmids. B, Schematic of the experiment depicting recording from both electroporated pyramidal neurons in layer II/III (either control XFP or shSLK) and non-electroporated neighboring neurons (paired-control PC). Postsynaptic currents were evoked by stimulating the subcortical white matter with a bipolar electrode. C, Minimum stimulation intensities required to evoke PSCs in the recorded cells. Bar represents mean ± SEM of the data. D, Representative IPSCs recorded at 0 mV to minimize the contribution of glutamatergic transmission. Large outward currents were blocked by gabazine (10 µM, blue traces). PSCs were completely blocked by additional application of CNQX and D-AP5 (50 µM and 200 µM, respectively, grey traces). E, Representative EPSCs elicited with electrical stimulation while holding neurons at -80 mV. EPSCs were blocked by the combined application of CNQX and D-AP5 (grey traces). PSC amplitudes were normalized to the ACSF condition. Bars represent the mean of the data.

We found a dramatic reduction of the amplitude of evoked IPSCs in neurons expressing shSLK compared to adjacent paired-control PCs, and cells electroporated with control XFP (**Fig. 7A, B,** two-way repeated-measures ANOVA main effects, XFP vs shSLK: $F_{(1,17)}$=10.15, p=0.005; electroporated vs paired-control: F(1,17)=3.519, p=0.078; interaction: $F_{(1,17)}$=5.846, p=0.027; Bonferroni's post-test, shSLK vs paired-control p=0.008; shSLK vs XFP p<0.001). If the amount of IPSC reduction was expressed as a ratio to the adjacent paired-control PC, the IPSCs were strongly reduced in the shSLK neurons (**Fig. 7C**, XFP and shSLK 80 and 23% of paired-control IPSCs, respectively, Mann-Whitney U test, p=0.001). In contrast, stimulation-evoked EPSCs showed a decreasing tendency but were not significantly reduced in neurons expressing shSLK

compared to XFP and paired control neurons (**Fig. 7D-E,** two-way repeated-measures ANOVA, XFP vs shSLK: $F_{(1,17)}$=1.7, p=0.214). The EPSC ratio of shSLK neurons to adjacent paired-controls also remained unaltered (**Fig. 7F**, Mann-Whitney U test, p=0.135). IPSC trains evoked at 10 Hz showed strong depressing features in control cells. In contrast, SLK-deficient neurons displayed altered short-term plasticity as suggested by their similar normalized IPSC amplitudes across the whole stimulation train (**Fig. 7G**). We did not observe alterations in short-term plasticity for EPSCs in shSLK electroporated neurons (**Fig. 7H**).

Measuring EPSC and IPSC magnitudes in the same neuron allowed us to compute a ratio between excitatory and inhibitory inputs for each cell. As expected, the excitation/inhibition (E/I) balance was significantly shifted toward excitation in SLK-deficient neurons (**Fig. 7I**, two-way ANOVA, XFP vs shSLK: $F_{(1,34)}$=14.58, p<0.001; electroporated vs paired-control $F_{(1,34)}$=6.81, p=0.013; interaction: $F_{(1,34)}$=10.81, p=0.002; Bonferroni's post-test, shSLK vs paired-control p<0.001; shSLK vs XFP p<0.001). Thus, decreasing SLK expression leads to a selective loss of circuit-based inhibition and a shift in E/I balance in pyramidal neurons.

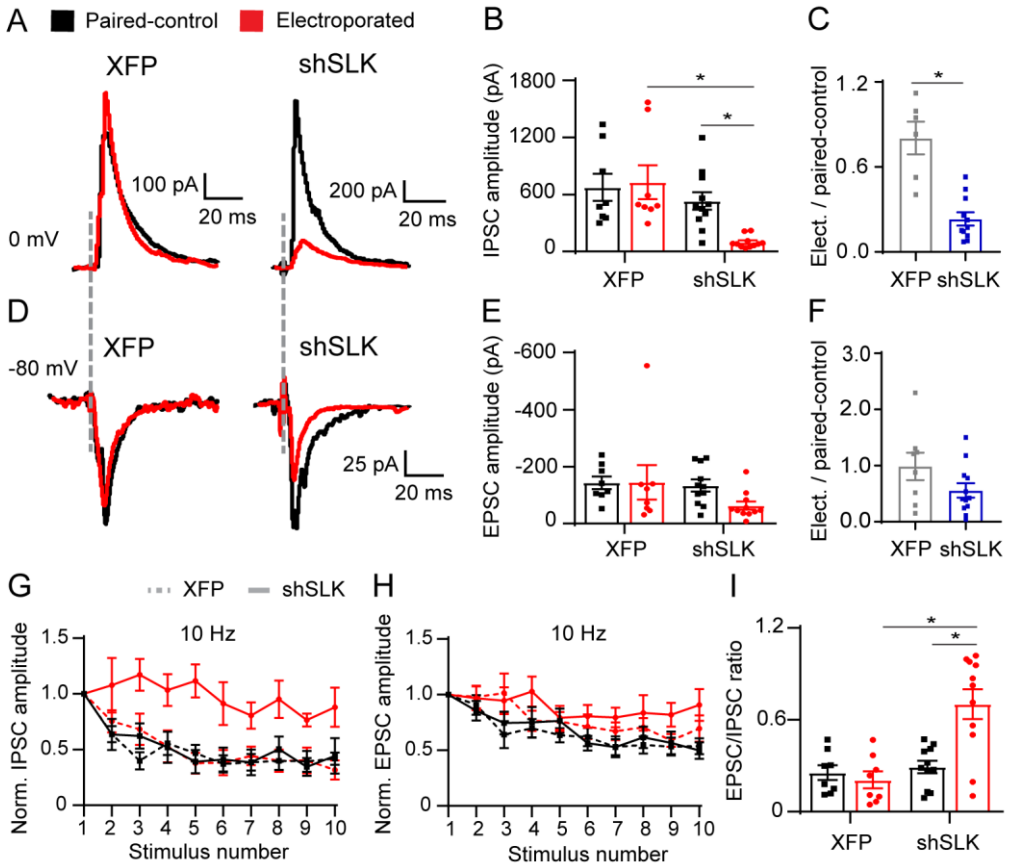

Figure 7: SLK-deficient neurons display a deficit in synaptic inhibition. A, D, Representative examples of IPSCs (A) and EPSCs (D) in electroporated XFP and shSLK neurons (red traces), and adjacent paired-control PCs in the same slice preparation (black traces). Dashed grey lines represent the time point of the stimulus onset. B, E, Comparison of evoked IPSC (B) and EPSC (E) amplitudes in neurons expressing shSLK or control XFP compared to their respective, adjacent paired-control PCs. Asterisks indicate post-tests after two-way repeated-measures ANOVA, IPSCs (panel B): Bonferroni's post-test, shSLK vs paired-control p=0.008; shSLK vs XFP p<0.001. C, Ratio of IPSCs in XFP or shSLK neurons expressed as a fraction of IPSCs recorded in adjacent paired-control PCs. Asterisk indicates Mann-Whitney U test, p=0.001. F, As in panel C, ratios computed for EPSCs. G, H, IPSC (G), and EPSC (H) amplitudes (normalized to first response) of synaptic responses evoked by white matter stimulation trains at 10 Hz in neurons expressing shSLK or control XFP compared to their respective, adjacent paired-control PCs. I, E/I balance computed as the EPSC/IPSC ratio for each individual XFP or shSLK neuron and their respective paired-control PC. Asterisks indicate post-tests following two-way ANOVA. Bonferroni's post-test, shSLK vs. paired-control p<0.001; shSLK vs. XFP p<0.001. Data are represented as mean ± SEM.

3.2 SLK deficiency causes abnormal excitation/inhibition balance in a feedforward circuit

Inhibition in the cortex is organized into feedforward and feedback motifs. We next elucidated if the deficit in inhibition preferentially affects either one or both of these inhibitory motifs. We first examined feedforward inhibition using an optogenetic approach. We expressed ChR2 in the thalamus with AAV-mediated gene transfer. We used injection coordinates that led to an expression in thalamocortical neurons that project to cortical areas overlapping the IUE affected area (**Fig. 8C,** see Methods). Following the injection, we identified large numbers of ChR2-eYFP-expressing axons in the ipsilateral layer 4, as expected for thalamic afferents, as well as in layer 1, where direct thalamic afferents are also present (**Fig. 8A**). We recorded from electroporated neurons (XFP and shSLK) and adjacent paired-control PCS as in figure 6 (**Fig. 8B**). Feedforward excitation and inhibition were blocked by glutamatergic and GABAergic receptor antagonists, respectively (**Fig. 8D, E**). Light-evoked IPSCs, but not EPSCs were blocked after combined application of TTX and 4-AP (1µM and 200µM). This indicates that IPSCs are disynaptic, and result from feedforward activation of interneurons by thalamic inputs, whereas EPSCs are largely monosynaptic (**Fig. 8F, G**).

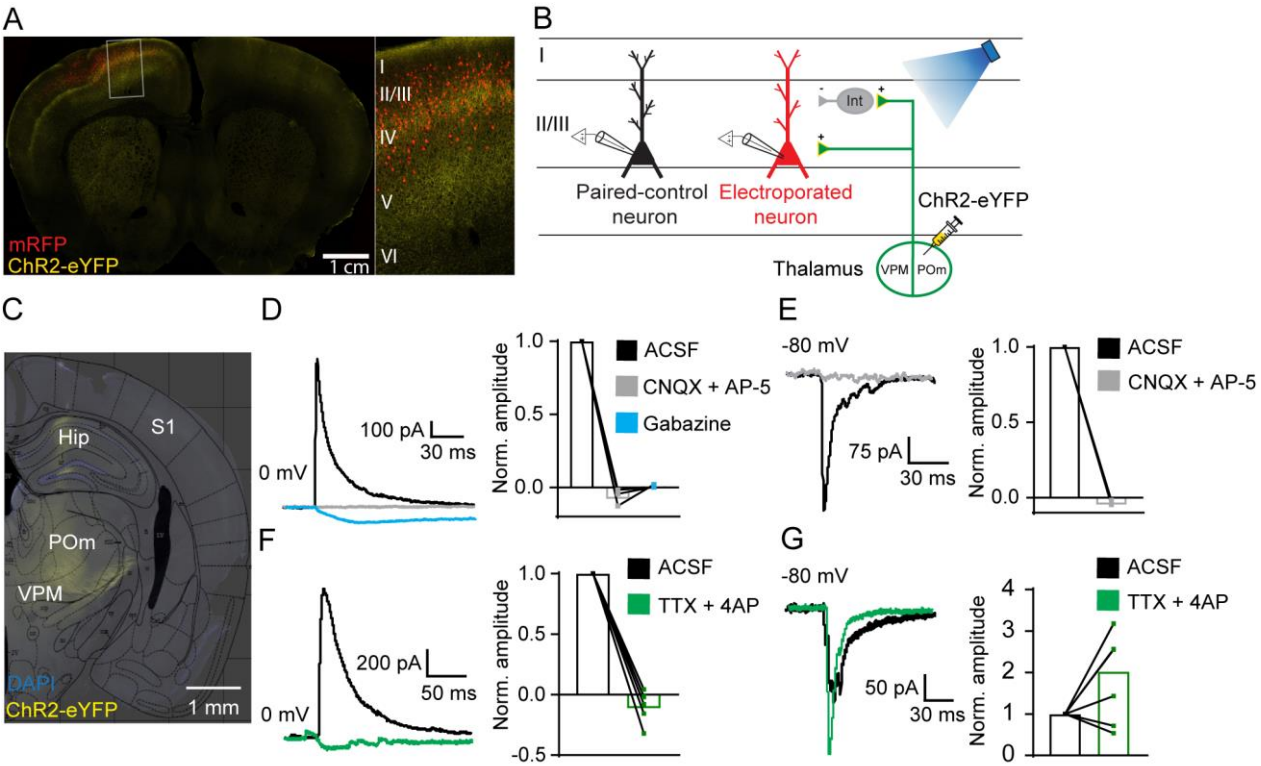

Figure 8: Optogenetic activation of thalamocortical axons evokes IPSCs and EPSCs in electroporated cortical neurons. A, Representative micrograph of cortical electroporated neurons and ChR2-eYFP-expressing thalamic axons reaching the electroporated area. B, Schematic of the experiment. ChR2-eYFP was expressed through stereotactic injections in thalamic nuclei projecting to M1 and S1. Patch-clamp recordings were carried out from both electroporated pyramidal neurons in layer II/III (either control XFP or shSLK) and non-electroporated neighboring neurons (paired-control). C, Representative micrograph showing ventral posteromedial nucleus (VPM) and the posteriormedial complex (POm) expressing ChR2-eYFP 2 weeks after intracranial injection of a ChR2-eYFP-expressing virus. Image is overlapped with a schematic brain slice from Paxinos and Franklin (2001). D, Representative light-evoked IPSCs recorded at 0 mV to minimize the contribution of glutamatergic transmission. Large outward currents were blocked by gabazine (10 µM, blue traces). PSCs were completely blocked by additional application of CNQX and D-AP5 (50 µM and 200 µM, respectively, grey traces). E, Representative EPSCs elicited by blue light-based stimulation of thalamic axons while holding neurons at -80 mV. EPSCs were blocked by the combined application of CNQX and D-AP5 (grey traces). F, G, Light-evoked IPSCs were disynaptic, while EPSCs were monosynaptic. IPSCs were completely blocked after the application of TTX and 4-AP (1 µM and 200 µM, panel F, green traces). EPSCs persist after combined application of TTX/4-AP due to direct optogenetic stimulation of glutamatergic terminals onto layer II/III pyramidal neurons (panel G). PSC amplitudes were normalized to the ACSF condition. Bars represent the mean of the data.

In neurons lacking SLK protein, a substantial reduction of IPSC amplitude (**Fig. 9A-C,** two-way repeated measures ANOVA (panel B), main effects XFP vs. shSLK: $F_{(1,21)}$=0.803,

p=0.380; electroporated vs. paired-control: $F_{(1,21)}$=21.98, p<0.001; interaction: $F_{(1,21)}$=29.33, p<0.001; Bonferroni's post-test, shSLK vs. paired-control p<0.001; shSLK vs. XFP p=0.009. Mann-Whitney U test (panel C), p<0.001) was observed compared to adjacent control PCs and XFP electroporated cells. This finding was stable over a large range of optogenetic stimulation intensities (**Fig. 9D**). Similarly, EPSC amplitudes were found to be reduced in shSLK neurons, but only when compared to their paired-control PCs (**Fig. 9E-G,** two-way repeated measures ANOVA (panel F), main effects XFP vs shSLK $F_{(1,21)}$=0.008, p=0.931; electroporated vs paired-control $F_{(1,21)}$=2.65, p=0.119; interaction: $F_{(1,21)}$=17.9, p<0.001; Bonferroni's post-test, shSLK vs. paired-control p<0.001. Mann-Whitney U test (panel G), p<0.001). As observed with white matter stimulation, the IPSC depression observed in control neurons was less robust in SLK-deficient neurons (**Fig. 9I**)

This striking finding resulted in significant differences between control and experimental animals. Even though both EPSCs and IPSCs were significantly reduced, inhibition was reduced to a greater extent. As a consequence, the E/I balance was significantly elevated in SLK-deficient neurons (**Fig. 9K,** two-way ANOVA, main effects XFP vs shSLK: $F_{(1,42)}$=4.072, p=0.050; electroporated vs paired-control: $F_{(1,42)}$=5.828, p=0.020; interaction: $F_{(1,42)}$=1.624, p=0.210; Bonferroni's post-test, shSLK vs. paired-control p=0.015; shSLK vs. XFP p=0.050).

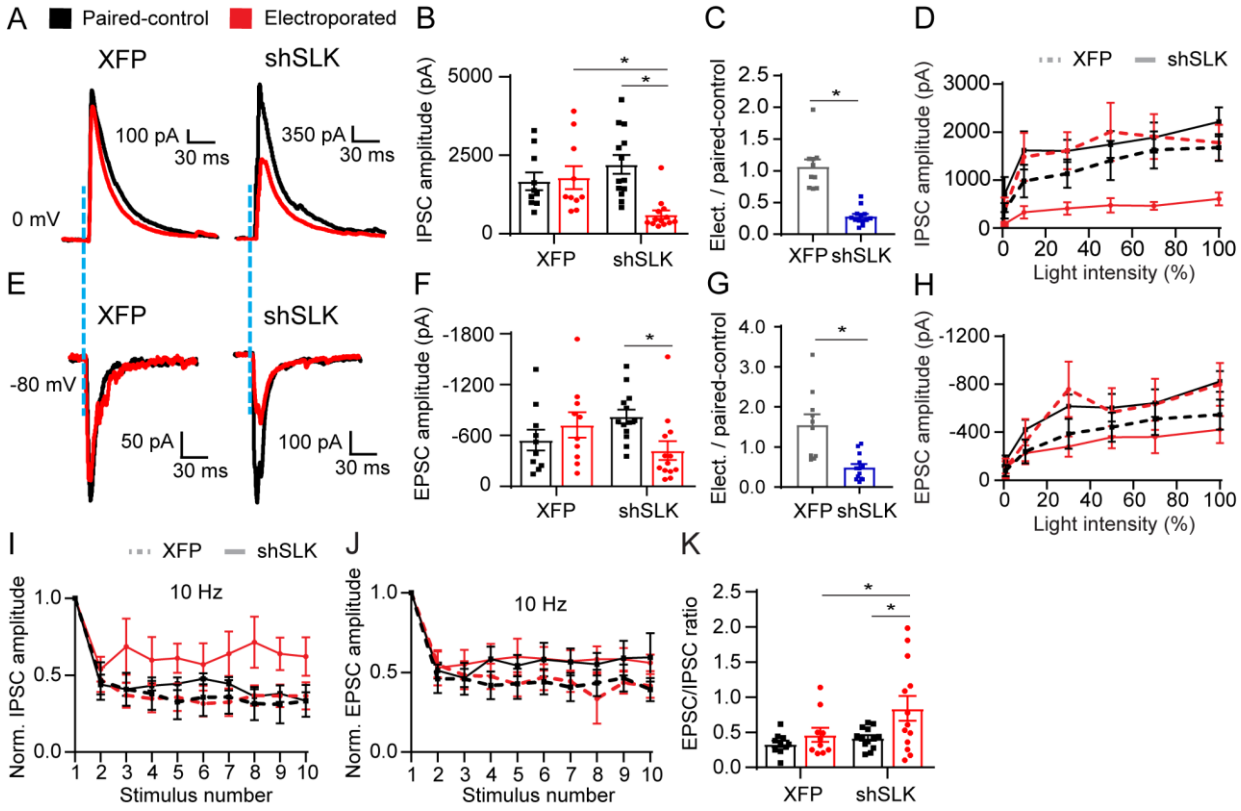

Figure 9: Abnormal excitation/inhibition balance in SLK-deficient neurons resides in a feedforward circuit. A, E, Representative examples of light-evoked IPSCs (A) and EPSCs (E) in electroporated XFP and shSLK neurons (red traces), and adjacent paired-control PCs in the same slice preparation (black traces). Dashed blue lines represent the time point of the stimulus onset. B, F, Comparison of light-evoked IPSCs (B) and EPSCs (F) in neurons expressing shSLK or control XFP compared to their respective, adjacent paired-control pyramidal neurons. Asterisks indicate post-tests after two-way repeated-measures ANOVA, IPSCs (panel B): Bonferroni's post-test, shSLK vs. paired-control $p<0.001$; shSLK vs. XFP $p=0.009$ EPSCs; (panel F): Bonferroni's post-test, shSLK vs. paired-control $p<0.001$. C, G, Ratio of light-evoked IPSCs (C) and EPSCs (G) in XFP or shSLK neurons expressed as a fraction of PSCs recorded in adjacent paired-control PCs. Asterisk indicates Mann-Whitney U test, $p<0.0001$ (C) and $p<0.001$ (G). D, H, Amplitudes of light-evoked feedforward IPSCs (D) and EPSCs (H) across different light stimulation intensities (100% = 20.96 mW light fiber output) in neurons expressing shSLK or control XFP compared to their respective, adjacent paired-control PCs. I, J, IPSC (I), and EPSC (J) amplitudes (normalized to first response) of synaptic responses evoked by light stimulation trains at 10 Hz of thalamic axons in neurons expressing shSLK or control XFP compared to their respective, adjacent paired-control PCs. K, E/I balance computed as the EPSC/IPSC ratio for each individual XFP, shSLK, and their respective paired-control PCs. Asterisks indicate Bonferroni's post-tests following two-way ANOVA. shSLK vs. paired-control $p=0.015$; shSLK vs. XFP $p=0.050$. Data are represented as mean ± SEM.

3.3 Inhibition supplied by cortical feedback circuits is unaltered in SLK-deficient neurons

To assess whether feedback inhibition is also affected in SLK-deficient neurons, we expressed ChR2 in adjacent excitatory cortical cells using a dual viral approach injection of a virus expressing cre-recombinase under a CaMKII promoter only in excitatory neurons, in addition to a virus conditionally expressing ChR2 (**Fig. 10A, B**, see Methods). In electroporated neurons, blue light stimulation evoked PSCs that could be separated into glutamatergic EPSCs and GABAergic IPSCs by clamping at different holding potentials (**Fig. 10C, D**). We applied long light-based stimuli in order to determine if recorded cells displayed direct photocurrents. Few electroporated neurons (3 of 35) displayed long-lasting currents that followed the 500 ms light-pulse, indicating intrinsic expression of ChR2. These neurons were excluded from further analysis (**Fig. 10E**).

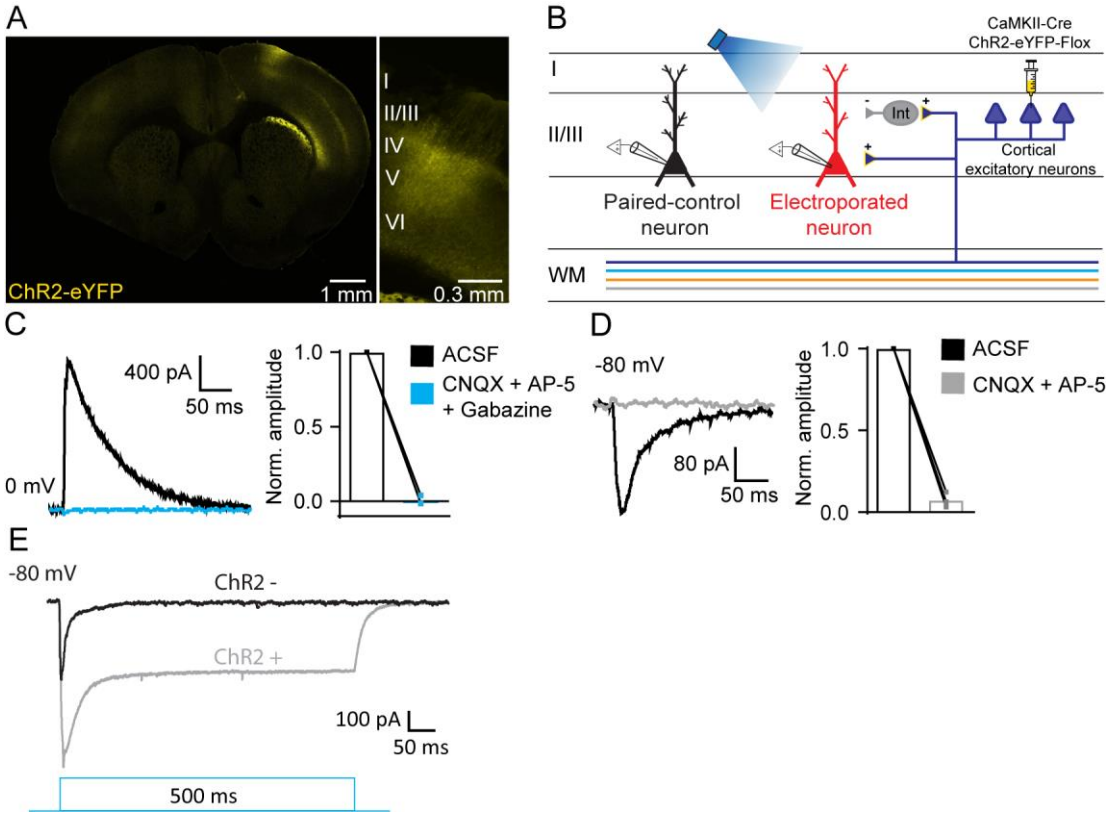

Figure 10: Optogenetic activation of intracortical connections evokes IPSCs and EPSCs in electroporated neurons. A, Representative micrograph of ChR2-eYFP-expressing axons of cortical excitatory neurons virally transduced with cre-recombinase under a CaMKII promoter and cre-conditional ChR2. B, Schematic of the experiment. ChR2 was expressed in cortical layer II/III excitatory neurons. Patch-clamp recordings were carried out from both electroporated pyramidal neurons in layer II/III (either control XFP or shSLK) and non-electroporated neighboring PCs (paired-control). C, Light-evoked IPSCs

recorded at 0 mV to minimize the contribution of glutamatergic transmission in ACSF and after the combined application of CNQX, D-AP5, and gabazine (50 µM, 200 µM, and 10µM respectively, blue traces). D, Representative EPSCs elicited by blue light stimulation of cortical neurons while holding neurons at -80 mV. Grey traces indicate the application of CNQX and D-AP5 (50 µM and 200 µM). E, Representative synaptic response of patched cortical neuron not expressing ChR2 (black) after light-based feedback activation. Neurons displaying long-lasting currents that followed the 500 ms light-pulse (grey) were considered to express ChR2 and were removed from further analysis. PSC amplitudes were normalized to the ACSF condition. Bars represent the mean of the data.

Surprisingly, neither IPSC (**Fig. 11A-D**, **I,** two-way repeated measures ANOVA, main effects XFP vs. shSLK: $F_{(1,15)}$=1.386, p=0.257; electroporated vs. paired-control: $F_{(1,15)}$=0.213, p=0.651; interaction: $F_{(1,15)}$=0.700, p=.416) nor EPSC amplitudes (**Fig. 11E-H, J,** two-way repeated measures ANOVA, main effects XFP vs. shSLK: $F_{(1,15)}$=0.366, p=.075; electroporated vs. paired-control: $F_{(1,15)}$=0.105, p=0.750; interaction: $F_{(1,15)}$=0.071, p=0.793) were affected in shSLK vs. adjacent non-electroporated or vs XFP neurons. As a consequence, the E/I balance evoked in feedback circuits was unchanged in SLK-deficient neurons (**Fig. 11K,** two-way ANOVA, XFP vs shSLK: $F_{(1,30)}$=0.342, p=0.563; electroporated vs paired-control $F_{(1,30)}$=0.00002, p=.997; interaction: $F_{(1,30)}$=0.541, p=0.468). This surprising finding indicates that the inhibitory deficit triggered after SLK loss is confined to feedforward inhibition, and does not affect feedback or lateral inhibitory circuits.

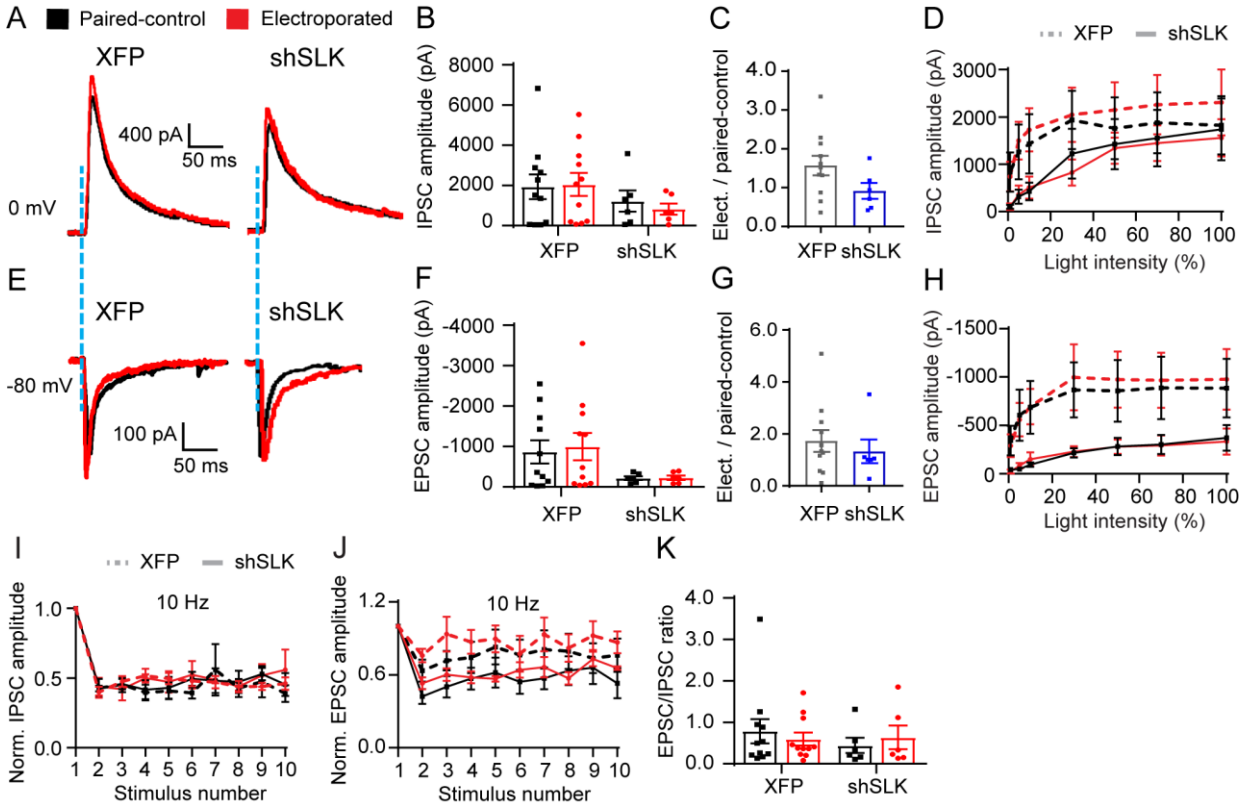

Figure 11: SLK-KD neurons do not show alterations in feedback inputs. A, E, Representative examples of light-evoked IPSCs (A) and EPSCs (E) in electroporated XFP and shSLK neurons (red traces), and adjacent paired-control neurons in the same slice preparation (black traces). Dashed blue lines represent the time point of the stimulus onset. B, F, Comparison of light-evoked IPSCs (B) and EPSCs (F) in neurons expressing shSLK or control XFP compared to their respective, adjacent paired-control PCs. C, G, Ratio of light-evoked IPSCs (C) or EPSCs (D) in XFP or shSLK neurons expressed as a fraction of PSCs recorded in adjacent paired-control PCs. D, H, Amplitudes of light-evoked feedback IPSCs (D) and EPSCs (H) across different light stimulation intensities (100% = 20.96 mW light fiber output) in neurons expressing shSLK or control XFP compared to their respective, adjacent paired-control PCs. I, J, IPSC (I), and EPSC (J) amplitudes (normalized to first response) of synaptic responses evoked by light-based stimulation trains at 10 Hz of intracortical axons in neurons expressing shSLK or control XFP compared to their respective, adjacent paired-control PCs. K, E/I balance computed as the EPSC/IPSC ratio for each individual XFP, shSLK, and the respective paired-control neurons. Data are represented as mean ± SEM.

3.4 Timing of inhibition is altered in shSLK neurons

Feedforward inhibition is normally fast and synchronous, due to the strong and fast excitation of feedforward interneurons, mainly of Parvalbumin (PV)-expressing interneurons. We therefore examined if the strong reduction of feedforward inhibition is associated with altered timing of inhibition. In optogenetic experiments in which we

stimulated thalamocortical axons, the remaining small residual IPSCs in shSLK neurons displayed a significantly slower rise time (**Fig. 12B**, two-way repeated-measures ANOVA, main effects XFP vs. shSLK: $F_{(1,20)}$=6.412, p=0.020; electroporated vs. paired-control: $F_{(1,20)}$=4.005, p=0.059; interaction: $F_{(1,20)}$=11.840, p=0.003; Bonferroni's post-test, shSLK vs. paired-control p<0.001; shSLK vs. XFP p<0.001) and time to peak (**Fig. 12D,** two-way repeated-measures ANOVA, main effects XFP vs. shSLK: F(1,20)=4.43, p=0.048; electroporated vs. paired-control: F(1,20)=4.46, p=0.047; interaction: F(1,20)=9.79, p=0.05; Bonferroni's post-test, shSLK vs. paired-control p=0.001; shSLK vs. XFP p=0.003) compared to paired-control and XFP electroporated cells. Only discreet changes were observed in the decay kinetics of feedforward EPSCs (**Fig. 12G,** two-way repeated-measures ANOVA, main effects XFP vs. shSLK: F(1,19)=0.060, p=0.81; electroporated vs. paired-control: F(1,19)=2.58, p=0.124; interaction: F(1,19)=5.44, p=0.031; Bonferroni's post-test, shSLK vs. paired-control p=0.014). Similar changes in IPSC kinetics were seen following electrical stimulation of the white matter. Also in this stimulation paradigm, which recruits feedforward, but also other forms of cortical inhibition, IPSCs showed a delayed time course in shSLK neurons (**Fig. 12I-L**). In contrast, the timing of feedback inhibition was not altered, consistent with the idea that this form of inhibition is not changed in SLK deficient neurons (**Fig. 12Q-X**). These data indicate a pronounced deficit in the amount and timing of thalamocortical feedforward inhibition provided to neurons lacking SLK.

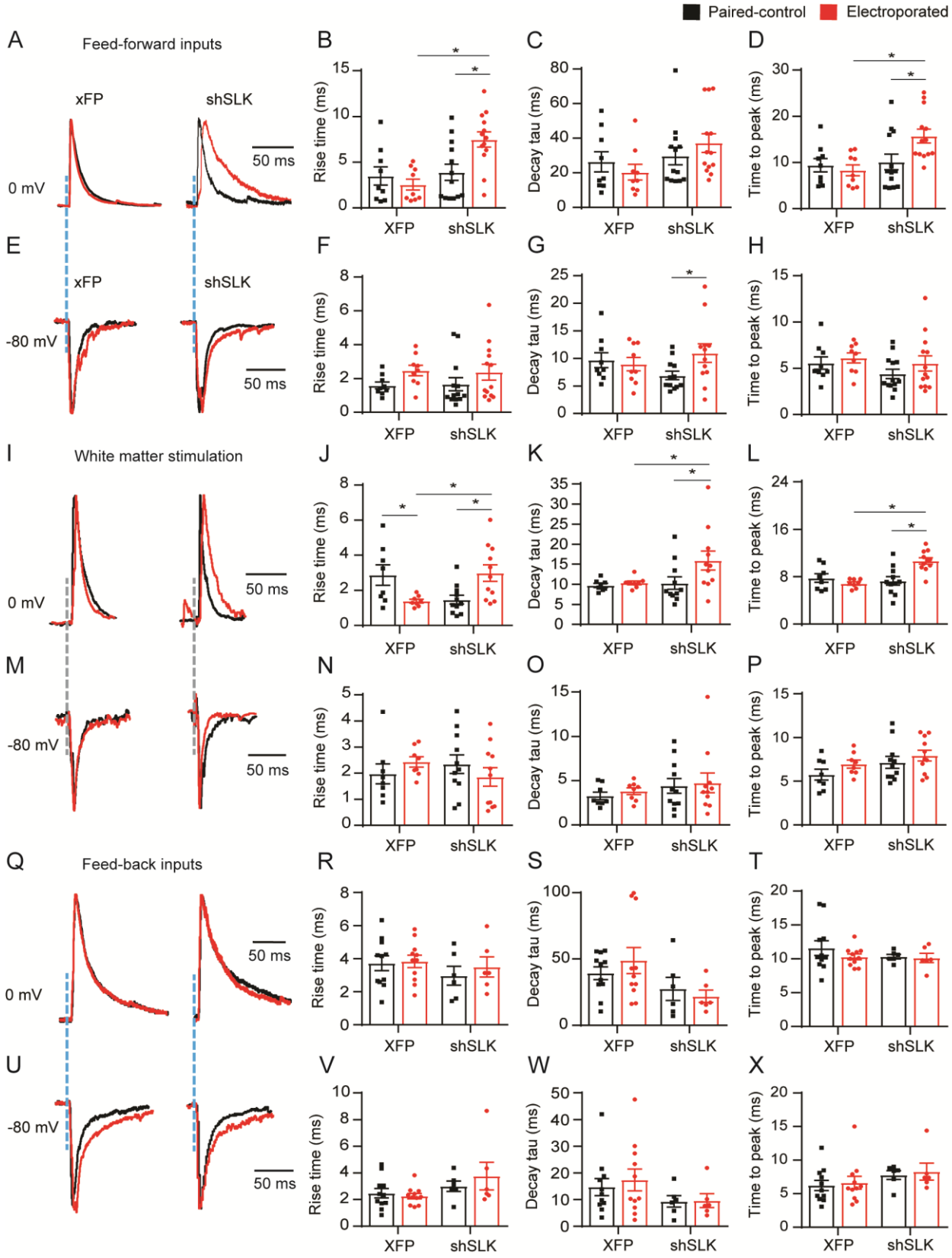
Paired-control
Electroporated
A
Feed-forward inputs
xFP
shSLK
0 mV
50 ms
B
Rise time (ms)
C
Decay tau (ms)
D
Time to peak (ms)
XFP
shSLK
E
-80 mV
F
G
H
I
White matter stimulation
J
K
L
M
N
O
P
Q
Feed-back inputs
R
S
T
U
V
W
X

Figure 12: Timing of inhibition is altered in SLK-deficient neurons. A, E, I, M, Q, U, Representative examples of PSCs after light-based feedforward activation (A, IPSCs; E, EPSCs), white matter stimulation (I, IPSCs; M, EPSCs), and light-based feedback activation (Q, IPSCs; U, EPSCs) in electroporated XFP and shSLK neurons (red traces) and adjacent paired-control PCs (black traces). Dashed lines represent the time point of the stimulus onset. The PSC amplitudes of electroporated cells were normalized to the amplitude of their paired-control PC in order to facilitate kinetics comparisons. B, F, J, N, R, V, Rise time quantifications of responses after light-based feedforward activation (B, F), white matter stimulation (J, N), and light-based feedback activation (R, V). Asterisks indicate post-tests after two-way repeated-measures ANOVA, feedforward IPSCs (B): Bonferroni's post-test, shSLK vs. paired-control $p<0.001$, shSLK vs. XFP $p=0.003$; white matter stimulation IPSCs (F): Bonferroni's post-test, shSLK vs. paired-control $p=0.0162$, shSLK vs. XFP $p=0.0169$, XFP vs paired-control $p=0.0446$. C, G, K, O, S, W, Decay tau quantifications of responses after light-based feedforward activation (C, G), white matter stimulation (K, O), and light-based feedback activation (S, W). Asterisks indicate post-tests after two-way repeated-measures ANOVA, feedforward EPSCs (G): Bonferroni's post-test, shSLK vs. paired-control $p=0.014$; white matter stimulation IPSCs (K): Bonferroni's post-test, shSLK vs. paired-control $p=0.0487$, shSLK vs. XFP $p=0.0243$. D, H, L, P, T, X, Time to peak quantifications of responses after light-based feedforward activation (D, H), white matter stimulation (L, P), and light-based feedback activation (T, X). Asterisks indicate post-tests after two-way repeated-measures ANOVA, feedforward IPSCs (D): Bonferroni's post-test, shSLK vs. paired-control $p=0.001$, shSLK vs. XFP $p=0.003$; white matter stimulation IPSCs (L): Bonferroni's post-test, shSLK vs. paired-control $p=0.0008$, shSLK vs. XFP $p=0.0002$. Data are represented as mean ± SEM.

3.5 Inhibition mediated by PV-expressing and not by SST-expressing interneurons is reduced in SLK-deficient neurons

Once we determined that SLK-deficient neurons display a profound inhibition impairment constrained to feedforward circuits, we aimed to address whether a specific interneuron subtype is responsible for the E/I imbalance observed after thalamic activation. The distribution of thalamic inputs differs across distinct GABAergic neuron-types in cortical areas, preferentially recruiting PV- over somatostatin (SST)-expressing interneurons in the somatosensory cortex (Sermet et al., 2019). In order to measure inhibitory inputs from either type of interneuron onto SLK-deficient cells, we expressed ChR2-eYFP in PV- or SST-expressing neurons in IUE brain areas using an AAV-mediated gene transfer in PV- or SST-cre mouse lines, respectively (**Fig 13A, B**). Two weeks after injection, selective ChR2-eYFP was detected in PV and SST interneurons (**Fig. 13C, G,** PV: 0.93 ± 0.05, SST: 0.78 ± 0.11), which reliably displayed direct photocurrents and action potentials after blue light stimulation (**Fig. 13D-E, H-I**). Light-evoked PSCs recorded in electroporated cells were unaffected by the addition of CNQX and D-AP5 (50µM and 200µM) to the

recording chamber but completely blocked after perfusing gabazine (10µM), indicating that light-evoked responses originate only from GABAergic interneurons in both cases (**Fig 13F, J**).

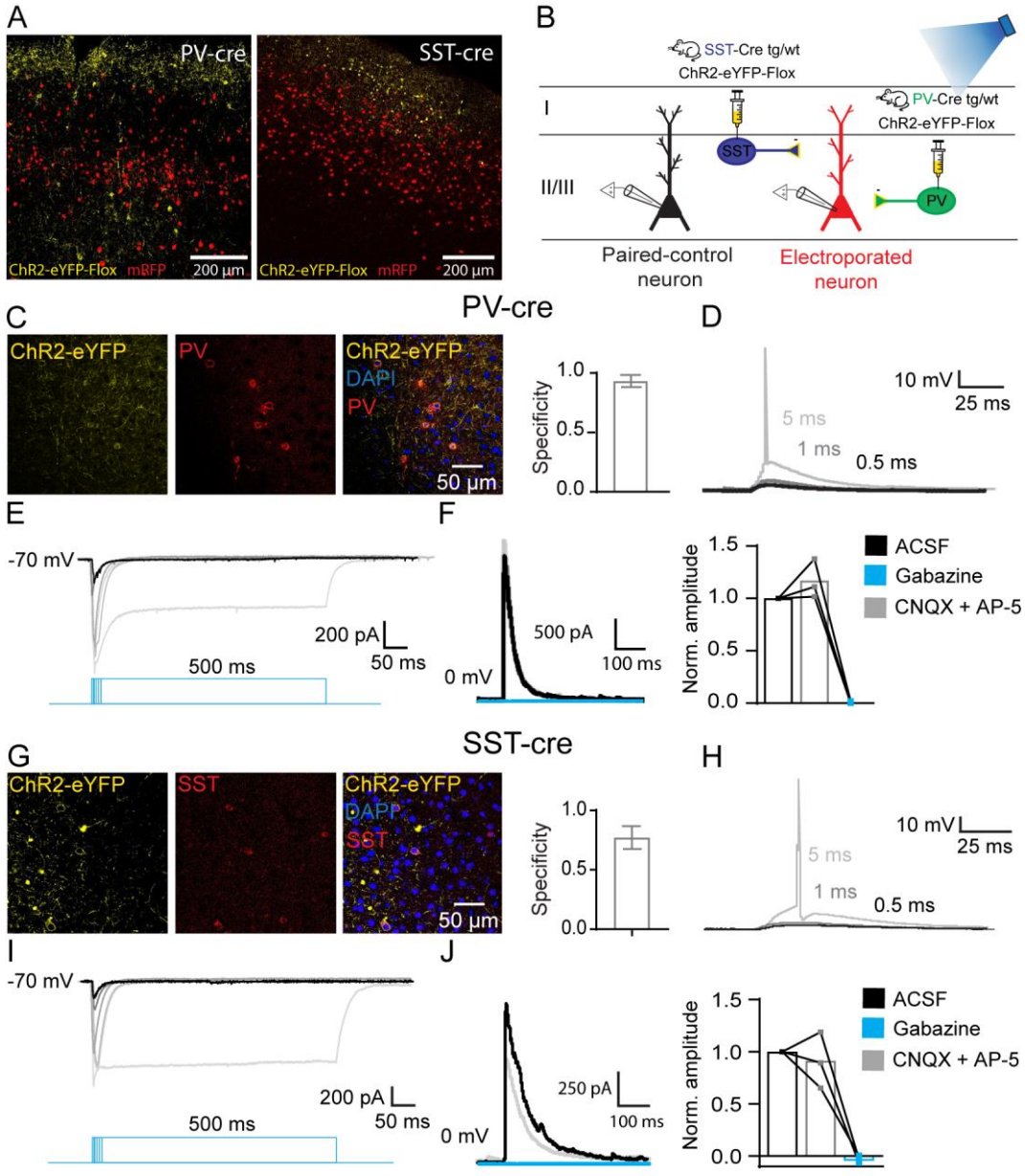

Figure 13: Specific light-based activation of PV- and SST-expressing interneurons. A, ChR2-eYFP expression in PV (left) and SST (right) interneurons in cortical slices electroporated with mRFP. B, Schematic of the experiment. Patch-clamp recordings were carried out from both electroporated pyramidal neurons in layer II/III (either control XFP or shSLK) and non-electroporated neighboring neurons (paired-control) from acute brain slices of PV- and SST-cre animals. C, Immunostaining of PV in cortical slices from PV-cre animals 2 weeks after stereotactic injection of a virus conditionally expressing ChR2. Bar plot shows the fraction of ChR2 positive cells that were reactive to PV antibodies (0.93 ±

0.05). Data are represented as mean ± SEM. D, E, Patch-clamp recordings of ChR2-expressing cells in acute slices from PV-cre animals revealed direct photocurrents that increased in amplitude and duration when light stimulation duration was increased (E). Increasing stimulus duration led to increased depolarization that ultimately resulted in reliable action potential firing (D). F, Representative IPSCs recorded in cortical excitatory neurons after blue light-based stimulation of PV-expressing interneurons while applying a holding voltage of 0 mV. IPSCs were unaffected by the combined application of CNQX and D-AP5 (50 µM and 200 µM, grey traces), but completely blocked by the application of gabazine (10µM, blue traces). PSC amplitudes were normalized to the ACSF condition. Bars represent the mean of the data. G, Immunostaining of SST in cortical slices from SST-cre animals 2 weeks after stereotactic injection of a virus conditionally expressing ChR2. Bar plot shows the fraction of ChR2 positive cells that were reactive to SST antibodies (0.78 ± 0.11). Data are represented as mean ± SEM. H, I, Patch-clamp recordings of ChR2-expressing cells in acute slices from SST-cre animals revealed direct photocurrents that increased in amplitude and duration when light stimulation duration was increased (I). Increasing stimulus duration led to increased depolarization that ultimately resulted in reliable action potential firing (H). J, Representative IPSCs recorded in cortical excitatory neurons after blue light-based stimulation of SST-expressing interneurons while applying a holding voltage of 0 mV. IPSCs were unaffected by the combined application of CNQX and D-AP5 (50 µM and 200 µM, grey traces), but completely blocked by the application of gabazine (10µM, blue traces). PSC amplitudes were normalized to the ACSF condition. Bars represent the mean of the data.

We then assessed the inhibitory responses following light-based stimulation of PV interneurons in both SLK/XFP electroporated pyramidal neurons, and paired-control cells in the same slice preparation. Neurons electroporated with shSLK loss showed a large reduction in IPSC amplitudes, compared to paired-control cells and neurons electroporated only with control XFP (**Fig. 14A-C**, two-way repeated measures ANOVA panel B, main effects XFP vs. shSLK: $F(1,23)=23.44$, $p<0.001$; electroporated vs. paired-control: $F(1,23)=1.34$, $p=0.259$; interaction: $F(1,23)=5.67$, $p=0.0259$; Bonferroni's post-test, shSLK vs. paired-control $p=0.0442$; shSLK vs. XFP $p<0.001$; Mann-Whitney U test panel C, $p=0.0013$). This finding was stable over a large range of optogenetic stimulation intensities and holding potentials (**Fig. 14D, E**). In contrast, no differences were observed in SST-mediated IPSC amplitudes (**Fig. 14F-H**, two-way repeated measures ANOVA panel G, main effects XFP vs. shSLK: $F(1,22)=1.002$, $p=0.33$; electroporated vs. paired-control: $F(1,22)=4.067$, $p=0.056$; interaction: $F(1,22)=0.04$, $p=0.82$; Mann-Whitney U test panel H, $p=0.98$).

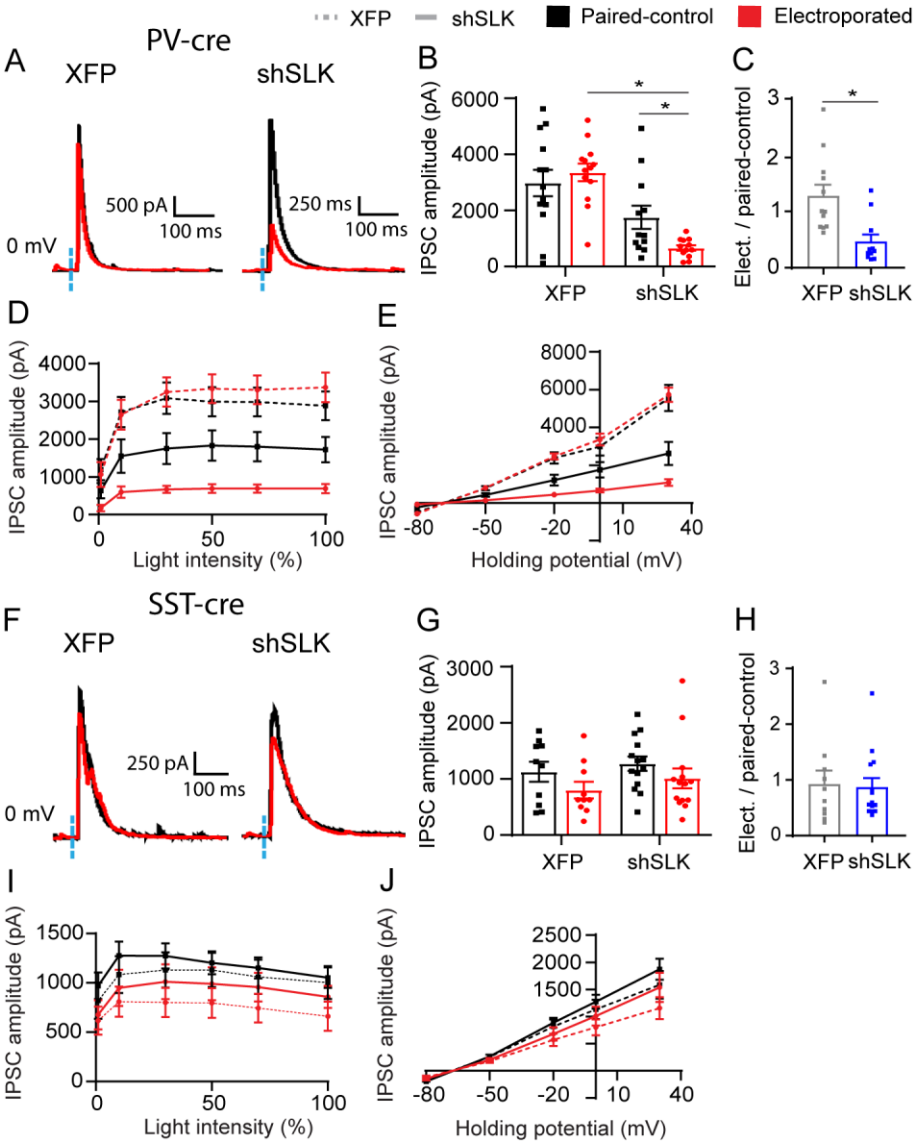

Figure 14: Inhibition supplied by PV-interneurons is reduced in SLK-deficient neurons. A, Representative examples of light-evoked IPSCs in PV-cre animals of electroporated XFP and shSLK neurons (red traces), and adjacent paired-control neurons in the same slice preparation (black traces). Dashed blue lines represent the time point of the stimulus onset. B, Comparison of light-evoked IPSCs in PV-cre animals of neurons expressing shSLK or control XFP compared to their respective, adjacent paired-control PCs. Asterisks indicate post-tests after two-way repeated-measures ANOVA, Bonferroni's post-test, shSLK vs. paired-control p=0.0442; shSLK vs. XFP p<0.001. C, Ratio of light-evoked IPSCs in PV-cre animals of XFP or shSLK neurons expressed as a fraction of IPSCs recorded in adjacent paired-control PCs. Asterisk indicates Mann-Whitney U test, p=0.0013. D, Amplitudes of IPSCs after light-based activation of PV-expressing interneurons across different stimulation intensities (100% = 20.96 mW light fiber output) in shSLK or XFP electroporated neurons compared to their respective, adjacent paired-control PCs. E, Amplitudes of IPSCs after light-based activation of PV-expressing interneurons across different holding potentials at 30% of light intensity in shSLK or XFP electroporated neurons compared to their respective, adjacent paired-control PCs. F,

Representative examples of light-evoked IPSCs in SST-cre animals of electroporated XFP and shSLK neurons (red traces), and adjacent paired-control neurons in the same slice preparation (black traces). Dashed blue lines represent the time point of the stimulus onset. G, Comparison of light-evoked IPSCs in SST-cre animals of neurons expressing shSLK or control XFP compared to their respective, adjacent paired-control PCs. H, Ratio of light-evoked IPSCs in SST-cre animals of XFP or shSLK neurons expressed as a fraction of IPSCs recorded in adjacent paired-control PCs. I, Amplitudes of IPSCs after light-activation of SST-expressing interneurons across different stimulation intensities (100% = 20.96 mW light fiber output) in shSLK or XFP electroporated neurons compared to their respective, adjacent paired-control PCs. J, Amplitudes of IPSCs after light-activation of SST-expressing interneurons across different holding potentials at 30% of light intensity in shSLK or XFP electroporated neurons compared to their respective, adjacent paired-control PCs. Data are represented as mean ± SEM.

PV interneuron-mediated IPSCs showed robust short-term depression without changes in shSLK electroporated neurons (**Fig. 15A**). As observed after white matter and thalamocortical stimulation, IPSCs originated from PV interneurons showed slower kinetics with reduced time to peak in SLK-deficient neurons compared to XFP control cells (**Fig. 15D,** two-way repeated-measures ANOVA, main effects XFP vs. shSLK: $F(1,23)=11.37$, $p=0.0026$; electroporated vs. paired-control: $F(1,23)=0.032$, $p=0.86$; interaction: $F(1,23)=0.80$, $p=0.38$; Bonferroni's post-test, shSLK vs. XFP $p=0.0092$). No changes were observed in the short-term plasticity features and kinetics of SST interneuron-mediated IPSCs (**Fig. 15E-H**).

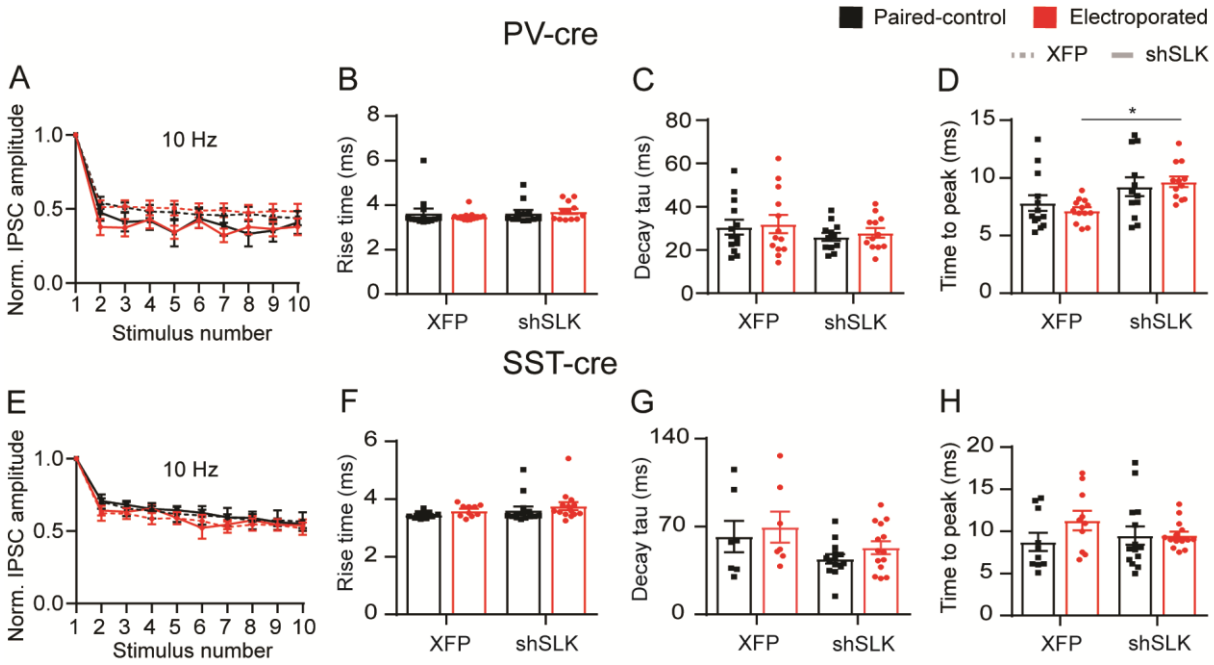

Figure 15. Short-term plasticity and kinetics of PV and SST interneuron-mediated inhibition in SLK-deficient neurons. A, E, IPSC amplitudes (normalized to first response) of synaptic responses evoked by 10 Hz light-based stimulation trains of PV- (A) and SST-expressing interneurons (E) in neurons electroporated with shSLK or control XFP compared to their respective, adjacent paired-control PCs. B-D, Rise time (B), decay tau (C), and time to peak (D) quantifications of PV interneuron-mediated IPSCs in shSLK and control XFP neurons, compared to their respective, adjacent paired-control PCs. Asterisks indicate post-tests after two-way repeated-measures ANOVA, time to peak (G): Bonferroni's post-test, shSLK vs. XFP p=0.003. F-H, Rise time (F), decay tau (G), and time to peak (H) quantifications of SST interneuron-mediated IPSCs in shSLK and control XFP neurons, compared to their respective, adjacent paired-control PCs. Data are represented as mean ± SEM.

This selective loss of PV interneuron-mediated inhibition could be due to a loss of specific inhibitory sites on SLK-deficient neurons driven by cell-autonomous mechanisms, but it could also be due to presynaptic changes. To address this possibility, we performed quantifications of interneuron numbers and paired-pulse experiments. Immunostaining of PV- and SST-expressing cells in brain slices from XFP and shSLK electroporated animals revealed that there were no changes in the density of either interneuron subtype across all cortical layers and when quantified only within electroporated areas (**Fig. 16A, B, D, E**). In addition, we found no differences in the paired-pulse ratio of responses recorded in shSLK neurons after specific PV- or SST interneuron activation (**Fig. 16C, F**). These results indicate that it is unlikely that changes in presynaptic release probability at the PV-pyramidal neuron synapses or changes in cell density contribute to the loss of inhibition after SLK loss. Moreover, our results suggest that SLK may play an important role in the establishment of inhibitory synapses between PV-expressing interneurons and cortical pyramidal cells.

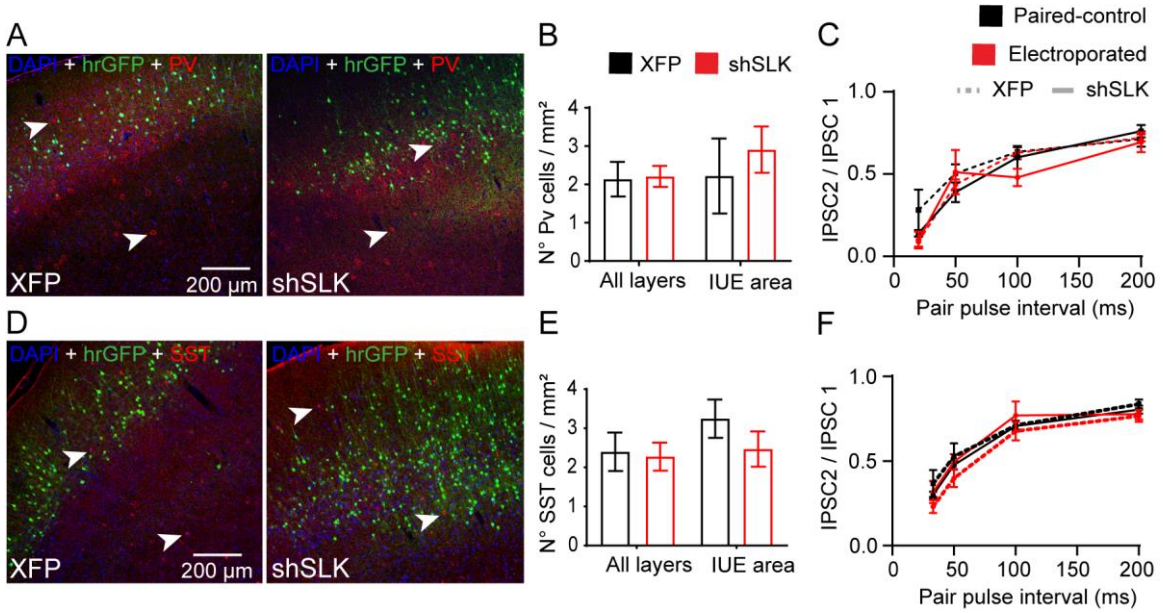

Figure 16. The number and paired-pulse ratio of PV and SST interneurons are unaltered in SLK-deficient animals. A, D, PV (A), and SST (D) immunostaining of cortical slices electroporated with control XFP (left panels) and shSLK (right panels). B, E, Quantification of the density of PV- (B) and SST-expressing neurons (E) across all cortical layers and only within the electroporated area. No changes in the number of either interneuron were observed in shSLK electroporated animals. C, F, Pair pulse ratio (faction of second to first response) recorded in electroporated and paired-control excitatory neurons after light-based activation of PV- (C) and SST-expressing interneurons (F). There were no differences between groups across any of the frequency stimulation performed. Data are represented as mean ± SEM.

3.6 shSLK neurons exhibit increased activity

The marked effect of SLK-KD on feedforward inhibition predicts that sensory recruitment of these neurons occurs with a pronounced deficit in inhibition, suggesting that they may be hyperactive in intact animals. We tested this idea using c-fos labeling, a technique that is useful to screen for general changes in the levels of neuronal activity. We assessed the c-fos immunolabelling in electroporated cells in animals that received control plasmids containing only hrGFP (**Fig. 17A**), and in animals electroporated with shSLK-hrGFP (**Fig. 17B**). A quantification of the number of hrGFP expressing cells that also expressed c-fos was significantly increased in shSLK electroporated animals (**Fig. 17C**, unpaired t-test, $t_{(21)}$=3.38, p=0.0028). Likewise, the c-fos fluorescence intensity measured in the somatic area of hrGFP expressing cells was markedly higher in neurons lacking SLK (**Fig. 17D,** unpaired t-test, $t_{(21)}$=3.39, p=0.0031). Thus, SLK-deficient neurons seem to constitute a more active cell population compared to control neurons in intact animals.

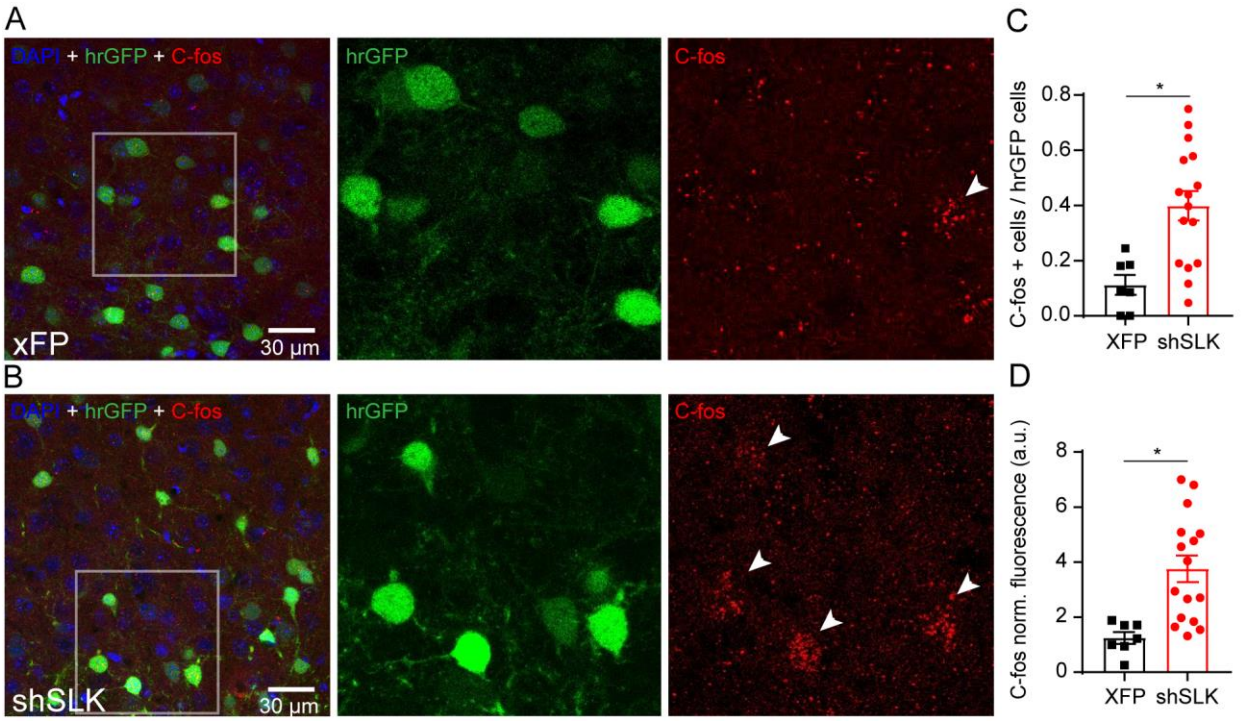

Figure 17: shSLK neurons exhibit increased levels of basal activity. A, B, C-fos immunostaining of cortical slices electroporated with control XFP (A) and shSLK (B). XFP electroporated cells showed sporadic expression of c-fos (arrowheads). In contrast, shSLK electroporated neurons displayed a more prominent c-fos protein expression (arrowheads). C, D, Quantification of the proportion of hrGFP-expressing neurons also expressing c-fos (C), and the c-fos labeling intensity (D) in control XFP and shSLK electroporated neurons. Asterisks indicate significance in unpaired t-test, p=0.0028 for panel C, p=0.0031 for panel D. Data are represented as mean ± SEM.

3.7 Identification of candidate molecular pathways correlated with altered inhibitory function in cortical pyramidal neurons using patch-seq

Our results establish that SLK is important for intact feedforward PV-mediated inhibition. This raises questions about what molecular, cell-autonomous pathways are responsible for the regulation of inhibition. To assess the specific connection between the E/I balance and the transcriptional landscape, we established patch-seq protocols, in which it is possible to correlate electrophysiological properties with gene expression patterns (**Fig. 18A**). The patch-seq technique combines whole-cell patch-clamping and single-cell RNA sequencing (scRNA-seq). In brief, cortical layer II/III neurons either expressing control XFP or shSLK (in addition to 3 striatal cells for downstream comparisons) were recorded with a patch-clamp electrode containing internal solution optimized for patch-seq. Following the electrophysiological recordings, the cell contents were aspirated into the

patch pipette and extruded into a tube containing lysis buffer for cDNA synthesis (**Fig. 18A**). We recorded and collected cell contents from 91 neurons, of which 71 samples were suitable for sequencing after showing ideal average cDNA concentration and length (< 200 pg/µl and < 1000 pb, respectively).

The functional analyses confirmed the selective reduction of inhibition in SLK-KD neurons reported before, with a reduction of mIPSC but unchanged mEPSC frequencies (**Fig. 18B, C**). Moreover, we identified a reduction in cell capacitance in neurons lacking SLK (**Fig. 18C**). Therefore, we correlated gene expression changes to IPSC frequency and cell capacitance, given that alterations in these electrophysiological features can be linked to an inhibitory or dendritic phenotype, respectively.

Sequenced reads were aligned to the mouse genome (see methods). The percentage of the total reads matched to the reference genome was variable across samples, with only a few samples showing alignment rates below 50% (**Fig. 18D**). We used reads aligned to both exonic and intronic gene sequences for further analyses in order to maximize gene counts as reported for other patch-seq datasets (Cadwell et al., 2017b; Scala et al., 2020). Similar to other studies, our samples showed variable proportions of reads originated from intronic unspliced transcripts, with an average intronic composition of 33.96 % ± 2.21 across samples (**Fig. 18E**) (Cadwell et al., 2017b; Scala et al., 2020).

In order to exclude poor-quality samples that may distort downstream analyses, we checked and computed basic quality control indicators that may reflect foreign DNA contamination, RNA degradation, or technical biases during library preparation and sequencing. We first checked whether samples displayed aligned reads to non-neuronal cell markers. Only 2 samples showed a considerably high number of reads mapped to the astrocyte marker GFAP, with none or very few reads observed for the oligodendrocyte marker Cldn11 (**Fig. 18F**). Next, basic quality control metrics were calculated to remove outlier samples displaying poor-quality features (Lun et al., 2016b; Amezquita et al., 2020). We used an adaptive threshold, which assumes that most of the dataset consists of high-quality cells, and removed samples with more than 3 median absolute deviations (MADs) below (library size and number of genes expressed) or above (proportion of mitochondrial genes) the median of the quality control metrics across samples (**Fig. 18G**).

Finally, we explored the expression profile of all genes in our dataset in order to identify low-abundance features and non-biological patterns of expression. We identified the 50 most highly expressed genes across all samples, which as expected, were dominated by constitutively expressed genes such as ribosomal, mitochondrial, and other house-keeping transcripts (**Fig. 18H**). Next, we selected genes with a minimum of 1 read in at least 28 samples, the smallest experimental group, in an attempt to dramatically reduce the number of low-abundance genes that do not contain enough information for reliable statistical inference (**Fig. 18I**). Thus, after applying quality control checks, we ended up with a dataset consisting of 69 samples (28 XFP, 38 shSLK, 3 striatum) and a total of 3889 genes, which was used for all downstream analyses.

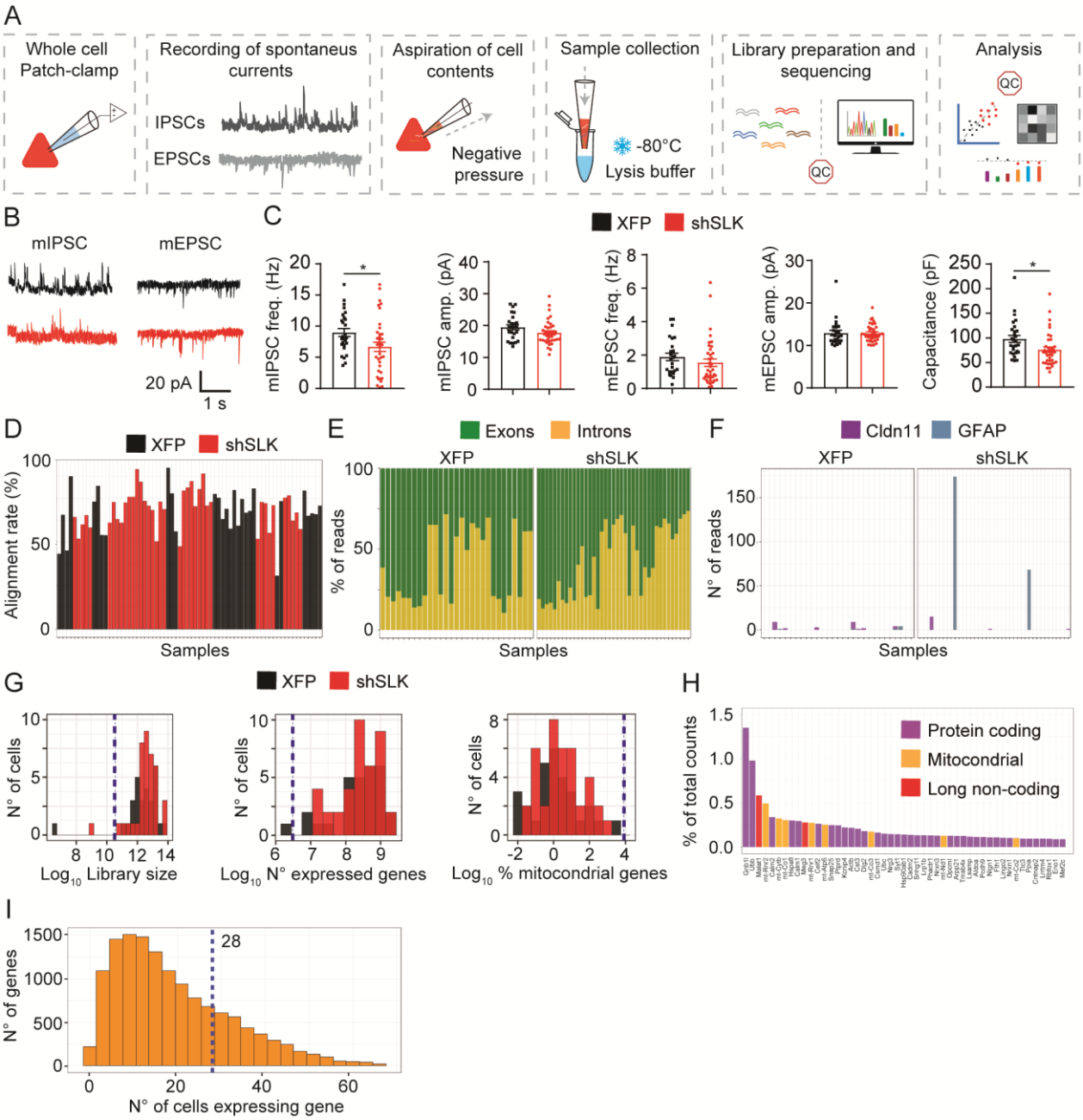

Figure 18: Patch-seq workflow and quality control checks. A, Workflow schematic of patch-seq methodology. Cortical layer II/III neurons either expressing control XFP or shSLK were recorded with a patch-clamp electrode containing internal solution optimized for patch-seq. Next, cell contents were aspirated into the patch pipette and extruded into a tube containing an optimized lysis buffer and stored at -80°C. Quality control (QC) checks were performed on cDNA library profiles and aligned reads to discard low-quality samples. B, Representative examples of miniature IPSCs in electroporated XFP (black traces) and shSLK neurons (red traces). C, IPSC/EPSC frequency and amplitude and cell capacitance comparisons of neurons expressing shSLK and control XFP. Asterisks indicate significance in unpaired t-test (p=0.029 for IPSC frequency, p=0.016 for cell capacitance). Data are represented as mean ± SEM. D, Percentage of reads per sample that were aligned to the mouse genome. E, Faction of aligned reads per sample mapped

to exonic or intronic sequences of the mouse genome. F, Raw reads per sample of Cldn11 and GFAP, cell markers of oligodendrocytes and astrocytes, respectively. G, Histograms of the log_{10}-transformed total number of reads (left), number of detected genes (middle), and percentage of mitochondrial genes (right) per sample. Samples with values deviating at least 3 times from the median absolute deviation (MAD, dashed lines) were classified as low quality and removed from further analysis. H, Percentage of total read count of the 50 most expressed genes across all samples by type of RNA. I, Histogram of the number of cells expressing each gene. Only genes expressed in at least 28 samples (size of the smallest experimental group, dashed line) were selected for further analysis.

We then performed t-distributed stochastic neighbor embedding (t-SNE) analyses in order to visualize how samples distribute in a reduced dimensional space according to the expression of the selected 3889 genes. Samples collected from XFP and shSLK neurons did not form separated clusters. In contrast, all samples collected from striatal cells grouped together in the reduced dimensional space (**Fig. 19A**). Next, we determined which genes were differentially expressed (DE) when comparing shSLK and XFP neurons. Using a recently described analysis approach that has been shown to be particularly suitable for scRNA-seq data with a high number of zero counts and a low number of samples (DEsingle) (Miao et al., 2018), we found 24 DE genes. Ten genes were downregulated in shSLK neurons, and 14 genes displayed upregulation (**Fig. 19B**, gene list in **Table 1**). In addition, DEsingle classifies DE genes in three categories: DEs (different expression status), DEa (different expression abundance), and DEg (general differential expression). All 24 DE genes were classified as DEa or DEg, indicating that these genes showed differences only in the actual RNA abundance or in both the actual RNA abundance and the proportion of cells with zero counts, respectively (**Table 1)**. For the 24 DE genes, we explored the association with human diseases using the Disgenet2r platform, which includes gene-disease associations from a large number of databases. Eighteen of the genes found to be altered in SLK-deficient neurons have been described to be involved in human disorders, especially in neoplasms and nervous system pathologies (**Fig. 19C**).

How does the abundance of the DE genes relate to the changes in electrophysiological parameters? Correlation of gene expression levels with functional parameters using a Spearman rank correlation yielded significant correlations with function in a subset of DE genes (**Fig. 19D**, gene list in **Table 2**). **Fig. 19E** shows functional parameters for each cell plotted above the relative abundance of genes found to be correlated to

electrophysiological features. Genes involved in neuronal growth and regulation of cellular morphology (SNX6, Dctn4, Spock2, and Ddx6) were found to be correlated with neuronal capacitance, which can be used as a functional proxy for neuronal membrane area. On the other hand, genes correlated with mIPSC frequency encode the transcription factors and guidance molecules Smarcc2, Sgms, and Megf9. It is important to note that only SNX6 and Smarcc2 have a sensible direction of expression change with respect to the direction of their correlation with the electrophysiological properties (**Fig. 19F**). Low expression of SNX6 and Smarcc2 correlated with the reduced capacitance or mIPSC frequency of SLK-deficient neurons, respectively.

Thus, our patch-seq experiments confirmed the alterations in synaptic inhibition and membrane properties produced after SLK loss reported previously (Schoch et al., 2021). In addition, we reported DE genes correlated and non-correlated with electrophysiological properties that can help to assess what molecular, cell-autonomous pathways are responsible for the morphologic and inhibitory synaptic phenotype observed after SLK loss.

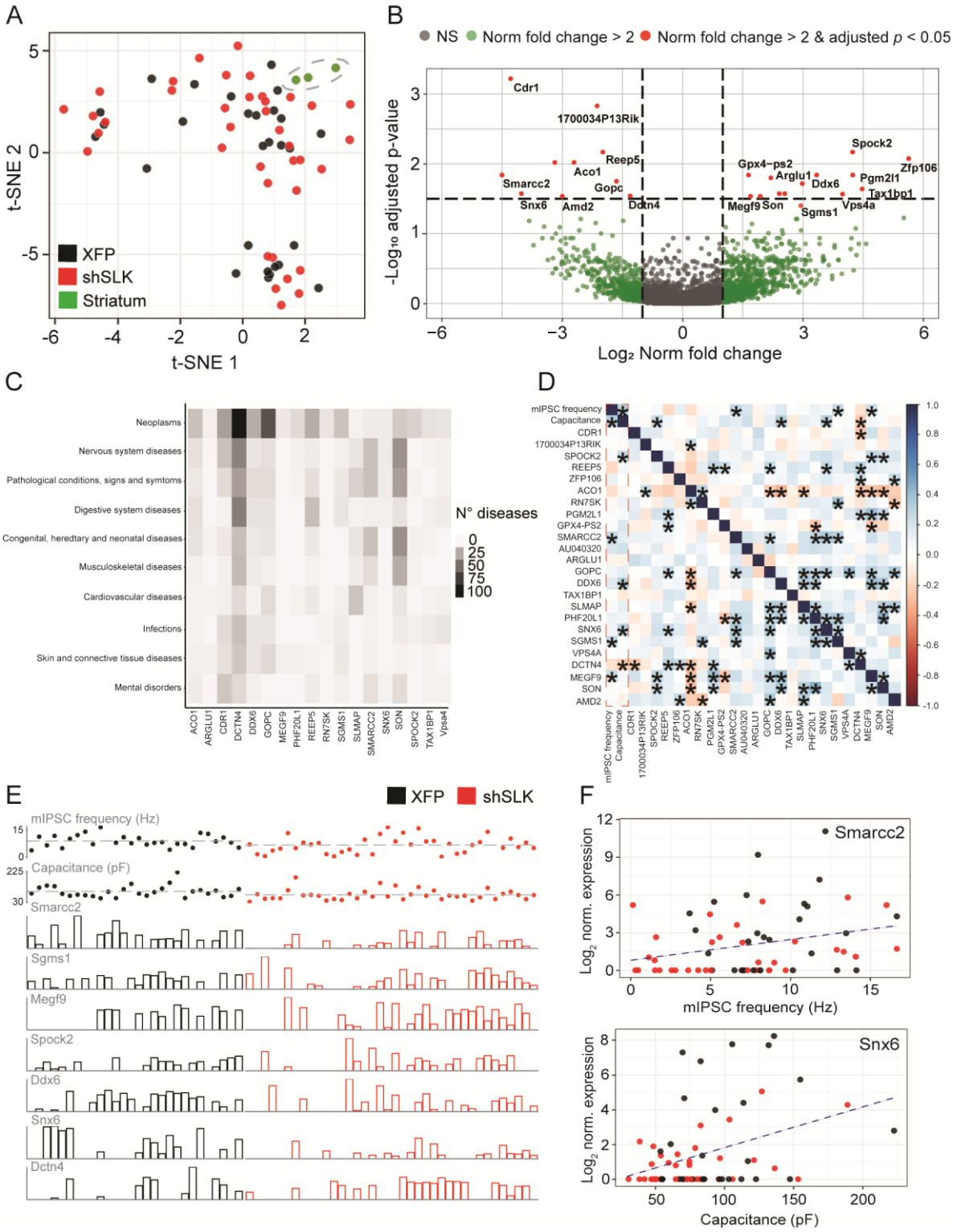

Figure 19: Correlation of altered inhibitory function of shSLK neurons with candidate molecular pathways using patch-seq. A, t-SNE analysis of log_2-transformed normalized read counts of samples collected from cortical XFP/shSLK electroporated cells and non-electroporated striatal cells. XFP and shSLK neurons did not form separated clusters. In contrast, striatal cells grouped together in the reduced-dimensional space (dashed grey circle). B, Volcano plot showing 24 differentially expressed genes (DE, red circles).

Dashed lines demark genes with an absolute normalized fold change higher than 2 (vertical dashed lines) and an adjusted p-value lower than 0.05 (horizontal dashed line). C, Heatmap displaying the number of diseases by type of disease associated with DE genes according to the gene discovery platform Disgenet2r. D, Correlation heatmap of the normalized expression of DE genes and electrophysiological parameters, showing 7 genes significantly correlated with either mIPSC frequency (3 genes) or cell capacitance (4 genes). Colour gradient indicates Spearman correlation coefficient (blue, positively correlated; red, negatively correlated), while asterisks indicate significant correlations with *p*-values <0.05. E, Plot showing mIPSC frequency, cell capacitance, and normalized expression of DE genes found to be significantly correlated to electrophysiological parameters from individual electroporated XFP and shSLK neurons. F, Scatter plots of normalized expression of selected genes (Smarcc2 and Snx6) and significant correlated electrophysiological properties (IPSC frequency and capacitance, respectively). Dashed lines represent the best-fitted line of linear correlation. Their positive slopes indicate positive correlations.

Table 1. Differentially expressed genes in shSLK neurons. Using a zero-inflated negative binomial model with DEsingle, we found 24 differentially expressed genes in shSLK compared to XFP neurons. DEsingle classifies genes with altered expression profiles in three categories: DEs (different expression status), DEa (different expression abundance), and DEg (general differential expression), depending on whether the genes showed differences in the proportion of cells with zero counts, the actual RNA abundance or both, respectively.

Gene name	Norm. fold change	Desingle DE type
Cdr1	0.046	DEg
1700034P13Rik	0.211	DEa
Spock2	16.718	DEa
Reep5	0.224	DEa
Zfp106	44.046	DEg
Aco1	0.136	DEg
Rn7sk	0.098	DEg
Pgm2l1	16.749	DEg
Gpx4-ps2	2.772	DEa
Smarcc2	0.039	DEg
AU040320	8.982	DEg
Arglu1	4.076	DEg
Gopc	0.283	DEg
Ddx6	7.014	DEa

Tax1bp1	19.712	DEg
Slmap	4.718	DEg
Phf20l1	5.178	DEg
Snx6	0.055	DEa
Sgms1	7.705	DEg
Vps4a	14.050	DEg
Dctn4	0.359	DEa
Megf9	2.870	DEg
Son	3.393	DEg
Amd2	0.111	DEg

Table 2. Correlation of gene expression levels with electrophysiological parameters. Spearman rank correlation yielded significant correlations of seven differentially expressed genes with either capacitance or IPSC frequency in shSLK neurons.

Capacitance		
Gene name	**Spearman correlation coefficient**	**p-value**
Ddx6	0.32	0.0094
Snx6	0.30	0.014
Dctn4	-0.24	0.048
Spock2	0.25	0.041
IPSC frequency		
Gene name	**Spearman correlation coefficient**	**p-value**
Megf9	0.25	0.049
Sgms1	0.28	0.025
Smarcc2	0.28	0.026

4. Discussion

Developmental focal lesions represent highly variable pathologies that require long-term treatment and even surgical removal of affected brain areas when refractory seizures arise. The wide spectrum of cortical abnormalities exhibits diverse anatomical alterations, genetic profiles, and clinical manifestations. This diversity has made it difficult to precisely determine what drives the emergence of hyperexcitability. In this study, we aimed to better understand the microcircuit features of morphological-altered neurons within cortical networks, a major shared hallmark of developmental focal lesions frequently associated with drug-resistant seizures. To this end, we used a newly generated model of dysplastic neurons that mimics the reduced expression of SLK found in dysmorphic cellular elements from human biopsies. shRNA-mediated KD of SLK strongly impairs dendritic and inhibitory synapse formation and leads to an aggravated seizure phenotype. We demonstrated that the downregulation of SLK in cortical neurons causes a selective loss of synaptic inhibition and a shift in the E/I balance. Using optogenetic approaches, we found that the inhibition impairment of SLK-deficient neurons is confined to feedforward inhibitory circuits, and does not affect feedback or lateral inhibition. Interestingly, only the inhibition mediated by PV-expressing interneurons seems to be affected in neurons lacking SLK. These results point to the downregulation of SLK as a key factor contributing to the excitatory-inhibitory imbalance observed within developmental focal lesions featuring dysplastic neurons. The fact that only feedforward PV-mediated inhibition is affected in SLK-deficient neurons, may suggest that cortical networks containing dysplastic neurons can be susceptible to generate hyperexcitability when sensory and motor information arrives from the thalamus. Finally, our results also suggest a relevant and cell-autonomous role for SLK in the establishment of inhibitory synapses between PV-expressing interneurons and pyramidal cells.

4.1 SLK deficiency leads to a strong impairment of synaptic inhibition and causes an excitatory-inhibitory imbalance in cortical neurons

We first intended to determine whether neurons with decreased SLK expression differentially recruit excitation and inhibition by electrically stimulating presynaptic axon tracks at the subcortical white matter. We observed a strong reduction in the amplitude of

evoked IPSCs in SLK-KD neurons compared to neurons electroporated with control plasmids and paired-control PCs. This result is in line with the reduction in inhibitory synapse density found in cells lacking SLK (Schoch et al., 2021). Importantly, 42.5% loss in inhibitory postsynapse density triggered 86.42% reduction (compared to XFP neurons) and 81.38% reduction (compared to paired-control PCs) in IPSC amplitude. This dichotomy is known from other manipulations that reduce inhibitory synapse density, where conditional knockout (KO) of neuroligin-2, a transsynaptic cell-adhesion molecule required for inhibitory synapse formation, decreases inhibitory synapse numbers ~15% but GABAergic transmission by ~45% (Liang et al., 2015). These observations may suggest non-linear effects from the loss of inhibitory postsynapses or impairments in additional synaptic mechanisms. We also observed changes in inhibitory short-term plasticity features of SLK-deficient neurons. In control neurons, we observed a strong short-term inhibitory synaptic depression characteristic of synapses with a high initial release probability that then decreases in strength mostly due to presynaptic vesicle depletion (Zucker and Regehr, 2002). In contrast, inhibitory synaptic depression was not observed in SLK-KD neurons after stimulation trains at 10 Hz, being their first responses considerably smaller compared to control cells and more similar to the subsequent IPSCs.

The functional inhibitory alterations observed after SLK loss might be explained by the reduced inhibitory postsynapse density that the downregulation of this protein causes in cortical neurons, given that similar structural postsynaptic changes have been reported to functionally translate into changes in evoked IPSC amplitudes, mIPSC frequencies, and E/I balance without altering spike firing properties (4 features observed in SLK-KD neurons) (Kneussel et al., 1999; Poulopoulos et al., 2009; Liang et al., 2015; Babaev et al., 2016; Chen et al., 2020; Kim et al., 2021). Interestingly, we did not observe any of these inhibitory alterations in paired-control neurons, suggesting that neighboring cells within networks containing SLK-deficient neurons do not show secondary or indirect effects on the recruitment of inhibitory inputs. Taken together, these results link the loss of SLK to a profound functional inhibitory impairment in cortical neurons. We will discuss the possible mechanisms by which SLK might modulate inhibitory synapses function later in this chapter.

In contrast, the EPSCs of SLK-KD neurons were not significantly altered compared to control cells. However, we did observe a tendency of reduction in their amplitudes. This may originate from the fact that the loss of SLK produces aberrant dendritic arbors with loss of secondary and high-order dendrites, perhaps causing a reduction in the total number of both inhibitory and excitatory synapses (Schoch et al., 2021). Importantly, distal dendrites of excitatory neurons are known to display large numbers of excitatory synapses (Megías et al., 2001). Nevertheless, only the inhibitory and not the excitatory postsynapse density is altered in the remaining dendrites of SLK-KD neurons, which is most likely driving the strong alterations we observed in synaptic inhibition.

Despite the small changes in excitation observed in SLK-deficient neurons, the impairment in inhibition was considerably more robust. This caused the E/I balance of these neurons to be significantly shifted towards excitation. An altered E/I balance is commonly thought to underlie epileptogenesis and seizure generation after insufficient or excessive regulatory mechanisms that cause augmented excitation, reduced inhibition, or both, favoring a hyperexcitable state (Fritschy, 2008; Shao et al., 2019; Sohal and Rubenstein, 2019). To avoid this, the activity of neuronal networks is maintained within a narrow window by complex and finely-regulated physiological processes at different scales (Marder and Goaillard, 2006; Fritschy, 2008). At a circuit level, features like the number of excitatory and inhibitory neurons, the pattern of synaptic connectivity, neuronal synchronization, interaction with non-neuronal cell types, among others, can drastically alter the E/I balance (Fritschy, 2008; Sohal and Rubenstein, 2019). At the neuronal level, the number of excitatory and inhibitory synapses is highly regulated in order to maintain appropriate ratios of excitatory versus inhibitory synaptic inputs and control neuronal output (Megías et al., 2001; Fares and Stepanyants, 2009; Sohal and Rubenstein, 2019; Iascone et al., 2020). Specifically, alterations in inhibitory synapses have been observed to increase the E/I balance and overall the excitability of neurons, similarly to what found in SLK-deficient neurons (Poulopoulos et al., 2009; Lionel et al., 2013; Babaev et al., 2016; Chen et al., 2020; Dzyubenko et al., 2021; Jami et al., 2021; Kim et al., 2021). Therefore, the reduction of inhibitory postsynapses caused by SLK loss may play an important role in contributing to the E/I imbalance and the emergence of network hyperexcitability observed in the most highly-epileptogenic developmental brain lesions featuring

dysplastic neurons (Cepeda et al., 2003, 2005a; André et al., 2004; Andres et al., 2005; Calcagnotto et al., 2005; Möddel et al., 2005; Koh et al., 2018; Goz et al., 2020)

4.2 SLK-deficient neurons lack proper feedforward inhibition mediated by PV-expressing interneurons

The cortex is formed by densely interconnected neuronal populations, whose cell diversity and sophisticated connectivity patterns define its capacity to process and integrate complex information (Harris and Mrsic-flogel, 2013). Incoming signals are filtered and processed within distinctive inhibitory circuit motifs featuring specialized computational roles. Feedforward inhibition produces input normalization by regulating the rate at which the neuron activity scales in response to increasing excitatory inputs (gain control) (Pouille and Scanziani, 2001; Isaacson and Scanziani, 2011; Delevich et al., 2015; Ferguson and Gao, 2018a). In contrast, feedback inhibition integrates the output of a given principal cell and feeds back inhibition, efficiently controlling population activity (Paz and Huguenard, 2015; Tremblay et al., 2016; Feldmeyer et al., 2018). Therefore, after we determined that the neuronal loss of SLK reduces the amplitude of inhibitory synaptic currents, we assessed whether this inhibition impairment preferentially affects feedforward or feedback inputs. This is relevant since different circuitry motifs preferentially recruit particular neuronal subtypes and are activated under specific signal processing mechanisms, providing us with relevant information about the network state and features in which the E/I balance of dysplastic neurons is triggered.

We first evaluated if feedforward circuits are affected in SLK-KD neurons. The thalamus, especially the ventral posteromedial nucleus and the posteriormedial complex (VPM and POm, respectively), are the main sources of feedforward excitation and inhibition in the motor and somatosensory cortices (Oberlaender et al., 2012; Hunnicutt et al., 2014; Sermet et al., 2019). Thalamic glutamatergic axons directly activate cortical excitatory neurons and produce disynaptic inhibition after the activation of local interneurons (Oberlaender et al., 2012; Tremblay et al., 2016). This innervation pattern and functional connectivity features were observed when we expressed ChR2-eYFP in VPM and POm through a viral approach and recorded from cortical neurons. Under this experimental setup, SLK-deficient neurons showed a strong reduction of light-based IPSC amplitudes compared to XFP and paired-control neurons. This result suggests that SLK-KD neurons

might face augmented excitability after thalamocortical activation, given that feedforward inhibition maintains cortical network stability by normalizing incoming sensory inputs (Pouille et al., 2009).

In addition, IPSCs displayed changes in their kinetics with longer rise time and time to peak. Despite its disynaptic nature, feedforward inhibition reaches cortical excitatory neurons with a delay of only about 1-2 ms after feedforward excitation (in our experiments: 2.18 ms delay; EPSC time to peak XFP neurons: 6.13 ± 0.54 ms; IPSC time to peak XFP neurons: 8.31 ± 1.17 ms) (Pinto et al., 2000; Alonso and Swadlow, 2005; Sermet et al., 2019), producing a limited time window for excitatory inputs to summate and evoke an output in the postsynaptic cell. The slower kinetics of feedforward inhibition in SLK-deficient neurons (delay increased to 9.61 ms) may be widening this tight time window and allowing persistent and asynchronous thalamic activity to over-activate cortical neurons. In this sense, failure in feedforward inhibition has been linked to an increased seizure propagation speed (Trevelyan et al., 2007), the development of hyperexcitability in focal cortical dysplasia generated by cortical freeze lesions (Sun et al., 2005), and animal models of absence epilepsy (Sasaki et al., 2006; Paz et al., 2011; Maheshwari et al., 2013) and autism (Antoine et al., 2019).

In the case of feed-forward excitation, EPSC amplitudes were reduced in SLK-deficient neurons compared to their paired-controls, which can be attributed to their reduced dendritic complexity as mentioned before. Nonetheless, the E/I balance of feedforward inputs onto SLK-KD neurons was shifted towards excitation, suggesting destabilized cortical networks as sensory information arrives from the periphery in the form of thalamic excitation. Remarkably, we did not find any difference in the amplitude IPSCs after light-based activation of local cortical excitatory neurons, indicating that the inhibition impairment of SLK-deficient neurons mostly affects feedforward circuits.

How can this inhibition impairment be specific to only one microcircuit motif? We hypothesized that the preferential recruitment of different types of interneurons by each cortical microcircuit motif is what may underlie the specificity of SLK-KD inhibitory impairment. Feedback circuits are known to recruit both, PV and SST interneurons. However, due to the differences in their synaptic (short-term facilitation) and intrinsic properties, SST interneurons seem to be more dependent on the increase in local

excitatory firing rates and therefore preferentially activated in cortical feedback inhibitory circuits (Silberberg and Markram, 2007; Kwan and Dan, 2012; Paz and Huguenard, 2015; Callaway, 2016). In contrast, feedforward thalamic inputs strongly activate cortical fast-spiking PV-expressing interneurons (Beierlein et al., 2003; Cruikshank et al., 2007; Sermet et al., 2019). Optogenetic experiments where ChR2 was expressed in VPM and POm thalamic nuclei (as done in this study), revealed that thalamic activation strongly recruits PV interneurons, showing synaptic depolarizations even larger than the ones recorded in excitatory neurons. In addition, SST expressing interneurons appeared to receive only weak feedforward inputs, with excitatory postsynaptic potential amplitudes and rate of rise 11.6 and 45.5 times smaller than in PV-expressing interneurons (Sermet et al., 2019). These results demonstrated that feedforward thalamic inputs preferentially recruit PV interneurons in the somatosensory cortex.

We therefore addressed whether SLK-deficient neurons display alterations in the inputs received directly from PV interneurons in comparison to inputs from SST-expressing cells. We found that the IPSC amplitude evoked after light-based stimulation of PV interneurons was significantly reduced when compared to XFP and paired-control neurons. In contrast, light activation of SST-expressing cells did not reveal any alteration in neurons lacking SLK. These remarkable results indicate that the inhibitory impairment observed in SLK-deficient neurons is mostly caused by the lack of PV interneuron-mediated inhibition, which may have important implications regarding the network consequences of the loss of SLK and the molecular mechanism by which this kinase modulates inhibition in cortical neurons.

As stated above, PV-expressing interneurons display unique cellular and molecular intrinsic properties that allow them to exert fast and temporally precise inhibition onto the perisomatic area and proximal dendrites of cortical pyramidal neurons (Martina and Jonas, 1997; Erisir et al., 1999; Zaitsev et al., 2007; Hull et al., 2009; Goldberg et al., 2011). PV interneurons control cortical excitability by limiting the time for excitatory input summation and by regulating the rate at which the neuron activity increases in response to incoming excitatory inputs (Pouille and Scanziani, 2001; Isaacson and Scanziani, 2011; Delevich et al., 2015; Ferguson and Gao, 2018a). In addition, inputs from PV interneurons reach cortical neurons highly synchronized, producing reliable inhibition that strongly limits cell

firing (Kvitsiani et al., 2013). Consequently, the failure of PV interneuron-mediated inhibition has been shown to lead to over-excitation of cortical networks and the emergence of seizures (Bekenstein and Lothman, 1993; Dutton et al., 2013; Rossignol et al., 2013; Gulyás and Freund, 2015; Drexel et al., 2017; Adotevi et al., 2021; Chen et al., 2021), being the loss of PV immunoreactivity described in epileptic tissue (Andrioli et al., 2007; Knopp et al., 2008; Drexel et al., 2011). In animal models of FCD featuring spontaneous seizures, pyramidal cells show decreased strength of inhibitory synaptic connections with PV-expressing interneurons (Sun et al., 2005; Zhou and Roper, 2014). Moreover, PV interneuron activity has been observed to help to prevent seizure initiation (Cammarota et al., 2013; Jiang et al., 2016), and to slow the progression and duration of epileptic activity (Trevelyan et al., 2007; Sessolo et al., 2015). Finally, in vivo experiments have shown that the optogenetic activation of PV-interneurons is effective to reduce the duration of spontaneous seizures (Krook-Magnuson et al., 2013, 2014; Panthi and Leitch, 2021) and its associated comorbidity of impaired spatial memory (Kim et al., 2020). Thus, our results suggest that the loss of PV-mediated inhibition in SLK-KD neurons may indeed promote the onset of hyperexcitability in cortical networks.

This selective loss of inhibition originated from PV interneurons could be due to a reduction of specific inhibitory sites induced by cell-intrinsic mechanisms after SLK loss, but it could also be due to changes in the number of PV interneurons or their synaptic properties. In our experiments, we did not find any difference in the cortical density of PV-immunoreactive cells in shSLK electroporated compared to control animals. In contrast, immunostaining analyses in epileptic specimens diagnosed with FCD and GG have found a reduced number of PV-expressing interneurons within dysplastic cortex (Zamecnik et al., 2006; Aronica et al., 2007; Medici et al., 2016; Nakagawa et al., 2017; Liang et al., 2020). In addition, different animal models of focal epileptogenic lesions display altered numbers and distribution of PV-expressing interneurons (Roper et al., 1999; Moroni et al., 2008; Akakin et al., 2013).

As opposed to epileptic specimens and other FCD animal models, to our knowledge shSLK animals do not show spontaneous generalized seizures, which can be a cause of interneuron loss in epileptogenic cortical malformations (Wong and Roper, 2016; Subramanian et al., 2020). In addition, we aimed to study the synaptic alterations of

morphologically altered neurons by reducing the expression of SLK specifically targeting excitatory neurons, reason why we do not expect direct induced changes in interneuron populations during the development. In this sense, inducing molecular changes that lead to the hyperactivation of mTOR only in PV-expressing interneurons, does not recapitulate the reduction in IPSC frequency and altered E/I balance in layer 2/3 excitatory neurons observed when this genetic modification was produced using a pan-neuronal approach (Zhao and Yoshii, 2019). Moreover, the lack of changes in paired-pulse ratio after light-based activation of PV interneurons indicates that it is unlikely that changes in presynaptic release probability at the PV-pyramidal neuron synapses contribute to the loss of inhibition. Thus, we hypothesize that the reduction of inhibitory inputs observed after the activation of PV-expressing interneurons is caused by cell-autonomous changes in SLK-KD neurons and not due to alterations in the number or synaptic properties of PV interneurons. Quantification of the number of synapses between PV interneurons and SLK-KD neurons may be key to confirm that the reduction in PV-mediated inhibition is caused due to improper formation/maintenance of synapses between these two neuronal types.

Hence, the impairment in feedforward inhibition timing and magnitude and E/I imbalance observed after SLK loss, suggest destabilized and hyperexcitable networks in cortical areas featuring dysplastic neurons. Due to the specific alteration in thalamocortical inhibition, the E/I imbalance in SLK-deficient neurons may be triggered as sensory information arrives to cortical areas from the periphery. In addition, the lack of changes in interneuron density, paired-pulse ratio, and alterations in non-electroporated neighboring pyramidal cells, implies that loss of SLK leads to cell-intrinsic changes that lead to dysregulations in inhibition originating from specific canonical circuits and interneuron subtypes.

4.3 In vivo implications of SLK loss in cortical neurons

After observing a reduced thalamocortical and PV interneuron-mediated inhibition in SLK-deficient neurons, we asked whether SLK loss produces any change in cortical neurons in intact animals. Therefore, we performed c-fos labeling in brain slices obtained from animals electroporated with shSLK or XFP control plasmids. C-fos is an immediate early gene that is used as a molecular marker of neural activity (Chung, 2015). C-fos expression

is maintained at low levels during basal conditions due to the instability of its mRNA and auto-repression by its protein form (Lucibello et al., 1989; Morgan and Curran, 1991). However, after strong and continued stimulation, intracellular Ca^{2+} elevations activate the MAPK pathway leading to c-fos transcription (Murphy et al., 1991; Liste et al., 1995; Rajadhyaksha et al., 1999; Chaudhuri et al., 2000). We found a significantly higher number of electroporated cells expressing c-fos protein in animals that received shSLK plasmids. In addition, the average intensity of c-fos labeling was higher in neurons electroporated with shSLK compared to neurons electroporated with control plasmids. These results demonstrate that the loss of SLK leads to an increased basal activity level of cortical neurons, which may be reflecting the over-activation of neurons in live animals.

The increased expression of neuronal activity markers and impaired inhibition, together with the reduced inhibitory synapse density and dendritic complexity, suggest that SLK loss can underlie the generation of ictal activity. In shSLK electroporated animals, Schoch and collaborators performed repetitive injections of pentylenetetrazol, a $GABA_A$ receptor blocker, and observed more severe chemically evoked seizures compared to mice electroporated with control plasmids (data not published), indicating that the focal cortical loss of SLK in mice translates into a more excitable phenotype. However, we have not observed spontaneous generalized seizures in animals electroporated with shSLK as reported for developmental brain lesions in humans and animal models (Sisodiya et al., 2009; Aronica and Crino, 2014; Jayalakshmi et al., 2019).

It is important to highlight that even though the downregulation of SLK recapitulates many of the features observed in dysplastic neurons, the epileptogenicity of developmental brain lesions is believed to be a multifactorial process (Abdijadid et al., 2015). Pathological alterations such as disrupted cellular growth and migration, neurotransmitter and ionic changes, acidosis, inflammation, immature neuronal networks, the emergence of a variety of morphologically altered cellular elements (dysmorphic neurons, cytomegalic neurons, balloon cells, immature cells, etc.), among others, may contribute to generating the drug-resistant seizures often observed in patients with developmental brain lesions (Aronica and Crino, 2014; Abdijadid et al., 2015; Pallud and McKhann, 2019). It seems that the focal KD of SLK in a subset of excitatory neurons is not enough to generate convulsive seizures in mice. In contrast, specific genetic alterations that lead to the hyperactivation

of mTOR in cortical neurons have been shown to be sufficient to trigger neuronal aberrant morphology, cortical dyslamination, and spontaneous behavioral seizures (Faustino et al., 2012; Lim et al., 2015, 2017; Hsieh et al., 2016; Koh et al., 2018; Ribierre et al., 2018; Goz et al., 2020; Slegers and Blumcke, 2020). Nonetheless, it is still remarkable that the downregulation of SLK during the development can trigger such strong circuit-based inhibitory impairment, which we hypothesized to be a key factor increasing the excitability of cortical networks within epileptogenic focal lesions. We do not exclude the possibility that focal loss of SLK may generate hyperactive cortical networks. Hence, in vivo local field potential recordings from electroporated areas would reveal whether cortical networks containing SLK-deficient neurons are able to trigger non-convulsive focal or generalized seizures or any other type of aberrant network activity.

The reduction in feedforward and PV interneuron-mediated inhibition of SLK-deficient neurons not only predicts increased excitability of cortical networks, but also sensory and cognitive impairments in vivo (Gonzalez-Burgos et al., 2015; Wood et al., 2017; Nahar et al., 2021). As stated before, PV-expressing interneurons are strongly depolarized by thalamic inputs, which subsequently modulate neuronal activity and tune sensory processing. PV-expressing interneuron activation is able to alter frequency selectivity and gain control of neuronal responses to sensory inputs in visual and auditory cortex (Cardin et al., 2009; Atallah et al., 2012; Lee et al., 2012; Wilson et al., 2012; Hamilton et al., 2013; Aizenberg et al., 2015; Agetsuma et al., 2018). Therefore, proper PV-mediated inhibition is necessary for the modulation of sensory responses, allowing neuronal responsiveness to represent a wide range of input levels in their activity patterns instead of producing simple binary outputs (Ferguson and Gao, 2018a).

In addition, PV-expressing interneurons have been implicated in synchronizing neuronal populations to generate gamma oscillations (30-80 Hz), an oscillation frequency linked to cognition and information processing (Ferguson and Gao, 2018a). Optogenetic experiments showed that PV interneuron’s suppression was sufficient to avoid the generation and maintenance of gamma oscillations, which was accompanied by loss of proper control of sensory responses in the neocortex (Cardin et al., 2009; Sohal et al., 2009). Moreover, PV-expressing interneurons are required for goal-directed behavior (Sparta et al., 2014; Kim et al., 2016a; Lagler et al., 2016; Ferguson and Gao, 2018b),

attention (Kim et al., 2016b), social behavior (Selimbeyoglu et al., 2017; Ferguson and Gao, 2018b), cognitive flexibility tasks, and certain types of learning (Letzkus et al., 2011; Rossi et al., 2012; Donato et al., 2013; Liu et al., 2014; Ferguson and Gao, 2018b). Thus, it is not surprising that a disrupted E/I balance after loss of PV interneuron-mediated inhibition has been linked to neurodevelopmental disorders associated with autism and intellectual disabilities (Mierau et al., 2016; Selimbeyoglu et al., 2017; Vogt et al., 2018; Patrizi et al., 2020; Amegandjin et al., 2021), Alzheimer disease (Iaccarino et al., 2016; Martinez-Losa et al., 2018; Hijazi et al., 2020), and schizophrenia (Mellios et al., 2009; Fung et al., 2010; Cohen et al., 2015; Huang et al., 2021). Therefore, given that cognitive impairments are common in patients with developmental brain lesions (Oki et al., 1999; Chilosi et al., 2001; Kimura et al., 2019), a decrease of inhibition originated from PV-expressing interneurons after SLK loss could be disrupting sensory processing and neuronal oscillations linked to cognition and contributing to alter behavior in mice.

In order to directly assess the consequences of the focal loss of SLK in vivo, two-photon Ca^{2+} imaging experiments can be performed in awake animals to simultaneously record Ca^{2+} transients from populations of neurons with single-cell resolution. The addition of sensory stimuli while the animal behaves would allow determining whether abnormal activity patterns arise after thalamocortical sensory activation, as predicted by the loss in feedforward and PV interneuron-mediated inhibition. If seizure-like activity is detected, it would be possible to determine whether it originates within networks containing dysplastic neurons or from adjacent areas, as it has been observed before (Represa, 2019). In addition, whisker-dependent tasks would reveal if animals with focal loss of SLK face sensory degradation. Working memory and social behavior tasks can be performed to link SLK-KD to impaired cognition. Moreover, optogenetic activation of PV-expressing interneurons during any of these experimental procedures would reveal if sensory and cognitive alterations are directly caused by the reduction of PV interneuron-mediated inhibition as done before in other studies (Selimbeyoglu et al., 2017; Cao et al., 2018). Finally, in order to obtain more reproducible and robust effects, general SLK ablation in cortical excitatory neurons or panneuronally can be beneficial to address the role of SLK in the establishment of inhibitory circuits and the consequences of its loss in vivo.

4.4 Possible molecular mechanisms of SLK

The results of this and previous studies have revealed the importance of SLK in the development of proper dendritic morphology and functional inhibitory connections in cortical neurons. However, the exact molecular mechanism and specific signaling pathways in which SLK participates to regulate dendritic and synaptic development are still unsolved. We hypothesize that the decreased number of distal dendrites underlies the mild reduction of excitation we observed in SLK-KD neurons, given that distal dendrites of pyramidal neurons display large numbers of excitatory synapses (Megías et al., 2001). As discussed by Schoch et al., 2021, the most likely mechanism underlying the dendritic phenotype observed after SLK loss is a modulation of cytoskeletal dynamics, since SLK interacts and regulates the stability of microtubules and actin filaments (Wagner et al., 2002; Wagner and Sabourin, 2009). SLK acts downstream of integrin receptors (Wagner et al., 2002) and it can phosphorylate key cytoskeletal proteins known to be important for dendrite outgrowth and branching (Moresco et al., 2005; Marrs et al., 2006; Chen and Firestein, 2007; Myers and Gomez, 2011), including RhoA (Guilluy et al., 2008), ezrin (Viswanatha et al., 2012), paxillin (Wagner et al., 2008) and the $p150^{Glued}$ dynactin subunit (Zhapparova et al., 2013). Thus, lack of SLK may be affecting dendritic branching due to the interruption of relevant cytoskeletal signaling pathways during the development of the brain. Nonetheless, the interaction of SLK with these proteins and cascades has been reported only in non-neuronal cells. Therefore, the study of SLK's interaction partners in neurons would be key to better understand how the loss of this protein leads to an aberrant morphological phenotype.

Regarding the reduction of inhibitory currents, the decrease in gephyrin puncta observed after SLK loss (Schoch et al., 2021) can be a direct indicator of impaired synaptic accumulation of $GABA_A$ receptors since gephyrin represents an essential scaffold protein for the clustering and stabilization of inhibitory neurotransmitter receptors (Tretter et al., 2008; Petrini et al., 2014; Choii and Ko, 2015). Genetic ablation or mutation of gephyrin drastically reduces synapse maintenance, postsynaptic $GABA_A$ receptor grouping, and the amplitude of GABAergic currents (Kneussel et al., 1999; Kim et al., 2021). Hence, loss of gephyrin after SLK-KD might be driving the functional inhibitory impairment we recorded in cortical neurons lacking SLK.

Schoch and collaborators showed that SLK is not required for the initial formation of postsynaptic structures, but rather for their stabilization at a later time point during postnatal development (Schoch et al., 2021). Intriguingly, our functional experiments revealed that loss of SLK leads to a specific deficit of PV interneuron-mediated inhibition in cortical neurons. This may suggest that SLK not only specifically participates in inhibitory synapse stabilization, but that it is especially important for the establishment of inhibitory synapses between PV-expressing interneurons and excitatory neurons. In accordance, perisomatic and basal dendrite innervation of PV interneurons onto cortical excitatory neurons has an intense development after the second week of postnatal development, which corresponds with the time point (P15) in which SLK-deficient neurons start showing deficits in inhibitory postsynapse density (Chattopadhyaya et al., 2004; Virtanen et al., 2018; Baho et al., 2019).

We hypothesize that cell-intrinsic changes in transsynaptic signaling pathways in SLK-KD neurons might be responsible for the selective loss of inhibition originating from PV-expressing interneurons. In general, the formation and stability of inhibitory synapses require the clustering of $GABA_A$ receptors, the transsynaptic adhesion molecule neuroligin-2, and the scaffold proteins collybistin and gephyrin at the postsynaptic site (Zacchi et al., 2014; Pizzarelli et al., 2020). Interestingly, even though neuroligin-2 is located at virtually all inhibitory synapses, different studies have pointed to its participation in mechanisms governing the synapse specificity between PV interneurons and pyramidal neurons (Ali et al., 2020). Genetic deletion of neuroligin-2 reduces gephyrin and $GABA_A$ receptor puncta specifically in the perisomatic area but not in the dendritic arbor of neurons (Poulopoulos et al., 2009; Babaev et al., 2016). In addition, loss of neuroligin-2 destabilizes already formed synapses and reduces circuit-based synaptic inhibition (Liang et al., 2015; Troyano-Rodriguez et al., 2019).

More importantly, neuronal loss of neuroligin-2 produces similar functional consequences as reported in this study after SLK-KD. In the somatosensory cortex, KO of neuroligin-2 decreased the amplitude of IPSCs originating from PV- but not from SST-expressing interneurons (Gibson et al., 2009). Furthermore, manipulating the expression of neuroligin-2 was shown to lead to changes in evoked IPSC amplitudes, mIPSC frequency and amplitude, and E/I balance without altering spike firing properties or excitatory

connectivity (Poulopoulos et al., 2009; Liang et al., 2015; Babaev et al., 2016; Chen et al., 2020). C-fos analysis of neuroligin-2-KO animals revealed that excitatory cells but not PV- or SST-positive interneurons display over-excitation in the amygdala after anxiogenic stimuli (Babaev et al., 2016). Therefore, since SLK accumulates at inhibitory postsynapses (Schoch et al., 2021), and phosphorylation is an important posttranslational modification that modulates the activity of neuroligin-2 (Bemben et al., 2015), we hypothesize that the direct or indirect interaction of SLK and neuroligin-2 may be a possible mechanism by which loss of SLK leads to a specific reduction in perisomatic inhibition originated from PV interneurons.

Aside from a neuroligin-2 mediated mechanism, there is an additional cascade that could potentially give rise to interneuron-specific changes of inhibition in excitatory cells. The ErbB4 signaling cascade selectively regulates inhibition via PV-interneurons (Fazzari et al., 2010; Sun et al., 2016; Luo et al., 2021). Recent evidence shows that ErbB4 can act in a kinase-independent manner as part of a transsynaptic complex promoting GABAergic synapse formation, endowing it in principle with the capability for cell-autonomous regulation of PV interneuron-mediated inhibition (Luo et al., 2021). However, the relation between SLK and the transsynaptic signaling molecules neuroligin-2 and ErbB4 is yet to be established.

In an attempt to assess what molecular, neuron-intrinsic pathways are responsible for the morphologic and inhibitory synaptic phenotype of SLK-deficient neurons, we investigated the specific connection between changes in electrophysiological properties and the transcriptional profile of cortical neurons using patch-seq protocols. This technique has been successfully used to study the molecular basis of morphological and functional diversity of cells and to integrate multimodal cell type atlases, both in vitro and in vivo (Fuzik et al., 2016; Cadwell et al., 2017b, 2017a, 2020; Ellender et al., 2019; Liu et al., 2020; Scala et al., 2020). Applying patch-seq, we were able to correlate expression changes of specific genes with the mIPSC frequency and cell capacitance of neurons electroporated with control and shSLK plasmids. These two electrophysiological properties were shown before to be affected in SLK-KD neurons (Schoch et al., 2021), and expression changes correlated to either of them can be linked to an inhibitory (IPSC frequency) or dendritic (cell capacitance) phenotype.

Due to the dependency of manual sample collection by the experimenter, RNase and mRNA contamination from adjacent cells and the extracellular space is a common problem in patch-seq experiments (Tripathy et al., 2018). For this reason and as done in other studies, we applied a modified version of the traditional patch-clamp protocol under RNase-free conditions, in addition to strict quality control checks to mitigate technical noise and artifacts in downstream analysis (Fuzik et al., 2016; Cadwell et al., 2017b, 2020; Tripathy et al., 2018; Ellender et al., 2019; Liu et al., 2020; Scala et al., 2020). Despite this, we obtain a read count matrix inflated with low and zero counts, where none or only a few transcripts for many genes were captured due to technical biases or low-quality samples (Brennecke et al., 2013).

A large number of zero counts introduces a great amount of technical noise that may mask biological variance in downstream analysis. Genes with substantial drop-out events do not provide sufficient information for reliable statistical inference (Bourgon et al., 2010), lead to the formation of distinct clusters that distort the characterization of population heterogeneity, and produce artificial upregulated genes after normalization of libraries with small sizes (Amezquita et al., 2020). To account for the excess of zero counts, we selected for downstream analysis only genes that were expressed in at least 28 samples, the size of our smallest experimental group. In addition, exonic and intronic aligned reads were added and used together to maximize gene counts as reported for other patch-seq datasets (Cadwell et al., 2017b; Scala et al., 2020), given that up to 50% of reads using this approach originate from unspliced transcripts (which is similar to our alignment rates), a feature that was shown to be correlated with the harvest of the cell nucleus (Scala et al., 2020). Finally, we used an analysis pipeline that was shown to be suitable for datasets with a large number of zero counts and a small number of samples (the main two features of our dataset), compared to more traditional pipelines made for bulk-RNAseq (Miao et al., 2018; Wang et al., 2019; Mou et al., 2020).

Differential expression (DE) analysis revealed 10 down and 14 upregulated genes in shSLK neurons compared to the control group. Gene-disease associations showed that 16 of these DE genes have been linked to human diseases, especially to neoplasms and nervous system disorders. It is interesting that many of these neurological diseases are related to cognitive disabilities and epilepsy, which are conditions in which impaired PV

interneuron-mediated inhibition has been reported (Iaccarino et al., 2016; Mierau et al., 2016; Selimbeyoglu et al., 2017; Martinez-Losa et al., 2018; Vogt et al., 2018; Hijazi et al., 2020; Patrizi et al., 2020; Amegandjin et al., 2021). In addition, since SLK was also observed to be downregulated in the cellular component of GGs, it is interesting that genes associated with neoplasms (including brain neoplasms) were found to be DE in SLK-deficient neurons.

Spearman rank correlations revealed that genes associated with membrane trafficking and cell morphology were correlated to the capacitance of neurons, which can be used as a functional proxy for neuronal membrane area. SNX6 encodes a member of the sorting nexin family, which is involved in intracellular trafficking and axon guidance (Simonetti et al., 2019). Interestingly, SNX6 was proposed to be able to interact with semaphorin 4C (Simonetti et al., 2019), a member of a molecular cascade that has been shown to transsynaptically regulate inhibitory synapse development (Frias et al., 2019), and whose members may interact with SLK (data not published). Modeling studies suggest that SNX6 may interact with SNX27 through its PDZ domain, which regulates neuroligin-2 surface levels and whose KD results in changes in inhibitory synapse composition, the number of gephyrin clusters, and reduced IPSC frequency (Binda et al., 2019; Halff et al., 2019; Yong et al., 2020). Thus, downregulation of SNX6 after SLK loss may be indirectly affecting the formation of inhibitory synapses.

Dctn4 encodes the dynactin subunit 4, which has a role in cytoskeletal dynamics and dynactin complexes, which in turn are key mediators of dendritogenesis (Tempes et al., 2020). A third gene that was correlated with neuronal capacitance was Spock2, which encodes an extracellular matrix protein that can bind to glycosaminoglycans. Spock2 has a documented role in process formation, inhibiting neurite extension in primary cerebellar neurons (Schnepp et al., 2005). Finally, Ddx6 encodes a member of the DEAD-box protein family and participates in miRNA-mediated cell fate specification in neural stem cells (Nicklas et al., 2015). Ddx6 is present in dendritic granules that contain ribosomes and is involved in translation suppression and mRNA degradation in response to mTOR activation (Elvira et al., 2006; Pimentel and Boccaccio, 2014; Nandagopal and Roux, 2015; Zhang et al., 2018).

We identified genes that encode transcription factors and guidance molecules correlated with the frequency of mIPSCs. These include Smarcc2, a subunit of the SWI/SNF molecular complex that acts as a transcriptional activator and repressor by chromatin remodeling. SWI/SNF complex helps to maintain a stable neuronal morphology by stabilizing the expression of genes that underlie axon and dendrite formation (Staahl and Crabtree, 2013). Sgms 1 encodes Sphingomyelin Synthase 1, which synthesizes the sphingolipid sphingomyelin, through the transfer of the phosphatidyl head group onto the primary hydroxyl of ceramide (Filippenkov et al., 2015). Finally, Megf9 is a transmembrane protein with multiple EGF-like repeats that is strongly expressed in the developing and adult CNS and that has been proposed to function as a guidance or signaling molecule (Brandt-Bohne et al., 2007). Interestingly, Megf9 is predicted to interact with laminins, a family of extracellular matrix glycoproteins that are effective stimulators of neurite outgrowth (Powell and Kleinman, 1997; Brandt-Bohne et al., 2007).

It is important to note that only SNX6 and Smarcc2 have a sensible direction of expression change with respect to the direction of their correlation with the electrophysiological properties (e.g. SNX6 is downregulated in shSLK neurons and it is positively correlated with the cell capacitance, connecting low expression of SNX6 with the reduced capacitance of SLK-deficient neurons). Nonetheless, it is still interesting to consider other DE genes to further investigate the possible molecular mechanism of SLK and the consequences of its neuronal loss. In this sense, we observed a downregulation of the Golgi-associated PDZ and coiled-coil motif-containing protein (GOPC) in neurons lacking SLK. GOPC is involved in vesicular trafficking in secretory and endocytic processes. It has been shown that GOPC interacts with neuroligin and Frizzled 8 via its PDZ domain. Frizzled genes are related to the development of cell polarity in the Wnt pathway. It is hypothesized that GOPC might function as an important link between neuroligin/neurexin and Wnt pathways, indicating a role in synapse and neurite formation (Li et al., 2006).

Despite our efforts, it is possible that the high number of zero counts masked relevant biological variance between experimental groups that did not allow us to find other DE genes and correlations with electrophysiological properties. To overcome this, it would be ideal to perform sc-RNA sequencing experiments from dissociated tissue, which would allow us to validate our patch-seq results and to more reliably discover DE genes in SLK-

deficient neurons (which can be identified by the expression of a fluorescence protein). Afterward, it can be checked whether these newly discovered DE genes were correlated with electrophysiological properties in our patch-seq experiments. Validation of interesting DE genes can be achieved by performing polymerase chain reaction or western blot experiments, and if the spatial pattern of expression of DE genes is desired, performing immunohistochemistry or RNA scope experiments would be ideal. This approach would give the additional advantage of being able to determine whether other cell types within electroporated areas also display transcriptomic alterations, more interestingly neighboring non-targeted pyramidal cells, and PV-expressing interneurons.

4.5 Conclusion and further remarks

The main goal of this study was to better understand the microcircuit features of cortical neurons with reduced expression of SLK as observed in dysplastic cells within epileptogenic brain lesions. We demonstrated that the downregulation of SLK causes a selective loss of circuit-based inhibition confined to thalamic inputs and a shift in the E/I balance in cortical neurons. This predicts the generation of over-excitation when sensory and motor information arrives from the thalamus in live animals. Remarkably, only the inhibition mediated by PV-expressing interneurons seems to be affected in neurons lacking SLK, indicating that this kinase might have a pivotal role in mechanisms of inhibitory synapse specificity. Our results point to the loss of SLK as a key factor contributing to the E/I imbalance observed within developmental focal lesions featuring dysplastic neurons.

In order to understand better the consequences of SLK-KD in-vivo, it would be ideal to combine this model with in vivo recordings of cell activity to determine the behavioral states in which the E/I balance of SLK-neurons is triggered and to assess whether neuronal networks featuring dysplastic neurons generate any type of aberrant activity. In addition, behavioral experiments can be performed to determine the consequences of SLK loss regarding sensory integration and cognitive performance. Finally, scRNA sequencing analyses from dissociated tissue together with phosphoproteomic and proximity assays would help to uncover the potential transsynaptic mechanism of SLK leading to the specific reduction of PV synapses.

The implementation of multimodal approaches and the development of new animal models are key to unravel the functional mechanisms that lead to the heterogeneity and epileptogenicity of developmental brain lesions. In this thesis, we showed how the use of in utero electroporation, electrophysiology, and molecular biology, is of advantage to determine how developmental somatic alterations of candidate genes affect neuronal circuits and might lead to hyperexcitability. Upcoming studies may focus on finding genetic alterations that recapitulate many of the pathological features observed in humans (where the mTOR pathway already seems to be a strong candidate), which may open possibilities for future effective molecular therapeutic targets.

5. Abstract

Focal epileptogenic lesions displaying morphologically altered neurons are frequently associated with devastating and therapy-refractory epilepsies. However, it is still unsolved how dysplastic neurons contribute to the striking increase in the propensity to generate seizures. In this study, we aimed to better understand the functional connectivity features at the microcircuit level of morphological-altered neurons within cortical networks. To this end, we used a newly generated model of dysplastic neurons that mimics the reduced expression of the Ste20-like kinase (SLK) as found in dysmorphic cellular elements from human cortical malformations. Loss of SLK strongly impairs dendritic and inhibitory synapse formation and leads to an aggravated phenotype of chemically-induced seizures. We demonstrated that the downregulation of SLK in cortical neurons causes a selective, cell-autonomous loss of synaptic inhibition accompanied by a shift in the excitation/inhibition (E/I) balance. Using optogenetic approaches we found that the inhibition impairment of SLK-deficient neurons is confined to feedforward inhibitory circuits, and does not affect feedback or lateral inhibition. Interestingly, SLK loss specifically reduced inhibition mediated by PV-expressing interneurons, but not by somatostatin-expressing interneurons. This deficit led to increased activity levels of SLK-deficient neurons in intact mice. Finally, to assess the specific connection between the E/I imbalance and the transcriptional changes triggered by the loss of SLK, we performed patch-clamp RNA sequencing. This yielded several differentially expressed candidate genes, as well as genes correlated with the affected functional properties of cortical neurons. These results point to the downregulation of SLK as a key factor contributing to the E/I imbalance observed within focal epileptogenic lesions featuring dysplastic neurons. Moreover, our results suggest a relevant and cell-autonomous role for SLK in mechanisms governing inhibitory synapse specificity.

6. List of figures

7. List of tables

8. References

Abdijadid S, Mathern GW, Levine MS, Cepeda C. Basic mechanisms of epileptogenesis in pediatric cortical dysplasia. CNS Neurosci Ther. 2015;21(2):92–103.

Adesnik H, Bruns W, Taniguchi H, Huang ZJ, Scanziani M. A neural circuit for spatial summation in visual cortex. Nature. 2012;490(7419):226–30.

Adesnik H, Naka A. Cracking the Function of Layers in the Sensory Cortex. Neuron. 2018;100(5):1028–43.

Adesnik H, Scanziani M. Lateral competition for cortical space by layer-specific horizontal circuits. Nature. 2010;464(7292):1155–60.

Adler A, Zhao R, Shin ME, Yasuda R, Gan WB. Somatostatin-Expressing Interneurons Enable and Maintain Learning-Dependent Sequential Activation of Pyramidal Neurons. Neuron. 2019;102(1):202-216.e7.

Adotevi N, Su A, Peiris D, Hassan M, Leitch B. Altered Neurotransmitter Expression in the Corticothalamocortical Network of an Absence Epilepsy Model with impaired Feedforward Inhibition. Neuroscience. 2021;467:73–80.

Agetsuma M, Hamm JP, Tao K, Fujisawa S, Yuste R. Parvalbumin-positive interneurons regulate neuronal ensembles in visual cortex. Cereb Cortex. 2018;28(5):1831–45.

Aizenberg M, Mwilambwe-Tshilobo L, Briguglio JJ, Natan RG, Geffen MN. Bidirectional Regulation of Innate and Learned Behaviors That Rely on Frequency Discrimination by Cortical Inhibitory Neurons. PLoS Biol. 2015;13(12).

Akakin D, Martinez-Diaz H, Chen HX, Roper SN. Reduced densities of parvalbumin- and somatostatin-expressing interneurons in experimental cortical dysplasia and heterotopia in early postnatal development. Epilepsy Res. 2013;104(3):226–33.

Al-Zahrani KN, Baron KD, Sabourin LA. Ste20-like kinase SLK, at the crossroads: A matter of life and death. Cell Adhes Migr. 2013;7(1):1–10.

Al-Zahrani KN, Sekhon P, Tessier DR, Yockell-Lelievre J, Pryce BR, Baron KD, Howe GA, Sriram RK, Daniel K, McKay M, Lo V, Quizi J, Addison CL, Gruslin A, Sabourin LA. Essential role for the SLK protein kinase in embryogenesis and placental tissue development. Dev Dyn. 2014;243(5):640–51.

Ali H, Marth L, Krueger-Burg D. Neuroligin-2 as a central organizer of inhibitory synapses in health and disease. Sci Signal. 2020;13(663).

Alonso JM, Swadlow HA. Thalamocortical specificity and the synthesis of sensory cortical receptive fields. J Neurophysiol. 2005;94(1):26–32.

Amegandjin CA, Choudhury M, Jadhav V, Carriço JN, Quintal A, Berryer M, Snapyan M, Chattopadhyaya B, Saghatelyan A, Di Cristo G. Sensitive period for rescuing parvalbumin interneurons connectivity and social behavior deficits caused by TSC1 loss. Nat Commun. 2021;12(1).

Amezquita RA, Lun ATL, Becht E, Carey VJ, Carpp LN, Geistlinger L, Marini F, Rue-Albrecht K, Risso D, Soneson C, Waldron L, Pagès H, Smith ML, Huber W, Morgan M, Gottardo R, Hicks SC. Orchestrating single-cell analysis with Bioconductor. Nat Methods. 2020;17(2):137–45.

André VM, Flores-Hernández J, Cepeda C, Starling AJ, Nguyen S, Lobo MK, Vinters H V., Levine MS, Mathern GW. NMDA receptor alterations in neurons from pediatric cortical dysplasia tissue. Cereb Cortex. 2004;14(6):634–46.

Andres M, Andre VM, Nguyen S, Salamon N, Cepeda C, Levine MS, Leite JP, Neder L, Vinters H V., Mathern GW. Human cortical dysplasia and epilepsy: An ontogenetic hypothesis based on volumetric MRI and NeuN neuronal density and size measurements. Cereb Cortex. 2005;15(2):194–210.

Andrioli A, Alonso-Nanclares L, Arellano JI, DeFelipe J. Quantitative analysis of parvalbumin-immunoreactive cells in the human epileptic hippocampus. Neuroscience. 2007;149(1):131–43.

Antoine MW, Langberg T, Schnepel P, Feldman DE. Increased Excitation-Inhibition Ratio Stabilizes Synapse and Circuit Excitability in Four Autism Mouse Models. Neuron. 2019;101(4):648-661.e4.

Arkhipov A, Gouwens NW, Billeh YN, Gratiy S, Iyer R, Wei Z, Xu Z, Abbasi-Asl R, Berg J, Buice M, Cain N, da Costa N, de Vries S, Denman D, Durand S, Feng D, Jarsky T, Lecoq J, Lee B, Li L, Mihalas S, Ocker GK, Olsen SR, Reid RC, Soler-Llavina G, Sorensen SA, Wang Q, Waters J, Scanziani M, Koch C. Visual physiology of the layer 4 cortical circuit in silico. PLoS Comput Biol. 2018;14(11).

Aronica E, Crino PB. Epilepsy Related to Developmental Tumors and Malformations of Cortical Development. Neurotherapeutics. 2014;11(2):251–68.

Aronica E, Redeker S, Boer K, Spliet WGM, van Rijen PC, Gorter JA, Troost D. Inhibitory networks in epilepsy-associated gangliogliomas and in the perilesional epileptic

cortex. Epilepsy Res. 2007;74(1):33–44.

Aronica E, Yankaya B, Jansen GH, Leenstra S, Van Veelen CWM, Gorter JA, Troost D. Ionotropic and metabotropic glutamate receptor protein expression in glioneuronal tumours from patients with intractable epilepsy. Neuropathol Appl Neurobiol. 2001;27(3):223–37.

Asami M, Pilz GA, Ninkovic J, Godinho L, Schroeder T, Huttner WB, Götz M. The role of Pax6 in regulating the orientation and mode of cell division of progenitors in the mouse cerebral cortex. Development. 2011;138(23):5067–78.

Ascoli GA, Alonso-Nanclares L, Anderson SA, Barrionuevo G, Benavides-Piccione R, Burkhalter A, Buzsáki G, Cauli B, DeFelipe J, Fairén A, Feldmeyer D, Fishell G, Fregnac Y, Freund TF, Gardner D, Gardner EP, Goldberg JH, Helmstaedter M, Hestrin S, Karube F, Kisvárday ZF, Lambolez B, Lewis DA, Marin O, Markram H, Mũoz A, Packer A, Petersen CCH, Rockland KS, Rossier J, Rudy B, Somogyi P, Staiger JF, Tamas G, Thomson AM, Toledo-Rodriguez M, Wang Y, West DC, Yuste R. Petilla terminology: Nomenclature of features of GABAergic interneurons of the cerebral cortex. Nat Rev Neurosci. 2008;9(7):557–68.

Atallah B V., Bruns W, Carandini M, Scanziani M. Parvalbumin-Expressing Interneurons Linearly Transform Cortical Responses to Visual Stimuli. Neuron. 2012;73(1):159–70.

Ayaz A, Saleem AB, Schölvinck ML, Carandini M. Locomotion controls spatial integration in mouse visual cortex. Curr Biol. 2013;23(10):890–4.

Ayzenshtat I, Karnani MM, Jackson J, Yuste R. Cortical control of spatial resolution by VIP+ interneurons. J Neurosci. 2016;36(45):11498–509.

Baas PW, Deitch JS, Black MM, Banker GA. Polarity orientation of microtubules in hippocampal neurons: Uniformity in the axon and nonuniformity in the dendrite. Proc Natl Acad Sci U S A. 1988;85(21):8335–9.

Babaev O, Botta P, Meyer E, Müller C, Ehrenreich H, Brose N, Lüthi A, Krueger-Burg D. Neuroligin 2 deletion alters inhibitory synapse function and anxiety-associated neuronal activation in the amygdala. Neuropharmacology. 2016;100:56–65.

Babb TL, Ying Z, Hadam J, Penrod C. Glutamate receptor mechanisms in human epileptic dysplastic cortex. Epilepsy Res. 1998;32(1–2):24–33.

Bacci A, Rudolph U, Huguenard JR, Prince DA. Major Differences in Inhibitory Synaptic

Transmission onto Two Neocortical Interneuron Subclasses. J Neurosci. 2003;23(29):9664–74.

Baho E, Chattopadhyaya B, Lavertu-Jolin M, Mazziotti R, Awad PN, Chehrazi P, Groleau M, Jahannault-Talignani C, Vaucher E, Ango F, Pizzorusso T, Baroncelli L, Cristo G Di. p75 neurotrophin receptor activation regulates the timing of the maturation of cortical parvalbumin interneuron connectivity and promotes Juvenile-like plasticity in adult visual cortex. J Neurosci. 2019;39(23):4489–510.

Barba C, Coras R, Giordano F, Buccoliero AM, Genitori L, Blümcke I, Guerrini R. Intrinsic epileptogenicity of gangliogliomas may be independent from co-occurring focal cortical dysplasia. Epilepsy Res. 2011;97(1–2):208–13.

Barber M, Pierani A. Tangential migration of glutamatergic neurons and cortical patterning during development: Lessons from Cajal-Retzius cells. Dev Neurobiol. 2016;76(8):847–81.

Barkovich AJ, Guerrini R, Kuzniecky RI, Jackson GD, Dobyns WB. A developmental and genetic classification for malformations of cortical development: Update 2012. Brain. 2012;135(5):1348–69.

Barth AL, Poulet JFA. Experimental evidence for sparse firing in the neocortex. Trends Neurosci. 2012;35(6):345–55.

Baybis M, Yu J, Lee A, Golden JA, Weiner H, McKhann G, Aronica E, Crino PB. mTOR cascade activation distinguishes tubers from focal cortical dysplasia. Ann Neurol. 2004;56(4):478–87.

Beierlein M, Gibson JR, Connors BW. A network of electrically coupled interneurons drives synchronized inhibition in neocortex. Nat Neurosci. 2000;3(9):904–10.

Beierlein M, Gibson JR, Connors BW. Two Dynamically Distinct Inhibitory Networks in Layer 4 of the Neocortex. J Neurophysiol. 2003;90(5):2987–3000.

Bekenstein JW, Lothman EW. Dormancy of inhibitory interneurons in a model of temporal lobe epilepsy. Science (80-). 1993;259(5091):97–100.

Bemben MA, Shipman SL, Nicoll RA, Roche KW. The cellular and molecular landscape of neuroligins. Trends Neurosci. 2015;38(8):496–505.

Benova B, Jacques TS. Genotype-phenotype correlations in focal malformations of cortical development: a pathway to integrated pathological diagnosis in epilepsy surgery. Brain Pathol. 2019;29(4):473–84.

Berg AT, Berkovic SF, Brodie MJ, Buchhalter J, Cross JH, Van Emde Boas W, Engel J, French J, Glauser TA, Mathern GW, Moshé SL, Nordli D, Plouin P, Scheffer IE. Revised terminology and concepts for organization of seizures and epilepsies: Report of the ILAE Commission on Classification and Terminology, 2005-2009. Epilepsia. 2010;51(4):676–85.

Berg AT, Scheffer IE. New concepts in classification of the epilepsies: Entering the 21st century. Epilepsia. 2011. p. 1058–62.

Binda CS, Nakamura Y, Henley JM, Wilkinson KA. Sorting nexin 27 rescues neuroligin 2 from lysosomal degradation to control inhibitory synapse number. Biochem J. 2019;476(2):293–306.

Blümcke I, Thom M, Aronica E, Armstrong DD, Vinters H V., Palmini A, Jacques TS, Avanzini G, Barkovich AJ, Battaglia G, Becker A, Cepeda C, Cendes F, Colombo N, Crino P, Cross JH, Delalande O, Dubeau F, Duncan J, Guerrini R, Kahane P, Mathern G, Najm I, Özkara Ç, Raybaud C, Represa A, Roper SN, Salamon N, Schulze-Bonhage A, Tassi L, Vezzani A, Spreafico R. The clinicopathologic spectrum of focal cortical dysplasias: A consensus classification proposed by an ad hoc Task Force of the ILAE Diagnostic Methods Commission. Epilepsia. 2011;52(1):158–74.

Blümcke I, Wiestler OD. Gangliogliomas: An intriguing tumor entity associated with focal epilepsies. J Neuropathol Exp Neurol. 2002;61(7):575–84.

Boer K, Lucassen PJ, Spliet WGM, Vreugdenhil E, van Rijen PC, Troost D, Jansen FE, Aronica E. Doublecortin-like (DCL) expression in focal cortical dysplasia and cortical tubers. Epilepsia. 2009;50(12):2629–37.

Boer K, Troost D, Timmermans W, Van Rijen PC, Spliet WGM, Aronica E. Pi3K-mTOR signaling and AMOG expression in epilepsy-associated glioneuronal tumors. Brain Pathol. 2010;20(1):234–44.

Bourgon R, Gentleman R, Huber W. Independent filtering increases detection power for high-throughput experiments. Proc Natl Acad Sci U S A. 2010;107(21):9546–51.

Brandt-Bohne U, Keene DR, White FA, Koch M. MEGF9: A novel transmembrane protein with a strong and developmentally regulated expression in the nervous system. Biochem J. 2007;401(2):447–57.

Brecht M, Sakmann B. Dynamic representation of whisker deflection by synaptic potentials in spiny stellate and pyramidal cells in the barrels and septa of layer 4 rat

somatosensory cortex. J Physiol. 2002;543(1):49–70.

van Breemen MS, Wilms EB, Vecht CJ. Epilepsy in patients with brain tumours: epidemiology, mechanisms, and management. Lancet Neurol. 2007;6(5):421–30.

Brennecke P, Anders S, Kim JK, Kołodziejczyk AA, Zhang X, Proserpio V, Baying B, Benes V, Teichmann SA, Marioni JC, Heisler MG. Accounting for technical noise in single-cell RNA-seq experiments. Nat Methods. 2013;10(11):1093–8.

Cadwell CR, Palasantza A, Jiang X, Berens P, Deng Q, Yilmaz M, Reimer J, Shen S, Bethge M, Tolias KF, Sandberg R, Tolias AS. Electrophysiological , transcriptomic and morphologic profiling of single neurons using Patch-seq. Nat Biotechnol. 2015;34(2):199–203.

Cadwell CR, Sandberg R, Jiang X, Tolias AS. Q & A : using Patch-seq to profile single cells. 2017a;:1–7.

Cadwell CR, Scala F, Fahey PG, Kobak D, Mulherkar S, Sinz FH, Papadopoulos S, Tan ZH, Johnsson P, Hartmanis L, Li S, Cotton RJ, Tolias KF, Sandberg R, Berens P, Jiang X, Tolias AS. Cell type composition and circuit organization of clonally related excitatory neurons in the juvenile mouse neocortex. Elife. 2020;9.

Cadwell CR, Scala F, Li S, Livrizzi G, Shen S, Sandberg R, Jiang X, Tolias AS. Multimodal profiling of single-cell morphology, electrophysiology, and gene expression using Patch-seq. Nat Protoc. 2017b;12(12):2531–53.

Calcagnotto ME, Paredes MF, Tihan T, Barbaro NM, Baraban SC. Dysfunction of synaptic inhibition in epilepsy associated with focal cortical dysplasia. J Neurosci. 2005;25(42):9649–57.

Callaway EM. Inhibitory cell types, circuits and receptive fields in mouse visual cortex. Res Perspect Neurosci. 2016;(9783319277769):11–8.

Cammarota M, Losi G, Chiavegato A, Zonta M, Carmignoto G. Fast spiking interneuron control of seizure propagation in a cortical slice model of focal epilepsy. J Physiol. 2013;591(4):807–22.

Cao W, Lin S, Xia Q qiang, Du Y lan, Yang Q, Zhang M ying, Lu Y qing, Xu J, Duan S min, Xia J, Feng G, Xu J, Luo J hong. Erratum: Gamma Oscillation Dysfunction in mPFC Leads to Social Deficits in Neuroligin 3 R451C Knockin Mice (S0896627318301004 (2018) 97(6) (1253–1260.e7) (S0896627318301004) (10.1016/j.neuron.2018.02.001)). Neuron. 2018;98(3):670.

Cardin JA. Inhibitory Interneurons Regulate Temporal Precision and Correlations in Cortical Circuits. Trends Neurosci. 2018;41(10):689–700.

Cardin JA, Carlén M, Meletis K, Knoblich U, Zhang F, Deisseroth K, Tsai LH, Moore CI. Driving fast-spiking cells induces gamma rhythm and controls sensory responses. Nature. 2009;459(7247):663–7.

Casanova MF, Trippe J. Regulatory mechanisms of cortical laminar development. Brain Res Rev. 2006;51(1):72–84.

Cepeda C, André VM, Flores-Hernández J, Nguyen OK, Wu N, Klapstein GJ, Nguyen S, Koh S, Vinters H V., Levine MS, Mathern GW. Pediatric cortical dysplasia: Correlations between neuroimaging, electrophysiology and location of cytomegalic neurons and balloon cells and glutamate/GABA synaptic circuits. Dev Neurosci. 2005a;27(1):59–76.

Cepeda C, André VM, Levine MS, Salamon N, Miyata H, Vinters H V., Mathern GW. Epileptogenesis in pediatric cortical dysplasia: The dysmature cerebral developmental hypothesis. Epilepsy Behav. 2006;9(2):219–35.

Cepeda C, André VM, Vinters H V., Levine MS, Mathern GW. Are cytomegalic neurons and balloon cells generators of epileptic activity in pediatric cortical dysplasia? Epilepsia. 2005b;46(SUPPL. 5):82–8.

Cepeda C, André VM, Wu N, Yamazaki I, Uzgil B, Vinters H V., Levine MS, Mathern GW. Immature neurons and GABA networks may contribute to epileptogenesis in pediatric cortical dysplasia. Epilepsia. 2007;48(SUPPL. 5):79–85.

Cepeda C, Chen JY, Wu JY, Fisher RS, Vinters H V., Mathern GW, Levine MS. Pacemaker GABA synaptic activity may contribute to network synchronization in pediatric cortical dysplasia. Neurobiol Dis. 2014;62:208–17.

Cepeda C, Hurst RS, Flores-herna J, Klapstein GJ, Boylan MK, Calvert CR, Jocoy EL, Nguyen OK, Andre M, Vinters H V, Ariano MA, Levine MS, Mathern GW. Morphological and Electrophysiological Characterization of Abnormal Cell Types in Pediatric Cortical Dysplasia. 2003;486(January):472–86.

Chattopadhyaya B, Di Cristo G, Higashiyama H, Knott GW, Kuhlman SJ, Welker E, Huang ZJ. Experience and activity-dependent maturation of perisomatic GABAergic innervation in primary visual cortex during a postnatal critical period. J Neurosci. 2004;24(43):9598–611.

Chaudhuri A, Zangenehpour S, Rahbar-Dehgan F, Ye F. Molecular maps of neural activity and quiescence. Acta Neurobiol Exp (Wars). 2000;60(3):403–10.

Chen G, Zhang Y, Li X, Zhao X, Ye Q, Lin Y, Tao HW, Rasch MJ, Zhang X. Distinct Inhibitory Circuits Orchestrate Cortical beta and gamma Band Oscillations. Neuron. 2017;96(6):1403-1418.e6.

Chen H, Firestein BL. RhoA regulates dendrite branching in hippocampal neurons by decreasing cypin protein levels. J Neurosci. 2007;27(31):8378–86.

Chen J, Dong B, Feng X, Jiang D, Chen G, Long C, Yang L. Aberrant mPFC GABAergic synaptic transmission and fear behavior in neuroligin-2 R215H knock-in mice. Brain Res. 2020;1730.

Chen SX, Kim AN, Peters AJ, Komiyama T. Subtype-specific plasticity of inhibitory circuits in motor cortex during motor learning. Nat Neurosci. 2015;18(8):1109–15.

Chen W, Luo B, Gao N, Li H, Wang H, Li L, Cui W, Zhang L, Sun D, Liu F, Dong Z, Ren X, Zhang H, Su H, Xiong WC, Mei L. Neddylation stabilizes Nav1.1 to maintain interneuron excitability and prevent seizures in murine epilepsy models. J Clin Invest. 2021;131(8).

Chilosi AM, Cipriani P, Bertuccelli B, Pfanner L, Cioni G. Early cognitive and communication development in children with focal brain lesions. J Child Neurol. 2001;16(5):309–16.

Choii G, Ko J. Gephyrin: a central GABAergic synapse organizer. Exp Mol Med. 2015;47:e158.

Chung L. A Brief Introduction to the Transduction of Neural Activity into Fos Signal. Dev Reprod. 2015;19(2):61–7.

Cohen SM, Tsien RW, Goff DC, Halassa MM. The impact of NMDA receptor hypofunction on GABAergic neurons in the pathophysiology of schizophrenia. Schizophr Res. 2015;167(1–3):98–107.

Couey JJ, Witoelar A, Zhang SJ, Zheng K, Ye J, Dunn B, Czajkowski R, Moser MB, Moser EI, Roudi Y, Witter MP. Recurrent inhibitory circuitry as a mechanism for grid formation. Nat Neurosci. 2013;16(3):318–24.

Crino PB. Focal cortical dysplasia. Semin Neurol. 2015a;35(3):201–8.

Crino PB. mTOR signaling in epilepsy: Insights from malformations of cortical development. Cold Spring Harb Perspect Med. 2015b;5(4):1–18.

Crino PB, Trojanowski JQ, Eberwine J. Internexin, MAP1B, and nestin in cortical dysplasia as markers of developmental maturity. Acta Neuropathol. 1997;93(6):619–27.

Cruikshank SJ, Lewis TJ, Connors BW. Synaptic basis for intense thalamocortical activation of feedforward inhibitory cells in neocortex. Nat Neurosci. 2007;10(4):462–8.

Cummings KA, Clem RL. Prefrontal somatostatin interneurons encode fear memory. Nat Neurosci. 2020;23(1):61–74.

Curatolo P, Moavero R, van Scheppingen J, Aronica E. mTOR dysregulation and tuberous sclerosis-related epilepsy. Expert Rev Neurother. 2018;18(3):185–201.

Cybulsky A V., Guillemette J, Papillon J, Abouelazm NT. Regulation of Ste20-like kinase, SLK, activity: Dimerization and activation segment phosphorylation. PLoS One. 2017;12(5):1–25.

Cybulsky A V., Papillon J, Guillemette J, Belkina N, Patino-Lopez G, Torban E. Ste20-like kinase, SLK, a novel mediator of podocyte integrity. Am J Physiol - Ren Physiol. 2018;315(1):F186–98.

Cybulsky A V., Takano T, Papillon J, Hao W, Mancini A, Di Battista JA, Cybulsky MI. The 3′-untranslated region of the Ste20-like kinase SLK regulates SLK expression. Am J Physiol - Ren Physiol. 2007;292(2).

Cybulsky A V., Takano T, Papillon J, Khadir A, Bijian K, Chien CC, Alpers CE, Rabb H. Renal expression and activity of the germinal center kinase SK2. Am J Physiol - Ren Physiol. 2004;286(1 55-1):16–25.

Dan I, Watanabe NM, Kusumi A. The Ste20 group kinases as regulators of MAP kinase cascades. Trends Cell Biol. 2001;11(5):220–30.

Delarosa S, Guillemette J, Papillon J, Han YS, Kristof AS, Cybulsky A V. Activity of the ste20-like kinase, SLK, is enhanced by homodimerization. Am J Physiol - Ren Physiol. 2011;301(3):554–64.

Delevich K, Tucciarone J, Huang ZJ, Li B. The mediodorsal thalamus drives feedforward inhibition in the anterior cingulate cortex via parvalbumin interneurons. J Neurosci. 2015;35(14):5743–53.

Dickson BJ. Molecular mechanisms of axon guidance. Science (80-). 2002;298(5600):1959–64.

Donato F, Rompani SB, Caroni P. Parvalbumin-expressing basket-cell network plasticity

induced by experience regulates adult learning. Nature. 2013;504(7479):272–6.

Dougherty MJ, Santi M, Brose MS, Ma C, Resnick AC, Sievert AJ, Storm PB, Biegel JA. Activating mutations in BRAF characterize a spectrum of pediatric low-grade gliomas. Neuro Oncol. 2010;12(7):621–30.

Douglas RJ, Koch C, Mahowald M, Martin KAC, Suarez HH. Recurrent excitation in neocortical circuits. Science (80-). 1995;269(5226):981–5.

Douglas RJ, Martin KAC. Neuronal circuits of the neocortex. Annu Rev Neurosci. 2004;27:419–51.

Drexel M, Preidt AP, Kirchmair E, Sperk G. Parvalbumin interneurons and calretinin fibers arising from the thalamic nucleus reuniens degenerate in the subiculum after kainic acid-induced seizures. Neuroscience. 2011;189(1–2):316–29.

Drexel M, Romanov RA, Wood J, Weger S, Heilbronn R, Wulff P, Tasan RO, Harkany T, Sperk G. Selective silencing of hippocampal parvalbumin interneurons induces development of recurrent spontaneous limbic seizures in mice. J Neurosci. 2017;37(34):8166–79.

Duong T, De Rosa MJ, Poukens V, Vinters H V., Fisher RS. Neuronal cytoskeletal abnormalities in human cerebral cortical dysplasia. Acta Neuropathol. 1994;87(5):493–503.

Dutton SB, Makinson CD, Papale LA, Shankar A, Balakrishnan B, Nakazawa K, Escayg A. Preferential inactivation of SCN1A in parvalbumin interneurons increases seizure susceptibility. Neurobiol Dis. 2013;49(1):211–20.

Dzyubenko E, Fleischer M, Manrique-Castano D, Borbor M, Kleinschnitz C, Faissner A, Hermann DM. Inhibitory control in neuronal networks relies on the extracellular matrix integrity. Cell Mol Life Sci. 2021;78(14):5647–63.

Ehrstedt C, Ahlsten G, Strömberg B, Lindskog C, Casar-Borota O. Somatostatin receptor expression and mTOR pathway activation in glioneuronal tumours of childhood. Seizure. 2020;76:123–30.

Ellender TJ, Avery S V., Mahfooz K, Scaber J, von Klemperer A, Nixon SL, Buchan MJ, van Rheede JJ, Gatti A, Waites C, Pavlou HJ, Sims D, Newey SE, Akerman CJ. Embryonic progenitor pools generate diversity in fine-scale excitatory cortical subnetworks. Nat Commun. 2019;10(1).

Elvira G, Wasiak S, Blandford V, Tong XK, Serrano A, Fan X, del Rayo Sánchez-Carbente

M, Servant F, Bell AW, Boismenu D, Lacaille JC, McPherson PS, DesGroseillers L, Sossin WS. Characterization of an RNA granule from developing brain. Mol Cell Proteomics. 2006;5(4):635–51.

Englot DJ, Berger MS, Barbaro NM, Chang EF. Factors associated with seizure freedom in the surgical resection of glioneuronal tumors. Epilepsia. 2012;53(1):51–7.

Erisir A, Lau D, Rudy B, Leonard CS. Function of specific K+ channels in sustained high-frequency firing of fast-spiking neocortical interneurons. J Neurophysiol. 1999;82(5):2476–89.

Ethell IM, Pasquale EB. Molecular mechanisms of dendritic spine development and remodeling. Prog Neurobiol. 2005;75(3):161–205.

Fanselow EE, Richardson KA, Connors BW. Selective, state-dependent activation of somatostatin-expressing inhibitory interneurons in mouse neocortex. J Neurophysiol. 2008;100(5):2640–52.

Fares T, Stepanyants A. Cooperative synapse formation in the neocortex. Proc Natl Acad Sci U S A. 2009;106(38):16463–8.

Faustino A, Couto JP, Pópulo H, Rocha AS, Pardal F, Cameselle-Teijeiro JM, Lopes JM, Sobrinho-Simões M, Soares P. mTOR pathway overactivation in BRAF mutated papillary thyroid carcinoma. J Clin Endocrinol Metab. 2012;97(7).

Fazzari P, Paternain A V., Valiente M, Pla R, Luján R, Lloyd K, Lerma J, Marín O, Rico B. Control of cortical GABA circuitry development by Nrg1 and ErbB4 signalling. Nature. 2010;464(7293):1376–80.

Feldmeyer D. Excitatory neuronal connectivity in the barrel cortex. 2012;6(July):1–22.

Feldmeyer D, Brecht M, Helmchen F, Petersen CCH, Poulet JFA, Staiger JF, Luhmann HJ, Schwarz C. Barrel cortex function. Prog Neurobiol. 2013;103:3–27.

Feldmeyer D, Qi G, Emmenegger V, Staiger JF. Inhibitory interneurons and their circuit motifs in the many layers of the barrel cortex. Neuroscience. 2018;368:132–51.

Férézou I, Cauli B, Hill EL, Rossier J, Hamel E, Lambolez B. 5-HT3 receptors mediate serotonergic fast synaptic excitation of neocortical vasoactive intestinal peptide/cholecystokinin interneurons. J Neurosci. 2002;22(17):7389–97.

Ferguson BR, Gao WJ. Pv interneurons: critical regulators of E/I balance for prefrontal cortex-dependent behavior and psychiatric disorders. Front Neural Circuits. 2018a;12(May):1–13.

Ferguson BR, Gao WJ. Thalamic Control of Cognition and Social Behavior Via Regulation of Gamma-Aminobutyric Acidergic Signaling and Excitation/Inhibition Balance in the Medial Prefrontal Cortex. Biol Psychiatry. 2018b;83(8):657–69.

Fernández V, Llinares-Benadero C, Borrell V. Cerebral cortex expansion and folding: what have we learned? EMBO J. 2016;35(10):1021–44.

Filippenkov IB, Sudarkina OY, Limborska SA, Dergunova L V. Circular RNA of the human sphingomyelin synthase 1 gene: Multiple splice variants, evolutionary conservatism and expression in different tissues. RNA Biol. 2015;12(9):1030–42.

Fino E, Yuste R. Dense inhibitory connectivity in neocortex. Neuron. 2011;69(6):1188–203.

Fisher RS, Acevedo C, Arzimanoglou A, Bogacz A, Cross JH, Elger CE, Engel J, Forsgren L, French JA, Glynn M, Hesdorffer DC, Lee BI, Mathern GW, Moshé SL, Perucca E, Scheffer IE, Tomson T, Watanabe M, Wiebe S. ILAE Official Report: A practical clinical definition of epilepsy. Epilepsia. 2014;55(4):475–82.

Fisher RS, Cross JH, D'Souza C, French JA, Haut SR, Higurashi N, Hirsch E, Jansen FE, Lagae L, Moshé SL, Peltola J, Roulet Perez E, Scheffer IE, Schulze-Bonhage A, Somerville E, Sperling M, Yacubian EM, Zuberi SM. Instruction manual for the ILAE 2017 operational classification of seizure types. Epilepsia. 2017a;58(4):531–42.

Fisher RS, Cross JH, French JA, Higurashi N, Hirsch E, Jansen FE, Lagae L, Moshé SL, Peltola J, Roulet Perez E, Scheffer IE, Zuberi SM. Operational classification of seizure types by the International League Against Epilepsy: Position Paper of the ILAE Commission for Classification and Terminology. Epilepsia. 2017b;58(4):522–30.

Fisher RS, Van Emde Boas W, Blume W, Elger C, Genton P, Lee P, Engel J. Epileptic seizures and epilepsy: Definitions proposed by the International League Against Epilepsy (ILAE) and the International Bureau for Epilepsy (IBE). Epilepsia. 2005;46(4):470–2.

Frias CP, Liang J, Bresser T, Scheefhals L, Van Kesteren M, Van Dorland R, Yin Hu H, Bodzeta A, Van Bergen En Henegouwen PMP, Hoogenraad CC, Wierenga CJ. Semaphorin4D induces inhibitory synapse formation by rapid stabilization of presynaptic boutons via MET coactivation. J Neurosci. 2019;39(22):4221–37.

Fritschy JM. Epilepsy, E/I balance and GABAA receptor plasticity. Front Mol Neurosci.

2008;1(MAR).

Fu Y, Kaneko M, Tang Y, Alvarez-Buylla A, Stryker MP. A cortical disinhibitory circuit for enhancing adult plasticity. Elife. 2015;2015(4).

Fu Y, Tucciarone JM, Espinosa JS, Sheng N, Darcy DP, Nicoll RA, Huang ZJ, Stryker MP. A cortical circuit for gain control by behavioral state. Cell. 2014;156(6):1139–52.

Fung SJ, Webster MJ, Sivagnanasundaram S, Duncan C, Elashoff M, Weickert CS. Expression of interneuron markers in the dorsolateral prefrontal cortex of the developing human and in schizophrenia. Am J Psychiatry. 2010;167(12):1479–88.

Fuzik J, Zeisel A, Mate Z, Calvigioni D, Yanagawa Y, Szabo G, Linnarsson S, Harkany T. Integration of electrophysiological recordings with single-cell RNA-seq data identifies neuronal subtypes. Nat Biotechnol. 2016;34(2):175–83.

Galarreta M, Hestrin S. A network of fast-spiking cells in the neocortex connected by electrical synapses. Nature. 1999;402(6757):72–5.

Gatto L, Franceschi E, Nunno V Di, Tomasello C, Bartolini S, Brandes AA. Glioneuronal tumors: Clinicopathological findings and treatment options. Future Neurol. 2020;15(3).

Gentet LJ, Kremer Y, Taniguchi H, Huang ZJ, Staiger JF, Petersen CCH. Unique functional properties of somatostatin-expressing GABAergic neurons in mouse barrel cortex. Nat Neurosci. 2012;15(4):607–12.

Gibson JR, Belerlein M, Connors BW. Two networks of electrically coupled inhibitory neurons in neocortex. Nature. 1999;402(6757):75–9.

Gibson JR, Huber KM, Südhof TC. Neuroligin-2 deletion selectively decreases inhibitory synaptic transmission originating from fast-spiking but not from somatostatin-positive interneurons. J Neurosci. 2009;29(44):13883–97.

Giulioni M. Epilepsy associated tumors: Review article. World J Clin Cases. 2014;2(11):623.

Goldberg EM, Jeong HY, Kruglikov I, Tremblay R, Lazarenko RM, Rudy B. Rapid developmental maturation of neocortical FS cell intrinsic excitability. Cereb Cortex. 2011;21(3):666–82.

Gonzalez-Burgos G, Cho RY, Lewis DA. Alterations in cortical network oscillations and parvalbumin neurons in schizophrenia. Biol Psychiatry. 2015;77(12):1031–40.

Goz RU, Akgül G, LoTurco JJ. BRAFV600E expression in neural progenitors results in a

hyperexcitable phenotype in neocortical pyramidal neurons. J Neurophysiol. 2020;123(6):2449–64.

Grote A, Robens BK, Blümcke I, Becker AJ, Schoch S, Gembé E. LRP12 silencing during brain development results in cortical dyslamination and seizure sensitization. Neurobiol Dis. 2016;86:170–6.

Grueber WB, Jan LY, Jan YN. Different levels of the homeodomain protein cut regulate distinct dendrite branching patterns of Drosophila multidendritic neurons. Cell. 2003;112(6):805–18.

Guilluy C, Rolli-Derkinderen M, Loufrani L, Bourgá A, Henrion D, Sabourin L, Loirand G, Pacaud P. Ste20-related kinase SLK phosphorylates serl88 of RhoA to induce vasodilation in response to angiotensin II type 2 receptor activation. Circ Res. 2008;102(10):1265–74.

Gulyás AI, Freund TT. Generation of physiological and pathological high frequency oscillations: The role of perisomatic inhibition in sharp-wave ripple and interictal spike generation. Curr Opin Neurobiol. 2015;31:26–32.

Halff EF, Szulc BR, Lesept F, Kittler JT. SNX27-Mediated Recycling of Neuroligin-2 Regulates Inhibitory Signaling. Cell Rep. 2019;29(9):2599-2607.e6.

Hamilton LS, Sohl-Dickstein J, Huth AG, Carels VM, Deisseroth K, Bao S. Optogenetic Activation of an Inhibitory Network Enhances Feedforward Functional Connectivity in Auditory Cortex. Neuron. 2013;80(4):1066–76.

Hammers A, Koepp MJ, Richardson MP, Labbé C, Brooks DJ, Cunningham VJ, Duncan JS. Central benzodiazepine receptors in malformations of cortical development: A quantitative study. Brain. 2001;124(8):1555–65.

Hanai S, Saito T, Nakagawa E, Arai A, Otsuki T, Sasaki M, Goto Y ichi, Itoh M. Abnormal maturation of non-dysmorphic neurons in focal cortical dysplasia: Immunohistochemical considerations. Seizure. 2010;19(5):274–9.

Hao W, Takano T, Guillemette J, Papillon J, Ren G, Cybulsky A V. Induction of apoptosis by the Ste20-like kinase SLK, a germinal center kinase that activates apoptosis signal-regulating kinase and p38. J Biol Chem. 2006;281(6):3075–84.

Hardingham NR, Read JCA, Trevelyan AJ, Nelson JC, Jack JJB, Bannister NJ. Quantal analysis reveals a functional correlation between presynaptic and postsynaptic efficacy in excitatory connections from rat neocortex. J Neurosci. 2010;30(4):1441–

51.

Harris KD, Mrsic-flogel TD. Cortical connectivity and sensory coding. Nature. 2013;503(7474):51–8.

Harris KD, Shepherd GMG. The neocortical circuit: Themes and variations. Nat Neurosci. 2015;18(2):170–81.

Hashimoto K, Kano M. Synapse elimination in the developing cerebellum. Cell Mol Life Sci. 2013;70(24):4667–80.

Hijazi S, Heistek TS, Scheltens P, Neumann U, Shimshek DR, Mansvelder HD, Smit AB, van Kesteren RE. Early restoration of parvalbumin interneuron activity prevents memory loss and network hyperexcitability in a mouse model of Alzheimer's disease. Mol Psychiatry. 2020;25(12):3380–98.

Hsieh LS, Wen JH, Claycomb K, Huang Y, Harrsch FA, Naegele JR, Hyder F, Buchanan GF, Bordey A. Convulsive seizures from experimental focal cortical dysplasia occur independently of cell misplacement. Nat Commun. 2016;7:1–12.

Hu H, Gan J, Jonas P. Fast-spiking, parvalbumin+ GABAergic interneurons: From cellular design to microcircuit function. Science (80-). 2014;345(6196).

Huang Y, Jiang H, Zheng Q, Fok AHK, Li X, Lau CG, Lai CSW. Environmental enrichment or selective activation of parvalbumin-expressing interneurons ameliorates synaptic and behavioral deficits in animal models with schizophrenia-like behaviors during adolescence. Mol Psychiatry. 2021;

Huberfeld G, Vecht CJ. Seizures and gliomas - Towards a single therapeutic approach. Nat Rev Neurol. 2016;12(4):204–16.

Hull C, Isaacson JS, Scanziani M. Postsynaptic mechanisms govern the differential excitation of cortical neurons by thalamic inputs. J Neurosci. 2009;29(28):9127–36.

Hunnicutt BJ, Long BR, Kusefoglu D, Gertz KJ, Zhong H, Mao T. A comprehensive thalamocortical projection map at the mesoscopic level. Nat Neurosci. 2014;(August):1–13.

Iaccarino HF, Singer AC, Martorell AJ, Rudenko A, Gao F, Gillingham TZ, Mathys H, Seo J, Kritskiy O, Abdurrob F, Adaikkan C, Canter RG, Rueda R, Brown EN, Boyden ES, Tsai LH. Gamma frequency entrainment attenuates amyloid load and modifies microglia. Nature. 2016;540(7632):230–5.

Iascone DM, Li Y, Sümbül U, Doron M, Chen H, Andreu V, Goudy F, Blockus H, Abbott

LF, Segev I, Peng H, Polleux F. Whole-Neuron Synaptic Mapping Reveals Spatially Precise Excitatory/Inhibitory Balance Limiting Dendritic and Somatic Spiking. Neuron. 2020;106(4):566-578.e8.

Iffland PH, Carson V, Bordey A, Crino PB. GATORopathies: The role of amino acid regulatory gene mutations in epilepsy and cortical malformations. Epilepsia. 2019;60(11):2163–73.

Iffland PH, Crino PB. Focal Cortical Dysplasia: Gene Mutations, Cell Signaling, and Therapeutic Implications. Annu Rev Pathol Mech Dis. 2017;12:547–71.

Inoue T, Imoto K. Feedforward inhibitory connections from multiple thalamic cells to multiple regular-spiking cells in layer 4 of the somatosensory cortex. J Neurophysiol. 2006;96(4):1746–54.

Isaacson JS, Scanziani M. How inhibition shapes cortical activity. Neuron. 2011;72(2):231–43.

Itoh S, Kameda Y, Yamada E, Tsujikawa K, Mimura T, Kohama Y. Molecular cloning and characterization of a novel putative STE20-like kinase in guinea pigs. Arch Biochem Biophys. 1997;340(2):201–7.

Jaberi A, Hooker E, Guillemette J, Papillon J, Kristof AS, Cybulsky A V. Identification of Tpr and α-actinin-4 as two novel SLK-interacting proteins. Biochim Biophys Acta - Mol Cell Res. 2015;1853(10):2539–52.

Jami SA, Cameron S, Wong JM, Daly ER, McAllister AK, Gray JA. Increased excitation-inhibition balance and loss of gabaergic synapses in the serine racemase knockout model of nmda receptor hypofunction. J Neurophysiol. 2021;126(1):11–27.

Jayalakshmi S, Nanda SK, Vooturi S, Vadapalli R, Sudhakar P, Madigubba S, Panigrahi M. Focal cortical dysplasia and refractory epilepsy: Role of multimodality imaging and outcome of surgery. Am J Neuroradiol. 2019;40(5):892–8.

Jiang X, Lachance M, Rossignol E. Involvement of cortical fast-spiking parvalbumin-positive basket cells in epilepsy. Prog Brain Res. 2016;226:81–126.

Jiang X, Nardelli J. Cellular and molecular introduction to brain development. Neurobiol Dis. 2016;92(Part A):3–17.

Kapfer C, Glickfeld LL, Atallah B V., Scanziani M. Supralinear increase of recurrent inhibition during sparse activity in the somatosensory cortex. Nat Neurosci. 2007;10(6):743–53.

Karube F, Kubota Y, Kawaguchi Y. Axon Branching and Synaptic Bouton Phenotypes in GABAergic Nonpyramidal Cell Subtypes. J Neurosci. 2004;24(12):2853–65.

Kato HK, Gillet SN, Isaacson JS. Flexible Sensory Representations in Auditory Cortex Driven by Behavioral Relevance. Neuron. 2015;88(5):1027–39.

Kawaguchi Y, Kubota Y. Physiological and morphological identification of somatostatin- or vasoactive intestinal polypeptide-containing cells among GABAergic cell subtypes in rat frontal cortex. J Neurosci. 1996;16(8):2701–15.

Kim D, Jeong H, Lee J, Ghim JW, Her ES, Lee SH, Jung MW. Distinct Roles of Parvalbumin- and Somatostatin-Expressing Interneurons in Working Memory. Neuron. 2016a;92(4):902–15.

Kim H, Ährlund-Richter S, Wang X, Deisseroth K, Carlén M. Prefrontal Parvalbumin Neurons in Control of Attention. Cell. 2016b;164(1–2):208–18.

Kim HK, Gschwind T, Nguyen TM, Bui AD, Felong S, Ampig K, Suh D, Ciernia A V., Wood MA, Soltesz I. Optogenetic intervention of seizures improves spatial memory in a mouse model of chronic temporal lobe epilepsy. Epilepsia. 2020;61(3):561–71.

Kim S, Kang M, Park D, Lee AR, Betz H, Ko J, Chang I, Um JW. Impaired formation of high-order gephyrin oligomers underlies gephyrin dysfunction-associated pathologies. iScience. 2021;24(2).

Kimura N, Takahashi Y, Shigematsu H, Imai K, Ikeda H, Ootani H, Takayama R, Mogami Y, Kimura N, Baba K, Matsuda K, Tottori T, Usui N, Kondou S, Inoue Y. Risk factors of cognitive impairment in pediatric epilepsy patients with focal cortical dysplasia. Brain Dev. 2019;41(1):77–84.

Kneussel M, Brandstätter JH, Laube B, Stahl S, Müller U, Betz H. Loss of postsynaptic GABA(A) receptor clustering in gephyrin-deficient mice. J Neurosci. 1999;19(21):9289–97.

Knopp A, Frahm C, Fidzinski P, Witte OW, Behr J. Loss of GABAergic neurons in the subiculum and its functional implications in temporal lobe epilepsy. Brain. 2008;131(6):1516–27.

Koh HY, Kim SH, Jang J, Kim H, Han S, Lim JS, Son G, Choi J, Park BO, Do Heo W, Han J, Lee HJ, Lee D, Kang HC, Shong M, Paik SB, Kim DS, Lee JH. BRAF somatic mutation contributes to intrinsic epileptogenicity in pediatric brain tumors. Nat Med. 2018;24(11):1662–8.

Kolodkin AL, Tessier-Lavigne M. Mechanisms and molecules of neuronal wiring: A primer. Cold Spring Harb Perspect Biol. 2011;3(6):1–14.

Krook-Magnuson E, Armstrong C, Oijala M, Soltesz I. On-demand optogenetic control of spontaneous seizures in temporal lobe epilepsy. Nat Commun. 2013;4.

Krook-Magnuson E, Szabo GG, Armstrong C, Oijala M, Soltesz I. Cerebellar directed optogenetic intervention inhibits spontaneous hippocampal seizures in a mouse model of temporal lobe epilepsy. eNeuro. 2014;1(1).

Kuzniecky R. Epilepsy and malformations of cortical development: New developments. Curr Opin Neurol. 2015;28(2):151–7.

Kvitsiani D, Ranade S, Hangya B, Taniguchi H, Huang JZ, Kepecs A. Distinct behavioural and network correlates of two interneuron types in prefrontal cortex. Nature. 2013;498(7454):363–6.

Kwan AC, Dan Y. Dissection of cortical microcircuits by single-neuron stimulation in vivo. Curr Biol. 2012;22(16):1459–67.

Lagler M, Ozdemir AT, Lagoun S, Malagon-Vina H, Borhegyi Z, Hauer R, Jelem A, Klausberger T. Divisions of Identified Parvalbumin-Expressing Basket Cells during Working Memory-Guided Decision Making. Neuron. 2016;91(6):1390–401.

Lamparello P, Baybis M, Pollard J, Hol EM, Eisenstat DD, Aronica E, Crino PB. Developmental lineage of cell types in cortical dysplasia with balloon cells. Brain. 2007;130(9):2267–76.

Larkum ME, Senn W, Lüscher HR. Top-down dendritic input increases the gain of layer 5 pyramidal neurons. Cereb Cortex. 2004;14(10):1059–70.

Larkum ME, Zhu JJ, Sakmann B. A new cellular mechanism for coupling inputs arriving at different cortical layers. Nature. 1999;398(6725):338–41.

Lee J. Malformations of cortical development : genetic mechanisms and diagnostic approach. 2017;60(1):1–9.

Lee JH. Somatic mutations in disorders with disrupted brain connectivity. 2016;48(6):e239-9.

Lee S, Kruglikov I, Huang ZJ, Fishell G, Rudy B. A disinhibitory circuit mediates motor integration in the somatosensory cortex. Nat Neurosci. 2013;16(11):1662–70.

Lee SH, Hjerling-Leffler J, Zagha E, Fishell G, Rudy B. The largest group of superficial neocortical GABAergic interneurons expresses ionotropic serotonin receptors. J

Neurosci. 2010;30(50):16796–808.

Lee SH, Kwan AC, Zhang S, Phoumthipphavong V, Flannery JG, Masmanidis SC, Taniguchi H, Huang ZJ, Zhang F, Boyden ES, Deisseroth K, Dan Y. Activation of specific interneurons improves V1 feature selectivity and visual perception. Nature. 2012;488(7411):379–83.

Lefort S, Tomm C, Floyd Sarria JC, Petersen CCH. The Excitatory Neuronal Network of the C2 Barrel Column in Mouse Primary Somatosensory Cortex. Neuron. 2009;61(2):301–16.

Letzkus JJ, Wolff SBE, Meyer EMM, Tovote P, Courtin J, Herry C, Lüthi A. A disinhibitory microcircuit for associative fear learning in the auditory cortex. Nature. 2011;480(7377):331–5.

Li LY, Li YT, Zhou M, Tao HW, Zhang LI. Intracortical multiplication of thalamocortical signals in mouse auditory cortex. Nat Neurosci. 2013a;16(9):1179–81.

Li N, Chen TW, Guo Z V., Gerfen CR, Svoboda K. A motor cortex circuit for motor planning and movement. Nature. 2015;519(7541):51–6.

Li X, Zhang J, Cao Z, Wu J, Shi Y. Solution structure of GOPC PDZ domain and its interaction with the C-terminal motif of neuroligin. Protein Sci. 2006;15(9):2149–58.

Li YT, Ibrahim LA, Liu BH, Zhang LI, Tao HW. Linear transformation of thalamocortical input by intracortical excitation. Nat Neurosci. 2013b;16(9):1324–30.

Li Z, Sheng M. Some assembly required: The development of neuronal synapses. Nat Rev Mol Cell Biol. 2003;4(11):833–41.

Liang C, Zhang CQ, Chen X, Wang LK, Yue J, An N, Zhang L, Liu SY, Yang H. Differential Expression Hallmarks of Interneurons in Different Types of Focal Cortical Dysplasia. J Mol Neurosci. 2020;70(5):796–805.

Liang J, Xu W, Hsu YT, Yee AX, Chen L, Südhof TC. Conditional neuroligin-2 knockout in adult medial prefrontal cortex links chronic changes in synaptic inhibition to cognitive impairments. Mol Psychiatry. 2015;20(7):850–9.

Lien AD, Scanziani M. Tuned thalamic excitation is amplified by visual cortical circuits. Nat Neurosci. 2013;16(9):1315–23.

Lim JS, Gopalappa R, Kim SH, Ramakrishna S, Lee M, Kim W-I, Kim J, Park SM, Lee J, Oh J-H, Kim HD, Park C-H, Lee JS, Kim S, Kim DS, Han JM, Kang H-C, Kim H (Henry), Lee JH. Somatic Mutations in TSC1 and TSC2 Cause Focal Cortical

Dysplasia. Am J Hum Genet. 2017;100(3):454–72.

Lim JS, Kim W Il, Kang HC, Kim SH, Park AH, Park EK, Cho YW, Kim S, Kim HM, Kim JA, Kim J, Rhee H, Kang SG, Kim HD, Kim D, Kim DS, Lee JH. Brain somatic mutations in MTOR cause focal cortical dysplasia type II leading to intractable epilepsy. Nat Med. 2015;21(4):395–400.

Lionel AC, Vaags AK, Sato D, Gazzellone MJ, Mitchell EB, Chen HY, Costain G, Walker S, Egger G, Thiruvahindrapuram B, Merico D, Prasad A, Anagnostou E, Fombonne E, Zwaigenbaum L, Roberts W, Szatmari P, Fernandez BA, Georgieva L, Brzustowicz LM, Roetzer K, Kaschnitz W, Vincent JB, Windpassinger C, Marshall CR, Trifiletti RR, Kirmani S, Kirov G, Petek E, Hodge JC, Bassett AS, Scherer SW. Rare exonic deletions implicate the synaptic organizer gephyrin (GPHN) in risk for autism, schizophrenia and seizures. Hum Mol Genet. 2013;22(10):2055–66.

Liste I, Rozas G, Guerra MJ, Labandeira-Garcia JL. Cortical stimulation induces Fos expression in striatal neurons via NMDA glutamate and dopamine receptors. Brain Res. 1995;700(1–2):1–12.

Liu D, Gu X, Zhu J, Zhang X, Han Z, Yan W, Cheng Q, Hao J, Fan H, Hou R, Chen Z, Chen Y, Li CT. Medial prefrontal activity during delay period contributes to learning of a working memory task. Science (80-). 2014;346(6208):458–63.

Liu J, Wang M, Sun L, Pan NC, Zhang C, Zhang J, Zuo Z, He S, Wu Q, Wang X. Integrative analysis of in vivo recording with single-cell RNA-seq data reveals molecular properties of light-sensitive neurons in mouse V1. Protein Cell. 2020;11(6):417–32.

Ljungberg MC, Bhattacharjee MB, Lu Y, Armstrong DL, Yoshor D, Swann JW, Sheldon M, D'Arcangelo G. Activation of mammalian target of rapamycin in cytomegalic neurons of human cortical dysplasia. Ann Neurol. 2006;60(4):420–9.

Lübke J, Feldmeyer D. Excitatory signal flow and connectivity in a cortical column: Focus on barrel cortex. Brain Struct Funct. 2007;212(1):3–17.

Lucibello FC, Lowag C, Neuberg M, Müller R. Trans-repression of the mouse c-fos promoter: A novel mechanism of fos-mediated trans-regulation. Cell. 1989;59(6):999–1007.

Luhovy AY, Jaberi A, Papillon J, Guillemette J, Cybulsky A V. Regulation of the Ste20-like kinase, SLK: Involvement of activation segment phosphorylation. J Biol Chem. 2012;287(8):5446–58.

Lun ATL, Bach K, Marioni JC. Pooling across cells to normalize single-cell RNA sequencing data with many zero counts. Genome Biol. 2016a;17(1).

Lun ATL, McCarthy DJ, Marioni JC. A step-by-step workflow for low-level analysis of single-cell RNA-seq data with Bioconductor. F1000Research. 2016b;5.

Luo B, Liu Z, Lin D, Chen W, Ren D, Yu Z, Xiong M, Zhao C, Fei E, Li B. ErbB4 promotes inhibitory synapse formation by cell adhesion, independent of its kinase activity. Transl Psychiatry. 2021;11(1):361.

Ma Y, Hu H, Berrebi AS, Mathers PH, Agmon A. Distinct subtypes of somatostatin-containing neocortical interneurons revealed in transgenic mice. J Neurosci. 2006;26(19):5069–82.

Maheshwari A, Nahm WK, Noebels JL. Paradoxical proepileptic response to NMDA receptor blockade linked to cortical interneuron defect in stargazer mice. Front Cell Neurosci. 2013;7(SEP).

Majolo F, Marinowic DR, Machado DC, Costa J, Costa D. Epilepsy & Behavior MTOR pathway in focal cortical dysplasia type 2 : What do we know ? Epilepsy Behav. 2018;85:157–63.

Makino H, Hwang EJ, Hedrick NG, Komiyama T. Circuit Mechanisms of Sensorimotor Learning. Neuron. 2016;92(4):705–21.

Marder E, Goaillard JM. Variability, compensation and homeostasis in neuron and network function. Nat Rev Neurosci. 2006;7(7):563–74.

Marín O, Valdeolmillos M, Moya F. Neurons in motion: same principles for different shapes? Trends Neurosci. 2006;29(12):655–61.

Markram H, Toledo-Rodriguez M, Wang Y, Gupta A, Silberberg G, Wu C. Interneurons of the neocortical inhibitory system. Nat Rev Neurosci. 2004;5(10):793–807.

Marrs GS, Honda T, Fuller L, Thangavel R, Balsamo J, Lilien J, Dailey ME, Arregui C. Dendritic arbors of developing retinal ganglion cells are stabilized by β1-integrins. Mol Cell Neurosci. 2006;32(3):230–41.

Marsan E, Baulac S. Review: Mechanistic target of rapamycin (mTOR) pathway, focal cortical dysplasia and epilepsy. Neuropathol Appl Neurobiol. 2018;44(1):6–17.

Martina M, Jonas P. Functional differences in Na+ channel gating between fast-spiking interneurones and principal neurones of rat hippocampus. J Physiol. 1997;505(3):593–603.

Martinez-Losa M, Tracy TE, Ma K, Verret L, Clemente-Perez A, Khan AS, Cobos I, Ho K, Gan L, Mucke L, Alvarez-Dolado M, Palop JJ. Nav1.1-Overexpressing Interneuron Transplants Restore Brain Rhythms and Cognition in a Mouse Model of Alzheimer's Disease. Neuron. 2018;98(1):75-89.e5.

Mateo C, Avermann M, Gentet LJ, Zhang F, Deisseroth K, Petersen CCH. In vivo optogenetic stimulation of neocortical excitatory neurons drives brain-state-dependent inhibition. Curr Biol. 2011;21(19):1593–602.

Mathern GW, Cepeda C, Hurst RS, Flores-Hernandez J, Mendoza D, Levine MS. Neurons recorded from pediatric epilepsy surgery patients with cortical dysplasia. Epilepsia. 2000;41(SUPPL. 6).

Medici V, Rossini L, Deleo F, Tringali G, Tassi L, Cardinale F, Bramerio M, de Curtis M, Garbelli R, Spreafico R. Different parvalbumin and GABA expression in human epileptogenic focal cortical dysplasia. Epilepsia. 2016;57(7):1109–19.

Megías M, Emri Z, Freund TF, Gulyás AI. Total number and distribution of inhibitory and excitatory synapses on hippocampal CA1 pyramidal cells. Neuroscience. 2001;102(3):527–40.

Mellios N, Huang HS, Baker SP, Galdzicka M, Ginns E, Akbarian S. Molecular Determinants of Dysregulated GABAergic Gene Expression in the Prefrontal Cortex of Subjects with Schizophrenia. Biol Psychiatry. 2009;65(12):1006–14.

Miao Z, Deng K, Wang X, Zhang X. DEsingle for detecting three types of differential expression in single-cell RNA-seq data. Bioinformatics. 2018;34(18):3223–4.

Mierau SB, Patrizi A, Hensch TK, Fagiolini M. Cell-Specific Regulation of N-Methyl-D-Aspartate Receptor Maturation by Mecp2 in Cortical Circuits. Biol Psychiatry. 2016;79(9):746–54.

Miller CJ, Lou HJ, Simpson C, Van De Kooij B, Hak Ha B, Fisher OS, Pirman NL, Boggon TJ, Rinehart J, Yaffe MB, Linding R, Turk BE. Comprehensive profiling of the STE20 kinase family defines features essential for selective substrate targeting and signaling output. PLoS Biol. 2019.

Miller KD. Canonical computations of cerebral cortex. Curr Opin Neurobiol. 2016;37:75–84.

Miyata H, Chiang ACY, Vinters H V. Insulin signaling pathways in cortical dysplasia and TSC-tubers: Tissue microarray analysis. Ann Neurol. 2004;56(4):510–9.

Möddel G, Jacobson B, Ying Z, Janigro D, Bingaman W, González-Martínez J, Kellinghaus C, Prayson RA, Najm IM. The NMDA receptor NR2B subunit contributes to epileptogenesis in human cortical dysplasia. Brain Res. 2005;1046(1–2):10–23.

Møller RS, Weckhuysen S, Chipaux M, Marsan E, Taly V, Martina Bebin E, Hiatt SM, Prokop JW, Bowling KM, Mei D, Conti V, De La Grange P, Ferrand-Sorbets S, Dorfmüller G, Lambrecq V, Larsen LHG, Leguern E, Guerrini R, Rubboli G, Cooper GM, Baulac S. Germline and somatic mutations in the MTOR gene in focal cortical dysplasia and epilepsy. Neurol Genet. 2016;2(6).

Momose-Sato Y, Sato K. Optical imaging of the spontaneous depolarization wave in the mouse embryo: Origins and pharmacological nature. Ann N Y Acad Sci. 2013;1279(1):60–70.

Moosa ANV, Wyllie E. Focal epileptogenic lesions. 1st ed. Handb. Clin. Neurol. 2013.

Moresco EMY, Donaldson S, Williamson A, Koleske AJ. Integrin-mediated dendrite branch maintenance requires Abelson (Abl) family kinases. J Neurosci. 2005;25(26):6105–18.

Morgan JI, Curran T. Stimulus-transcription coupling in the nervous system: Involvement of the inducible proto-oncogenes fos and jun. Annu Rev Neurosci. 1991;14:421–51.

Moroni RF, Inverardi F, Regondi MC, Panzica F, Spreafico R, Frassoni C. Altered spatial distribution of PV-cortical cells and dysmorphic neurons in the somatosensory cortex of BCNU-treated rat model of cortical dysplasia. Epilepsia. 2008;49(5):872–87.

Mou T, Deng W, Gu F, Pawitan Y, Vu TN. Reproducibility of Methods to Detect Differentially Expressed Genes from Single-Cell RNA Sequencing. Front Genet. 2020;10.

Mühlebner A, Bongaarts A, Sarnat HB, Scholl T, Aronica E. New insights into a spectrum of developmental malformations related to mTOR dysregulations: challenges and perspectives. J Anat. 2019;235(3):521–42.

Mühlebner A, Gröppel G, Dressler A, Reiter-Fink E, Kasprian G, Prayer D, Dorfer C, Czech T, Hainfellner JA, Coras R, Blümcke I, Feucht M. Epilepsy surgery in children and adolescents with malformations of cortical development-Outcome and impact of the new ILAE classification on focal cortical dysplasia. Epilepsy Res. 2014;108(9):1652–61.

Muñoz W, Rudy B. Spatiotemporal specificity in cholinergic control of neocortical function.

Curr Opin Neurobiol. 2014;26:149–60.

Murayama M, Pérez-Garci E, Nevian T, Bock T, Senn W, Larkum ME. Dendritic encoding of sensory stimuli controlled by deep cortical interneurons. Nature. 2009;457(7233):1137–41.

Murphy TH, Worley PF, Baraban JM. L-type voltage-sensitive calcium channels mediate synaptic activation of immediate early genes. Neuron. 1991;7(4):625–35.

Myers JP, Gomez TM. Focal adhesion kinase promotes integrin adhesion dynamics necessary for chemotropic turning of nerve growth cones. J Neurosci. 2011;31(38):13585–95.

Nahar L, Delacroix BM, Nam HW. The Role of Parvalbumin Interneurons in Neurotransmitter Balance and Neurological Disease. Front Psychiatry. 2021;12.

Najm IM, Sarnat HB, Blümcke I. Review: The international consensus classification of Focal Cortical Dysplasia – a critical update 2018. Neuropathol Appl Neurobiol. 2018;44(1):18–31.

Najm IM, Ying Z, Babb T, Mohamed A, Hadam J, LaPresto E, Wyllie E, Kotagal P, Bingaman W, Foldvary N, Morris H, Luders HO. Epileptogenicity correlated with increased N-methyl-D-aspartate receptor subunit NR2A/B in human focal cortical dysplasia. Epilepsia. 2000;41(8):971–6.

Naka A, Veit J, Shababo B, Chance RK, Risso D, Stafford D, Snyder B, Egladyous A, Chu D, Sridharan S, Mossing DP, Paninski L, Ngai J, Adesnik H. Complementary networks of cortical somatostatin interneurons enforce layer specific control. Elife. 2019;8.

Nakagawa JM, Donkels C, Fauser S, Schulze-Bonhage A, Prinz M, Zentner J, Haas CA. Characterization of focal cortical dysplasia with balloon cells by layer-specific markers: Evidence for differential vulnerability of interneurons. Epilepsia. 2017;58(4):635–45.

Nakashima M, Saitsu H, Takei N, Tohyama J, Kato M, Kitaura H, Shiina M, Shirozu H, Masuda H, Watanabe K, Ohba C, Tsurusaki Y, Miyake N, Zheng Y, Sato T, Takebayashi H, Ogata K, Kameyama S, Kakita A, Matsumoto N. Somatic Mutations in the MTOR gene cause focal cortical dysplasia type IIb. Ann Neurol. 2015;78(3):375–86.

Nandagopal N, Roux PP. Regulation of global and specific mRNA translation by the

mTOR signaling pathway. Translation. 2015;3(1):e983402.

Natan RG, Briguglio JJ, Mwilambwe-Tshilobo L, Jones SI, Aizenberg M, Goldberg EM, Geffen MN. Complementary control of sensory adaptation by two types of cortical interneurons. Elife. 2015;4(OCTOBER2015).

Nelson A, Mooney R. The Basal Forebrain and Motor Cortex Provide Convergent yet Distinct Movement-Related Inputs to the Auditory Cortex. Neuron. 2016;90(3):635–48.

Nicklas S, Okawa S, Hillje AL, González-Cano L, Sol A Del, Schwamborn JC. The RNA helicase DDX6 regulates cell-fate specification in neural stem cells via miRNAs. Nucleic Acids Res. 2015;43(5):2638–54.

Noctor SC, Martinez-Cerdeño V, Ivic L, Kriegstein AR. Cortical neurons arise in symmetric and asymmetric division zones and migrate through specific phases. Nat Neurosci. 2004;7(2):136–44.

Oberlaender M, De Kock CPJ, Bruno RM, Ramirez A, Meyer HS, Dercksen VJ, Helmstaedter M, Sakmann B. Cell type-specific three-dimensional structure of thalamocortical circuits in a column of rat vibrissal cortex. Cereb Cortex. 2012;22(10):2375–91.

Oki J, Miyamoto A, Takahashi S, Takei H. Cognitive deterioration associated with focal cortical dysplasia. Pediatr Neurol. 1999;20(1):73–7.

Otsuka T, Kawaguchi Y. Cell diversity and connection specificity between callosal projection neurons in the frontal cortex. J Neurosci. 2011;31(10):3862–70.

Pala A, Petersen CCH. State-dependent cell-type-specific membrane potential dynamics and unitary synaptic inputs in awake mice. Elife. 2018;7:1–13.

Pallud J, McKhann GM. Diffuse Low-Grade Glioma-Related Epilepsy. Neurosurg Clin N Am. 2019;30(1):43–54.

Panthi S, Leitch B. Chemogenetic Activation of Feed-Forward Inhibitory Parvalbumin-Expressing Interneurons in the Cortico-Thalamocortical Network During Absence Seizures. Front Cell Neurosci. 2021;15.

Panzeri S, Petersen RS, Schultz SR, Lebedev M, Diamond ME. The role of spike timing in the coding of stimulus location in rat somatosensory cortex. Neuron. 2001;29(3):769–77.

Park SM, Lim JS, Ramakrishina S, Kim DS, Kim HH, Lee JH, Park SM, Lim JS,

Ramakrishina S, Kim SH, Kim WK, Lee J. Brain Somatic Mutations in MTOR Disrupt Neuronal Ciliogenesis , Leading to Focal Cortical Article Brain Somatic Mutations in MTOR Disrupt Neuronal Ciliogenesis , Leading to Focal Cortical Dyslamination. Neuron. 2018;99(1):83-97.e7.

Parrish JZ, Kim MD, Lily YJ, Yuh NJ. Genome-wide analyses identify transcription factors required for proper morphogenesis of Drosophila sensory neuron dendrites. Genes Dev. 2006;20(7):820–35.

Pasquier B, Péoc'H M, Fabre-Bocquentin B, Bensaadi L, Pasquier D, Hoffmann D, Kahane P, Tassi L, Le Bas J-F, Benabid AL. Surgical pathology of drug-resistant partial epilepsy. A 10-year-experience with a series of 327 consecutive resections. Epileptic Disord. 2002;4(2):99–119.

Patrizi A, Awad PN, Chattopadhyaya B, Li C, Di Cristo G, Fagiolini M. Accelerated Hyper-Maturation of Parvalbumin Circuits in the Absence of MeCP2. Cereb Cortex. 2020;30(1):256–68.

Paxinos G, Franklin K. The Mouse Brain in Stereotaxic Coordinates. 2da Editio. 2001.

Paz JT, Bryant AS, Peng K, Fenno L, Yizhar O, Frankel WN, Deisseroth K, Huguenard JR. A new mode of corticothalamic transmission revealed in the Gria4 -/- model of absence epilepsy. Nat Neurosci. 2011;14(9):1167–75.

Paz JT, Huguenard JR. Microcircuits and their interactions in epilepsy : is the focus out of focus ? 2015;18(3):351–9.

Pennartz CMA, Dora S, Muckli L, Lorteije JAM. Towards a Unified View on Pathways and Functions of Neural Recurrent Processing. Trends Neurosci. 2019;42(9):589–603.

Peron S, Pancholi R, Voelcker B, Wittenbach JD, Ólafsdóttir HF, Freeman J, Svoboda K. Recurrent interactions in local cortical circuits. Nature. 2020;579(7798):256–9.

Petreanu L, Mao T, Sternson SM, Svoboda K. The subcellular organization of neocortical excitatory connections. Nature. 2009;457(7233):1142–5.

Petrini EM, Ravasenga T, Hausrat TJ, Iurilli G, Olcese U, Racine V, Sibarita JB, Jacob TC, Moss SJ, Benfenati F, Medini P, Kneussel M, Barberis A. Synaptic recruitment of gephyrin regulates surface GABA A receptor dynamics for the expression of inhibitory LTP. Nat Commun. 2014;5.

Pfeffer CK, Xue M, He M, Huang ZJ, Scanziani M. Inhibition of inhibition in visual cortex: The logic of connections between molecularly distinct interneurons. Nat Neurosci.

2013;16(8):1068–76.

Pi HJ, Hangya B, Kvitsiani D, Sanders JI, Huang ZJ, Kepecs A. Cortical interneurons that specialize in disinhibitory control. Nature. 2013;503(7477):521–4.

Picelli S, Faridani OR, Björklund ÅK, Winberg G, Sagasser S, Sandberg R. Full-length RNA-seq from single cells using Smart-seq2. Nat Protoc. 2014;9(1):171–81.

Pike ACW, Rellos P, Niesen FH, Turnbull A, Oliver AW, Parker SA, Turk BE, Pearl LH, Knapp S. Activation segment dimerization: A mechanism for kinase autophosphorylation of non-consensus sites. EMBO J. 2008;27(4):704–14.

Pimentel J, Boccaccio GL. Translation and silencing in RNA granules: A tale of sand grains. Front Mol Neurosci. 2014;7(JULY).

Piñero J, Bravo Á, Queralt-Rosinach N, Gutiérrez-Sacristán A, Deu-Pons J, Centeno E, García-García J, Sanz F, Furlong LI. DisGeNET: A comprehensive platform integrating information on human disease-associated genes and variants. Nucleic Acids Res. 2017;45(D1):D833–9.

Pinto DJ, Brumberg JC, Simons DJ. Circuit dynamics and coding strategies in rodent somatosensory cortex. J Neurophysiol. 2000;83(3):1158–66.

Pizzarelli R, Griguoli M, Zacchi P, Petrini EM, Barberis A, Cattaneo A, Cherubini E. Tuning GABAergic Inhibition: Gephyrin Molecular Organization and Functions. Neuroscience. 2020;439:125–36.

Polack PO, Friedman J, Golshani P. Cellular mechanisms of brain state-dependent gain modulation in visual cortex. Nat Neurosci. 2013;16(9):1331–9.

Pouille F, Marin-Burgin A, Adesnik H, Atallah B V., Scanziani M. Input normalization by global feedforward inhibition expands cortical dynamic range. Nat Neurosci. 2009;12(12):1577–85.

Pouille F, Scanziani M. Enforcement of temporal fidelity in pyramidal cells by somatic feed-forward inhibition. Science (80-). 2001;293(5532):1159–63.

Poulopoulos A, Aramuni G, Meyer G, Soykan T, Hoon M, Papadopoulos T, Zhang M, Paarmann I, Fuchs C, Harvey K, Jedlicka P, Schwarzacher SW, Betz H, Harvey RJ, Brose N, Zhang W, Varoqueaux F. Neuroligin 2 Drives Postsynaptic Assembly at Perisomatic Inhibitory Synapses through Gephyrin and Collybistin. Neuron. 2009;63(5):628–42.

Powell SK, Kleinman HK. Neuronal laminins and their cellular receptors. Int J Biochem

Cell Biol. 1997;29(3):401–14.

Prabowo AS, Iyer AM, Veersema TJ, Anink JJ, Schouten-Van Meeteren AYN, Spliet WGM, Van Rijen PC, Ferrier CH, Capper D, Thom M, Aronica E. BRAF V600E mutation is associated with mTOR signaling activation in glioneuronal tumors. Brain Pathol. 2014;24(1):52–66.

Prayson RA, Fong J, Najm I. Coexistent pathology in chronic epilepsy patients with neoplasms. Mod Pathol. 2010;23(8):1097–103.

Pryce BR, Al-Zahrani KN, Dufresne S, Belkina N, Labrèche C, Patino-Lopez G, Frenette J, Shaw S, Sabourin LA. Deletion of the Ste20-like kinase SLK in skeletal muscle results in a progressive myopathy and muscle weakness. Skelet Muscle. 2017;7(1):1–13.

Quezada S, Castillo-Melendez M, Walker DW, Tolcos M. Development of the cerebral cortex and the effect of the intrauterine environment. J Physiol. 2018;596(23):5665–74.

Rajadhyaksha A, Barczak A, Macías W, Leveque JC, Lewis SE, Konradi C. L-type Ca2+ channels are essential for glutamate-mediated CREB phosphorylation and c-fos gene expression in striatal neurons. J Neurosci. 1999;19(15):6348–59.

Rakic P. Mode of cell migration to the superficial layers of fetal monkey neocortex. J Comp Neurol. 1972;145(1):61–83.

Rakic P. Evolution of the neocortex: A perspective from developmental biology. Nat Rev Neurosci. 2009;10(10):724–35.

Rampp S, Rössler K, Hamer H, Illek M, Buchfelder M, Doerfler A, Pieper T, Hartlieb T, Kudernatsch M, Koelble K, Peixoto-Santos JE, Blümcke I, Coras R. Dysmorphic neurons as cellular source for phase-amplitude coupling in Focal Cortical Dysplasia Type II. Clin Neurophysiol. 2021;132(3):782–92.

Represa A. Why Malformations of Cortical Development Cause Epilepsy. Front Neurosci. 2019;13(March):1–10.

Resulaj A, Ruediger S, Olsen SR, Scanziani M. First spikes in visual cortex enable perceptual discrimination. Elife. 2018;7.

Reynolds JH, Heeger DJ. The Normalization Model of Attention. Neuron. 2009;61(2):168–85.

Ribierre T, Miles R, Baulac S, Ribierre T, Deleuze C, Bacq A, Baldassari S, Marsan E,

Chipaux M, Muraca G, Roussel D, Navarro V, Leguern E, Miles R, Baulac S. Second-hit mosaic mutation in mTORC1 repressor DEPDC5 causes focal cortical dysplasia – associated epilepsy Find the latest version : Second-hit mosaic mutation in mTORC1 repressor DEPDC5 causes focal cortical dysplasia – associated epilepsy. 2018;128(6):2452–8.

Riedemann T. Diversity and function of somatostatin-expressing interneurons in the cerebral cortex. Int J Mol Sci. 2019;20(12).

Riedemann T, Straub T, Sutor B. Two types of somatostatin-expressing GABAergic interneurons in the superficial layers of the mouse cingulate cortex. PLoS One. 2018;13(7):1–26.

Roesler R, Machado RLD, Quevedo J. Differential expression of glutamate and GABA-A receptor subunit mRNA in cortical dysplasia (multiple letters) [5]. Neurology. 2001;57(12):2325–6.

Roovers K, Wagner S, Storbeck CJ, O'Reilly P, Lo V, Northey JJ, Chmielecki J, Muller WJ, Siegel PM, Sabourin LA. The Ste20-like kinase SLK is required for ErbB2-driven breast cancer cell motility. Oncogene. 2009;28(31):2839–48.

Roper SN, Eisenschenk S, King MA. Reduced density of parvalbumin- and calbindin D28k-immunoreactive neurons in experimental cortical dysplasia. Epilepsy Res. 1999;37(1):63–71.

Rossi MA, Hayrapetyan VY, Maimon B, Mak K, Shawn Je H, Yin HH. Prefrontal cortical mechanisms underlying delayed alternation in mice. J Neurophysiol. 2012;108(4):1211–22.

Rossignol E, Kruglikov I, Van Den Maagdenberg AMJM, Rudy B, Fishell G. CaV2.1 ablation in cortical interneurons selectively impairs fast-spiking basket cells and causes generalized seizures. Ann Neurol. 2013;74(2):209–22.

Rossini L, de Santis D, Mauceri RR, Tesoriero C, Bentivoglio M, Maderna E, Maiorana A, Deleo F, de Curtis M, Tringali G, Cossu M, Tumminelli G, Bramerio M, Spreafico R, Tassi L, Garbelli R. Dendritic pathology, spine loss and synaptic reorganization in human cortex from epilepsy patients. Brain. 2021;144(1):251–65.

Rowitch DH. Glial specification in the vertebrate neural tube. Nat Rev Neurosci. 2004;5(5):409–19.

Rowitch DH, Kriegstein AR. Developmental genetics of vertebrate glial-cell specification.

Nature. 2010;468(7321):214–22.

Rudy B, Fishell G, Lee SH, Hjerling-Leffler J. Three groups of interneurons account for nearly 100% of neocortical GABAergic neurons. Dev Neurobiol. 2011;71(1):45–61.

Sabourin LA, Rudnicki MA. Induction of apoptosis by SLK, a Ste20-related kinase. Oncogene. 1999;18(52):7566–75.

Saliba AE, Westermann AJ, Gorski SA, Vogel J. Single-cell RNA-seq: Advances and future challenges. Nucleic Acids Res. 2014;42(14):8845–60.

Samadani U, Judkins AR, Akpalu A, Aronica E, Crino PB. Differential cellular gene expression in ganglioglioma. Epilepsia. 2007;48(1):646–53.

Sasaki S, Huda K, Inoue T, Miyata M, Imoto K. Impaired feedforward inhibition of the thalamocortical projection in epileptic Ca2+ channel mutant mice, tottering. J Neurosci. 2006;26(11):3056–65.

Scala F, Kobak D, Bernabucci M, Bernaerts Y, Cadwell CR, Castro JR, Hartmanis L, Jiang X, Laturnus S, Miranda E, Mulherkar S, Tan ZH, Yao Z, Zeng H, Sandberg R, Berens P, Tolias AS. Phenotypic variation of transcriptomic cell types in mouse motor cortex. Nature. 2020;

Scala F, Kobak D, Shan S, Bernaerts Y, Laturnus S, Cadwell CR, Hartmanis L, Froudarakis E, Castro JR, Tan ZH, Papadopoulos S, Patel SS, Sandberg R, Berens P, Jiang X, Tolias AS. Layer 4 of mouse neocortex differs in cell types and circuit organization between sensory areas. Nat Commun. 2019;10(1).

Scheffer IE, Berkovic S, Capovilla G, Connolly MB, French J, Guilhoto L, Hirsch E, Jain S, Mathern GW, Moshé SL, Nordli DR, Perucca E, Tomson T, Wiebe S, Zhang YH, Zuberi SM. ILAE classification of the epilepsies: Position paper of the ILAE Commission for Classification and Terminology. Epilepsia. 2017;58(4):512–21.

Schick V, Majores M, Engels G, Spitoni S, Koch A, Elger CE, Simon M, Knobbe C, Blümcke I, Becker AJ. Activation of Akt independent of PTEN and CTMP tumor-suppressor gene mutations in epilepsy-associated Taylor-type focal cortical dysplasias. Acta Neuropathol. 2006;112(6):715–25.

Schnepp A, Lindgren PK, Hülsmann H, Kröger S, Paulsson M, Hartmann U. Mouse testican-2: Expression, glycosylation, and effects on neurite outgrowth. J Biol Chem. 2005;280(12):11274–80.

Schoch S, Quatraccioni A, Robens BK, Maresch R, van Loo KMJ, Cases-Cunillera S,

Kelly T, Opitz T, Borger V, Dietrich D, Pitsch J, Beck H, Becker AJ. Ste20-like kinase is critical for inhibitory synapse maintenance and its deficiency confers a developmental dendritopathy. J Neurosci. 2021;JN-RM-0352-21.

Selimbeyoglu A, Kim CK, Inoue M, Lee SY, Hong ASO, Kauvar I, Ramakrishnan C, Fenno LE, Davidson TJ, Wright M, Deisseroth K. Modulation of prefrontal cortex excitation/inhibition balance rescues social behavior in CNTNAP2-deficient mice. Sci Transl Med. 2017;9(401).

Sermet BS, Truschow P, Feyerabend M, Mayrhofer JM, Oram TB, Yizhar O, Staiger JF, Petersen CCH. Pathway-, layer-and cell-type-specific thalamic input to mouse barrel cortex. Elife. 2019;8:1–28.

Sessolo M, Marcon I, Bovetti S, Losi G, Cammarota M, Ratto GM, Fellin T, Carmignoto G. Parvalbumin-positive inhibitory interneurons oppose propagation but favor generation of focal epileptiform activity. J Neurosci. 2015;35(26):9544–57.

Severino M, Geraldo AF, Utz N, Tortora D, Pogledic I, Klonowski W, Triulzi F, Arrigoni F, Mankad K, Leventer RJ, Mancini GMS, Barkovich JA, Lequin MH, Rossi A. Definitions and classification of malformations of cortical development: Practical guidelines. Brain. 2020;143(10):2874–94.

Shao L-R, Habela CW, Stafstrom CE. Pediatric Epilepsy Mechanisms: Expanding the Paradigm of Excitation/Inhibition Imbalance. Children. 2019;6(2):23.

Shao YR, Isett BR, Miyashita T, Chung J, Pourzia O, Gasperini RJ, Feldman DE. Plasticity of Recurrent L2/3 Inhibition and Gamma Oscillations by Whisker Experience. Neuron. 2013;80(1):210–22.

Shuler MG, Bear MF. Reward timing in the primary visual cortex. Science (80-). 2006;311(5767):1606–9.

Sigrist SJ, Schmitz D. Structural and functional plasticity of the cytoplasmic active zone. Curr Opin Neurobiol. 2011;21(1):144–50.

Silberberg G, Markram H. Disynaptic Inhibition between Neocortical Pyramidal Cells Mediated by Martinotti Cells. Neuron. 2007;53(5):735–46.

Simonetti B, Paul B, Chaudhari K, Weeratunga S, Steinberg F, Gorla M, Heesom KJ, Bashaw GJ, Collins BM, Cullen PJ. Molecular identification of a BAR domain-containing coat complex for endosomal recycling of transmembrane proteins. Nat Cell Biol. 2019;21(10):1219–33.

Sisodiya SM, Fauser S, Cross JH, Thom M. Focal cortical dysplasia type II: biological features and clinical perspectives. Lancet Neurol. 2009;8(9):830–43.

Slegers RJ, Blumcke I. Low-grade developmental and epilepsy associated brain tumors: A critical update 2020. Acta Neuropathol Commun. 2020;8(1):1–11.

Sohal VS, Rubenstein JLR. Excitation-inhibition balance as a framework for investigating mechanisms in neuropsychiatric disorders. Mol Psychiatry. 2019;24(9):1248–57.

Sohal VS, Zhang F, Yizhar O, Deisseroth K. Parvalbumin neurons and gamma rhythms enhance cortical circuit performance. Nature. 2009;459(7247):698–702.

Sparta DR, Hovelsø N, Mason AO, Kantak PA, Ung RL, Decot HK, Stuber GD. Activation of prefrontal cortical parvalbumin interneurons facilitates extinction of reward-seeking behavior. J Neurosci. 2014;34(10):3699–705.

Spruston N. Pyramidal neurons : dendritic structure and synaptic integration. 2008;9(march):206–21.

Staahl BT, Crabtree GR. Creating a neural specific chromatin landscape by npBAF and nBAF complexes. Curr Opin Neurobiol. 2013;23(6):903–13.

Stark E, Eichler R, Roux L, Fujisawa S, Rotstein HG, Buzsáki G. Inhibition-Induced theta resonance in cortical circuits. Neuron. 2013;80(5):1263–76.

Storbeck CJ, Wagner S, O'Reilly P, McKay M, Parks RJ, Westphal H, Sabourin LA. The Ldb1 and Ldb2 transcriptional cofactors interact with the Ste20-like kinase SLK and regulate cell migration. Mol Biol Cell. 2009;20(19):4174–82.

Subramanian L, Calcagnotto ME, Paredes MF. Cortical Malformations: Lessons in Human Brain Development. Front Cell Neurosci. 2020;13.

Sun QQ, Huguenard JR, Prince DA. Reorganization of barrel circuits leads to thalamically-evoked cortical epileptiform activity. Thalamus Relat Syst. 2005;3(4):261–73.

Sun Y, Ikrar T, Davis MF, Gong N, Zheng X, Luo ZD, Lai C, Mei L, Holmes TC, Gandhi SP, Xu X. Neuregulin-1/ErbB4 Signaling Regulates Visual Cortical Plasticity. Neuron. 2016;92(1):160–73.

Szczurkowska J, Cwetsch AW, Dal Maschio M, Ghezzi D, Ratto GM, Cancedda L. Targeted in vivo genetic manipulation of the mouse or rat brain by in utero electroporation with a triple-electrode probe. Nat Protoc. 2016;11(3):399–412.

Talos DM, Sun H, Kosaras B, Joseph A, Folkerth RD, Poduri A, Madsen JR, Black PM, Jensen FE. Altered inhibition in tuberous sclerosis and type IIb cortical dysplasia. Ann

Neurol. 2012;71(4):539–51.

Tamás G, Buhl EH, Lörincz A, Somogyi P. Proximally targeted GABAergic synapses and gap junctions synchronize cortical interneurons. Nat Neurosci. 2000;3(4):366–71.

Taniguchi H, Lu J, Huang ZJ. The spatial and temporal origin of chandelier cells in mouse neocortex. Science (80-). 2013;339(6115):70–4.

Tasic B, Menon V, Nguyen TN, Kim TK, Jarsky T, Yao Z, Levi B, Gray LT, Sorensen SA, Dolbeare T, Bertagnolli D, Goldy J, Shapovalova N, Parry S, Lee C, Smith K, Bernard A, Madisen L, Sunkin SM, Hawrylycz M, Koch C, Zeng H. Adult mouse cortical cell taxonomy revealed by single cell transcriptomics. Nat Neurosci. 2016;19(2):335–46.

Taylor PJ, Sater R, French J, Baltuch G, Crino PB. Transcription of intermediate filament genes is enhanced in focal cortical dysplasia. Acta Neuropathol. 2001;102(2):141–8.

Tempes A, Weslawski J, Brzozowska A, Jaworski J. Role of dynein–dynactin complex, kinesins, motor adaptors, and their phosphorylation in dendritogenesis. J Neurochem. 2020;155(1):10–28.

Tessier-Lavigne M, Goodman CS. The molecular biology of axon guidance. Science (80-). 1996;274(5290):1123–33.

Thomson AM, Lamy C. Functional Maps of Neocortical Local Circuitry. Front Neurosci. 2007;1(1):19–42.

Tremblay R, Lee S, Rudy B. GABAergic Interneurons in the Neocortex: From Cellular Properties to Circuits. Neuron. 2016;91(2):260–92.

Tretter V, Jacob TC, Mukherjee J, Fritschy JM, Pangalos MN, Moss SJ. The clustering of GABAA receptor subtypes at inhibitory synapses is facilitated via the direct binding of receptor α2 subunits to gephyrin. J Neurosci. 2008;28(6):1356–65.

Trevelyan AJ, Sussillo D, Yuste R. Feedforward inhibition contributes to the control of epileptiform propagation speed. J Neurosci. 2007;27(13):3383–7.

Tripathy SJ, Toker L, Bomkamp C, Mancarci BO, Belmadani M, Pavlidis P. Assessing Transcriptome Quality in Patch-Seq Datasets. Front Mol Neurosci. 2018;11.

Troyano-Rodriguez E, Wirsig-Wiechmann CR, Ahmad M. Neuroligin-2 Determines Inhibitory Synaptic Transmission in the Lateral Septum to Optimize Stress-Induced Neuronal Activation and Avoidance Behavior. Biol Psychiatry. 2019;85(12):1046–55.

Tyagarajan SK, Fritschy JM. Gephyrin: A master regulator of neuronal function? Nat Rev Neurosci. 2014;15(3):141–56.

Veit J, Hakim R, Jadi MP, Sejnowski TJ, Adesnik H. Cortical gamma band synchronization through somatostatin interneurons. Nat Neurosci. 2017;20(7):951–9.

Virtanen MA, Lacoh CM, Fiumelli H, Kosel M, Tyagarajan S, de Roo M, Vutskits L. Development of inhibitory synaptic inputs on layer 2/3 pyramidal neurons in the rat medial prefrontal cortex. Brain Struct Funct. 2018;223(4):1999–2012.

Viswanatha R, Ohouo PY, Smolka MB, Bretscher A. Local phosphocycling mediated by LOK/SLK restricts ezrin function to the apical aspect of epithelial cells. J Cell Biol. 2012;199(6):969–84.

Vogt D, Cho KKA, Shelton SM, Paul A, Huang ZJ, Sohal VS, Rubenstein JLR. Mouse Cntnap2 and Human CNTNAP2 ASD Alleles Cell Autonomously Regulate PV + Cortical Interneurons. Cereb Cortex. 2018;28(11):3868–79.

Wagner S, Flood TA, O'Reilly P, Hume K, Sabourin LA. Association of the Ste20-like kinase (SLK) with the microtubule. Role in Rac1-mediated regulation of actin dynamics during cell adhesion and spreading. J Biol Chem. 2002;277(40):37685–92.

Wagner S, Storbeck CJ, Roovers K, Chaar ZY, Kolodziej P, McKay M, Sabourin LA. FAK/src-family dependent activation of the Ste20-like kinase SLK is required for microtubule-dependent focal adhesion turnover and cell migration. PLoS One. 2008;3(4).

Wagner SM, Sabourin LA. A novel role for the Ste20 kinase SLK in adhesion signaling and cell migration. Cell Adhes Migr. 2009;3(2):182–4.

Wang K, Hong RL, Lu JB, Wang DL. Ste20-like kinase is upregulated in glioma and induces glioma invasion. Neoplasma. 2018a;65(2):185–91.

Wang T, Li B, Nelson CE, Nabavi S. Comparative analysis of differential gene expression analysis tools for single-cell RNA sequencing data. 2019;1–16.

Wang Y, Toledo-Rodriguez M, Gupta A, Wu C, Silberberg G, Luo J, Markram H. Anatomical, physiological and molecular properties of Martinotti cells in the somatosensory cortex of the juvenile rat. J Physiol. 2004;561(1):65–90.

Wang Y, Wang R, Tang DD. Ste20-like kinase-mediated control of actin polymerization is a new mechanism for thin filament-associated regulation of airway smooth muscle contraction. Am J Respir Cell Mol Biol. 2020;62(5):645–56.

Wang Y, Ye M, Kuang X, Li Y, Hu S. A simplified morphological classification scheme for pyramidal cells in six layers of primary somatosensory cortex of juvenile rats. IBRO

Reports. 2018b;5:74–90.

Williams MR, De-Spenza T, Li M, Gulledge AT, Luikart BW. Hyperactivity of newborn pten knock-out neurons results from increased excitatory synaptic drive. J Neurosci. 2015;35(3):943–59.

Wilson NR, Runyan CA, Wang FL, Sur M. Division and subtraction by distinct cortical inhibitory networks in vivo. Nature. 2012;488(7411):343–8.

Wimmer VC, Bruno RM, De Kock CPJ, Kuner T, Sakmann B. Dimensions of a projection column and architecture of VPM and POm axons in rat vibrissal cortex. Cereb Cortex. 2010;20(10):2265–76.

Witte H, Bradke F. The role of the cytoskeleton during neuronal polarization. Curr Opin Neurobiol. 2008;18(5):479–87.

Wolf HK, Birkholz T, Wellmer J, Blumcke I, Pletsch T, Wlestler OD. Neurochemical profile of glioneuronal lesions from patients with pharmacoresistant focal epilepsies. J Neuropathol Exp Neurol. 1995;54(5):689–97.

Wong M, Roper SN. Genetic animal models of malformations of cortical development and epilepsy. J Neurosci Methods. 2016;260:73–82.

Wood KC, Blackwell JM, Geffen MN. Cortical inhibitory interneurons control sensory processing. Curr Opin Neurobiol. 2017;46:200–7.

World Health Organization. Epilepsy. 2019.

Woychyshyn B, Papillon J, Guillemette J, Navarro-Betancourt JR, Cybulsky A V. Genetic ablation of SLK exacerbates glomerular injury in adriamycin nephrosis in mice. Am J Physiol - Ren Physiol. 2020;318(6):F1377–90.

Yamada E, Tsujikawa K, Itoh S, Kameda YI, Kohama Y, Yamamoto H. Molecular cloning and characterization of a novel human STE20-like kinase, hSLK. Biochim Biophys Acta - Mol Cell Res. 2000;1495(3):250–62.

Yamanouchi H. Activated remodeling and N-methyl-D-aspartate (NMDA) receptors in cortical dysplasia. J Child Neurol. 2005;20(4):303–7.

Yan Y, Tulasne D, Browaeys E, Cailliau K, Khayath N, Pierce RJ, Trolet J, Fafeur V, Younes A Ben, Dissous C. Molecular cloning and characterisation of SmSLK, a novel Ste20-like kinase in Schistosoma mansoni. Int J Parasitol. 2007;37(14):1539–50.

Yavorska I, Wehr M. Somatostatin-expressing inhibitory interneurons in cortical circuits. Front Neural Circuits. 2016;10(SEP):1–18.

Yazaki-Sugiyama Y, Kang S, Cteau H, Fukai T, Hensch TK. Bidirectional plasticity in fast-spiking GABA circuits by visual experience. Nature. 2009;462(7270):218–21.

Ying Z, Babb TL, Mikuni N, Najm I, Drazba J, Bingaman W. Selective coexpression of NMDAR2A/B and NMDAR1 subunit proteins in dysplastic neurons of human epileptic cortex. Exp Neurol. 1999;159(2):409–18.

Ying Z, Bingaman W, Najm IM. Increased Numbers of Coassembled PSD-95 to NMDA-receptor Subunits NR2B and NR1 in Human Epileptic Cortical Dysplasia. Epilepsia. 2004;45(4):314–21.

Yong X, Zhao L, Deng W, Sun H, Zhou X, Mao L, Hu W, Shen X, Sun Q, Billadeau DD, Xue Y, Jia D. Mechanism of cargo recognition by retromerlinked SNX-BAR proteins. PLoS Biol. 2020;18(3).

Yoshimura Y, Dantzker JLM, Callaway EM. Excitatory cortical neurons form fine-scale functional networks. Nature. 2005;433(7028):868–73.

Yu S, Li S, Shu H, Zhang C, He J, Fan X, Yang H. Upregulated expression of voltage-gated sodium channel Nav1.3 in cortical lesions of patients with focal cortical dysplasia type IIb. Neuroreport. 2012;23(7):407–11.

Zacchi P, Antonelli R, Cherubini E. Gephyrin phosphorylation in the functional organization and plasticity of GABAergic synapses. Front Cell Neurosci. 2014;8(1 APR).

Zaitsev A V., Povysheva N V., Lewis DA, Krimer LS. P/Q-type, but not N-type, calcium channels mediate GABA release from fast-spiking interneurons to pyramidal cells in rat prefrontal cortex. J Neurophysiol. 2007;97(5):3567–73.

Zamecnik J, Krsek P, Druga R, Marusic P, Benes V, Tichy M, Komarek V. Densities of parvalbumin-immunoreactive neurons in non-malformed hippocampal sclerosis-temporal neocortex and in cortical dysplasias. Brain Res Bull. 2006;68(6):474–81.

Zeisel A, M͡oz-Manchado AB, Codeluppi S, Lönnerberg P, Manno G La, Juréus A, Marques S, Munguba H, He L, Betsholtz C, Rolny C, Castelo-Branco G, Hjerling-Leffler J, Linnarsson S. Cell types in the mouse cortex and hippocampus revealed by single-cell RNA-seq. Science (80-). 2015;347(6226):1138–42.

Zhang N, Hu G, Pena H, Qiu J, Park Y-D, Uzel G, Datta SK, Steiner JP, Kelsall BL, Williamson PR. Formation of an Argonaut-independent miRNA-mRNA Complex with DDX6 Orchestrates MTOR- dependent Regulation of T-cell differentiation. J

Immunol. 2018;200(1 Supplement):45.34 LP-45.34.

Zhang S, Xu M, Kamigaki T, Do JPH, Chang WC, Jenvay S, Miyamichi K, Luo L, Dan Y. Long-range and local circuits for top-down modulation of visual cortex processing. Science (80-). 2014;345(6197):660–5.

Zhang Y, Hume K, Cadonic R, Thompson C, Hakim A, Staines W, Sabourin LA. E xpression of the Ste20-like kinase SLK during embryonic development and in the murine adult central nervous system. 2002;139:205–15.

Zhao JP, Yoshii A. Hyperexcitability of the local cortical circuit in mouse models of tuberous sclerosis complex. Mol Brain. 2019;12(1).

Zhapparova ON, Fokin AI, Vorobyeva NE, Bryantseva SA, Nadezhdina ES. Ste20-like protein kinase SLK (LOSK) regulates microtubule organization by targeting dynactin to the centrosome. Mol Biol Cell. 2013;24(20):3205–14.

Zhou FW, Roper SN. Reduced chemical and electrical connections of fast-spiking interneurons in experimental cortical dysplasia. J Neurophysiol. 2014;112(6):1277–90.

Ziv NE, Garner CC. Cellular and molecular mechanisms of presynaptic assembly. Nat Rev Neurosci. 2004;5(5):385–99.

Zucker RS, Regehr WG. Short-term synaptic plasticity. Annu Rev Physiol. 2002;64:355–405.

9. Acknowledgements

First of all, I would like to express my most sincere thanks to Prof. Heinz Beck for giving me the opportunity to carry out my Ph.D. project in his lab. From our very first meeting via Skype when I was still a Master student in Brazil, I have found support and encouragement in his kind words, which were crucial to successfully push my project until the end. I really appreciate our stimulating scientific conversations and how receptive and interested he always has been about my ideas. This has definitively encouraged me to develop independent thinking and gave me the confidence to trust and share my scientific thoughts. I thank Prof. Susanne Schoch and Prof. Albert Becker for all the technical and methodological support given by their labs and for always being there to discuss new ideas. I want to thank Prof. Dirk Isbrandt for accepting being the second supervisor of my thesis and for the advice and suggestions he shared during my progress reports.

I want to thank Anne Quatraccioni for her crucial contribution to my project. She was always keen to support me in the generation of animals and to help me solve any problem my project faced. I am are very grateful to Lea Keller and Thoralf Opitz for their technical support and help with the breeding and genotyping of animals. I thank Margit Reitze, Nicole Schoenfelder, and Sabrina Walch for their administrative assistance during these years. I thank all the members of my lab for their kind support but especially for all the good times, lunches, beer tasting, conferences, and carnival celebrations that we shared together. I especially thank Nico, Martin, Negar, Michela, André, Fabian, Daniel, and Kristian since sharing time, gossips, laughs and emotional support with them is one of the reasons these 5 years in Germany have been amazing. I thank my lifetime friends Despina, Eugenia, Nohelia, Andrea, Luis, Veronica, Alessandra, Mariana, and Rafael for teaching that real friendship is priceless. I especially thank my parents and brothers for their unconditional love and support. Finally, thank you Katty for making me feel at home whenever I am by your side.